

Oxidation of *n*-octane over molybdenum oxide based catalysts

By

Ajij Golandaj

(M.Sc)

*Submitted in the fulfilment of the academic requirements for the degree of **Doctor of Philosophy** at the*

School of Chemistry and Physics

University of KwaZulu Natal

Durban

South Africa

December 2014

***Note:** This thesis has been written according to Format 3, as outlined in the guidelines from the Faculty of Science and Agriculture, University of KwaZulu-Natal, which states: This is a thesis in which the chapters are written as a set of discrete research papers, with an overall Introduction and a Final Discussion. These research papers would not be published yet, but at least one paper would have already been submitted for publication. The references are reformatted to a uniform standard.*

As the candidate's supervisor, I have approved this thesis for submission.

Name: Prof. H. B. Friedrich **Signature** _____ **Date** _____

Name: Dr. S. Singh **Signature** _____ **Date** _____

Dedicated
To my
Late
Grandfather and Grandmother

ABSTRACT

The research into alternative feedstocks has gained importance in recent years to replace olefins by alkanes. The use of alkanes is viable since they are cheap, abundant and can be easily sourced from Gas to liquid (GTL) plants and oil refineries. Oxidative dehydrogenation (ODH) is preferred over dehydrogenation (DH) as the catalysts regeneration and higher conversion can be achieved at comparatively lower temperature, and thus it is less energy intensive.

This study focussed on oxidative dehydrogenation of *n*-octane using molybdenum based catalysts. The choice of these oxides was based on their ability to form different oxides, among them, bulk MoO₃, monomeric and polymeric MoO_x, crystalline MoO₃ species, and cationic molybdates such as NiMoO₄, which were exploited for the ODH of *n*-octane. The catalysts were synthesized by the wet impregnation and co-precipitation methods. The prepared catalysts were characterised using ICP-OES, XRD, Raman, N₂-physisorption, SEM, TEM and TPR.

The catalytic testing was carried out with a continuous flow fixed bed reactor in the temperature range of 350 to 550 °C and the C:O ratios studied were 8:0, 8:1, 8:2, 8:3 and 8:4. The study was divided in to three parts, consisting of the effect of C:O ratio over bulk MoO₃, the effect of different weight loadings of Mo on SBA-15 and the effect of different phases of bulk and SBA-15 supported NiMoO₄ catalysts for the oxidative dehydrogenation of *n*-octane.

The catalytic and non-catalytic activation of *n*-octane was studied in the presence and absence of bulk MoO₃. Only cracked products were formed in a carborundum packed reactor tube, whereas with the catalyst, high selectivity to octenes was observed. Initially, octenes formation appeared due to lattice oxygen, after which their formation was ascribed to dehydrogenation over MoO₂, after depletion of lattice oxygen. The conversion increased with an increase in the oxygen content in both cases i.e. non-catalytic and catalytic, but it was higher for the catalytic route due to the operating redox cycle between MoO₃ and Mo₄O₁₁. With increase in oxygen content, the octene selectivity decreased and formation of CO_x increased. Highest 1-octene selectivity (16%) was observed when MoO₃ was used a catalyst, as opposed to the non-catalytic reactions where 1-octene selectivity was 8%.

When the molybdenum (4 to 18 wt%) was supported on SBA-15, formation of monomeric, polymeric MoO_x and crystalline MoO₃ was observed. The conversion of *n*-octane increased and

octenes selectivity decreased with an increase in the molybdenum loading. The catalyst with the 10 wt% molybdenum loading showed the highest yield towards ODH products. Furthermore, when the effect of temperature was examined over the 10 wt% catalyst, an increase in temperature resulted in an increase in the selectivity to aromatics. The conversion and selectivity to non-selective products increased with an increase in the oxygen content in the feed. The GHSV studies revealed that the octenes, cracked products and CO₂ are the primary products of the reaction.

For the study involving nickel molybdate (NiMoO₄) as a catalyst, the effect of C:O ratio (8:1, 8:2, and 8:3) at a GHSV of 4000 h⁻¹ was investigated over the α -phase of NiMoO₄. In which case, the C:O ratio of 8:1 was found optimum to produce octenes with a high selectivity. The unsupported β -NiMoO₄, α -NiMoO₄/SBA-15 and β -NiMoO₄/SBA-15 were then tested at the optimum C:O ratio of 8:1 at a GHSV of 4000 h⁻¹. When the conversions of all the catalysts were compared, the unsupported α -NiMoO₄ system showed the highest conversion. Octene was the dominant product observed and the highest octene selectivity was observed over the unsupported β -NiMoO₄ catalyst, whereas the highest aromatics selectivity was exhibited by the α -NiMoO₄/SBA-15 catalyst. In the case of supported catalysts, at temperatures of 350 and 400 °C, the reactions were driven by surface oxygen, whereas at temperatures of 450 and 500 °C, it is driven by the lattice oxygen.

PREFACE

The experimental work described in this thesis has been done in the School of Chemistry and Physics, University of KwaZulu-Natal (Westville Campus) from January 2011 to November 2014, under the supervision of Professor Holger B. Friedrich and Dr. Sooboo Singh.

The study mentioned in the thesis represents original work by the author and have not otherwise been submitted in any form for any degree or diploma to any other tertiary institution. Where use has been made of the work of others are duly acknowledged in the text.

Author: Mr. Ajij Golandaj

Sign: _____

Date: _____

DECLARATION-1

I, Mr. Ajij Jahangeer Golandaj, declare that:

- 1 The research reported in this thesis, except where otherwise indicated, and is my original research.
- 2 This thesis has not been submitted for any degree or examination at any other university.
- 3 This thesis does not contain other persons' data, pictures, graphs or other information, unless specifically acknowledged as being sourced from other persons.
- 4 This thesis does not contain other person's writing unless specifically acknowledged as being sourced from other researchers. Where other written sources have been quoted, then:
 - (a) Their words have been re-written but the general information attributed to them has been referenced.
 - (b) Where their exact words have been used, then their writing has been placed in italics and inside quotation marks, and referenced.
- 5 This thesis does not contain text, graphics or tables copied and pasted from the internet, unless specifically acknowledged, and the source being detailed in the thesis and in the Reference sections.

Signed:

Declaration Plagiarism 22/05/08 FHDR Approved

DECLARATION-2

Part of the work has been published and presented at conferences as detailed below:

Publication:

- 1 Oxidative dehydrogenation of *n*-octane over MoO₃, J. Mol. Catal. A: Chem (Communicated).
Authors: Ajij Golandaj, Abdul S. Mahomed, Holger B. Friedrich, and Sooboo Singh
- 2 Effect of different weight loadings of MoO_x on SBA15 over ODH of *n*-octane. J. Porous Mat (DOI 10.1007/s10934-015-9952-6).
Authors: Ajij Golandaj, Abdul S. Mahomed, Holger B. Friedrich, and Sooboo Singh
- 3 Oxidation dehydrogenation of *n*-octane over NiMoO₄ and NiMoO₄ supported on SBA-15 (Manuscript in preparation)
Authors: Ajij Golandaj, Abdul S. Mahomed, Holger B. Friedrich, and Sooboo Singh

Contribution: I carried out all the experimental work and the manuscript preparation under the supervision of Dr. A. S. Mahomed, Dr. S. Singh, and Prof. H. B. Friedrich.

Conference contributions:

- 1 Oxidation of *n*-paraffins by MoO₃ supported on SBA-15, Poster presentation, Catalysis Conference of South Africa (CATSA), November 2011.
- 2 Oxidation of *n*-octane over MoO₃ and SBA-15 supported MoO₃, Poster presentation, Catalysis Conference of South Africa (CATSA), November 2012.
- 3 Oxidation of *n*-octane over MoO₃ supported on SBA-15; effect of location of active species, Catalysis Conference of South Africa (CATSA), November 2013.

Author: Mr. Ajjj Golandaj

Sign: _____

Date: _____

ACKNOWLEDGEMENTS

Completion of this Doctoral thesis was possible with the support of few special people and I express my sincere and heart felt gratitude to them.

- I thank almighty for giving me perseverance, strength and guidance for successful completion of my doctoral research.
- My family has been my greatest support, I will always be grateful to them for having stood by me throughout this period, in particular my beloved mother, for being my motivation and continuous moral support in my life. I wouldn't have seen this day because of her sacrifices. I would also like to take this opportunity to thank my uncle Mr. Mansoor Mujawar, for his constant care and sustenance.
- I am extremely thankful to my late grandmother and grandfather for their positive influence and contribution in my life. Your love, affection and beautiful memories are treasured and dearly missed.
- No research would be possible without the resources and services the University of KwaZulu-Natal provides its students. I express my humble gratitude to this esteemed University
- This feat was possible only because of the support provided by Prof. Holger Friedrich and Dr. Sooboo Singh, I sincerely thank you both for keeping faith in me and all your support rendered until the completion and for being patient with me.
- I would also like to extend my gratitude to Dr. Abdul Samad Mahomed, for his valuable assistance and guidance in my research. You will always be remembered for the science I learnt from you in the field of catalysis.
- I duly acknowledge the financial support from THRIP, SASOL and University of KwaZulu Natal, which allowed me to completely focus on my doctoral studies.
- Dr. Michael Datt (SASOL) for his valuable and treasured guidance during my research. I sincerely thank you.
- I would like to thank the technical staff at the School of Chemistry and Physics, especially Mrs. Padayachee, Mr. Ishaan, Mr, Danny, Mr. Sagie and Mr. Moodley, whose generous technical support with instrumentation as well as specialised lab apparatus made my research less daunting task.

- I would like to extend my friendly & faithful appreciation to my close friends and lab mates Ziyad, Mohamed, Dr. Venkat, Charlene, and Ebrahim, without whose support, interactions, and suggestions this research would not have been rewarding. Thank you my dear friends.
- My stay in South Africa wouldn't have been so comfortable without my dear Indian friends Sachin, Hanif, Pramod, Suhas, and Sarvanan, who gave me a priceless support and company when most needed. I would also like to extend my sincere gratitude to my extended family in Durban Dr. Nizam Shaikh, Dr. Rajshekhar Karpoormath, and Mrs. Prithvi Narayan Karpoormath for always being there for me.
- Finally and most importantly, I would like to sincerely thank my beloved wife Nazia, for giving high priority to my research work and providing constant motivation. This work would not have been possible without your support.

TABLE OF CONTENTS

	Page No.
List of Figures	xv
List of Tables	xviii
List of Abbreviations	xix
Chapter 1: Introduction and Literature Survey	1
1.1 Oxidation	2
1.1.1 Non-catalytic oxidation	3
1.1.2 Catalytic oxidation of alkanes	6
1.1.2.1 Selective or partial oxidation of alkanes	6
1.1.2.2 Oxidative dehydrogenation of alkanes	9
1.2 Catalytic Systems	16
1.2.1 MoO ₃ and MoO _x supported catalysts	16
1.2.2 Supported NiMoO ₄ and NiMoO ₄ catalysts	19
1.2.3 SBA-15	23
1.3 Objectives of the study	25
References	27
Chapter 2: Oxidative dehydrogenation of <i>n</i>-octane over α-MoO₃	
Abstract	33
2.1 Introduction	33
2.2 Experimental	35
2.2.1 Catalyst synthesis and characterisation	35
2.2.2 Catalytic testing	35
2.3 Result and discussion	36
2.3.1 Catalyst characterization	36
2.3.1.1 Powder X-ray diffraction	36

	Page No.	
2.3.1.2	SEM and TEM	38
2.3.2	Catalytic testing	39
2.3.2.1	Effect of variation of oxygen	39
2.3.2.1.1	Blank reaction results	39
2.3.2.1.2	Catalytic testing of α -MoO ₃	41
2.3.2.1.3	Product selectivity	46
2.3.3	SEM analysis of used catalysts	49
2.4	Conclusion	50
	References	51
Chapter 3:	Effect of different weight loadings of Mo/SBA-15 on the oxidative dehydrogenation of <i>n</i>-octane	
	Abstract	54
3.1	Introduction	55
3.2	Experimental	56
3.2.1	Preparation of catalysts	56
3.2.1.1	Synthesis of SBA-15	56
3.2.1.2	Synthesis of molybdenum supported on SBA-15	57
3.2.2	Characterisation of catalysts	57
3.2.3	Catalytic testing	58
3.3	Result and discussion	58
3.3.1	Characterisation of catalysts	58
3.3.1.1	ICP-OES	58
3.3.1.2	BET analysis	58
3.3.1.3	Powder X-ray diffraction	60
3.3.1.4	Raman spectroscopy	62
3.3.1.5	SEM and TEM studies	63
3.3.2	Catalytic results	65
3.3.2.1	Catalytic testing of molybdenum oxide supported on SBA-15	65

	Page No.	
3.3.2.2	Effect of temperature on 10 wt % molybdenum supported on SBA-15	70
3.3.2.3	Effect of C:O ratio over 10 wt% molybdenum supported on SBA-15	71
3.3.2.4	Effect of GHSV over 10 wt% molybdenum supported on SBA-15	72
3.4	Summary and conclusions	74
	References	75
Chapter 4:	Oxidation dehydrogenation of <i>n</i>-octane over NiMoO₄ and NiMoO₄ supported on SBA-15	
	Abstract	78
4.1	Introduction	78
4.2	Experimental	80
4.2.1	Catalysts preparation	80
4.2.2	Catalyst characterization	81
4.2.3	Catalytic testing	81
4.3	Result and discussion	82
4.3.1	Characterisation of catalyst	82
4.3.1.1	Powder X-ray diffraction	82
4.3.1.2	SEM and TEM analyses	83
4.3.1.3	BET Studies	84
4.3.1.4	Temperature programmed reduction study	84
4.3.2	Catalytic results	85
4.3.2.1	Blank reaction details	85
4.3.2.2	Effect of C:O ratio for unsupported α -NiMoO ₄	86
4.3.2.3	Comparison of <i>n</i> -octane conversion for supported and unsupported NiMoO ₄	90
4.3.2.4	Comparison of product selectivity for all catalysts as a function of temperature	92

	Page No.	
4.3.2.5	Product selectivity at isoconversion	95
4.4	Summary and conclusions	97
	References	98
Chapter 5	Conclusion and summary	100
Appendix 1	Figures and Tables	103
Appendix 2	Product quantification	111

LIST OF FIGURES

		Page No.
Figure 1.1	Formation of cyclic ethers and ketones by gaseous oxygen	5
Figure 1.2	Mechanism of oxidation of <i>n</i> -pentane over VPO catalyst	8
Figure 1.3	Crystal structures of (A) α -MoO ₃ and (B) β -MoO ₃	16
Figure 1.4	MoO _x structures observed over SiO ₂ at different pH values	17
Figure 1.5	DTA cycle of stoichiometric NiMoO ₄ phase transitions	20
Figure 1.6	Arrangement of the oxygen octahedral in α -NiMoO ₄ , the octahedral containing Ni, Mo ions are shaded by line	20
Figure 1.7	TEM image and pore structure of SBA-15	23
Figure 2.1	XRD diffractogram of α -MoO ₃	36
Figure 2.2	SEM (A) and TEM (B) micrographs of α -MoO ₃	338
Figure 2.3	Time on line experiment at 550 °C without oxygen with MoO ₃ at a GHSV of 4000 h ⁻¹ (A) <i>n</i> -octane conversion and product selectivity (B) formation of octenes, hydrogen, and water as a function of time on line	42
Figure 2.4	XRD diffractograms of the used catalysts after reaction with <i>n</i> -octane at C:O ratio of 8:0 (A), 8:1(B) and 8:2 (C)	44
Figure 2.5	Schematic representation of α -MoO ₃ reduction/oxidation via Mo ₄ O ₁₁ under <i>n</i> -octane	45
Figure 2.6	Effect of oxygen content over octenes isomers at 550 °C (at carbon to oxygen ratio of 8:1 and 8:2 with a GHSV of 4000 h ⁻¹)	47
Figure 2.7	Aromatics breakdown at C:O ratio of 8:1 and 8:2 with a GHSV of 4000 h ⁻¹	48
Figure 2.8	SEM images of fresh catalyst (A) and used catalysts at C:O ratios of 8:0 (B), 8:1 (C) and 8:2 (D)	49

		Page No.
Figure 3.1	N ₂ adsorption-desorption isotherms of different loadings of molybdenum supported on SBA-15 catalysts	60
Figure 3.2	XRD diffractograms of catalysts with varying loadings of molybdenum supported on SBA-15 and SBA-15 support	61
Figure 3.3	Raman spectra of the catalysts with 4, 7, and 10 wt% molybdenum supported on SBA-15	62
Figure 3.4	Raman spectrum of 18% molybdenum supported on SBA-15	62
Figure 3.5	TEM images of 4 wt% (a), 7 wt% (b), 10 wt% (c) and 18 wt% (d) molybdenum supported on SBA-15	64
Figure 3.6	SEM images of 4 wt% (S), 7 wt% (b), 10 wt% (c) and 18 wt% (d) molybdenum supported on SBA-15	65
Figure 3.7	Conversion (oxygen and <i>n</i> -octane) and product selectivity as a function of weight loadings of molybdenum supported on SBA-15 (Temperature = 450 °C, GHSV = 4000 h ⁻¹ and C:O = 8:3)	66
Figure 3.8	Rate of <i>n</i> -octane consumption and rate of formation of octenes and aromatics over the different wt% of molybdenum supported on SBA-15 (Temperature = 450 °C, GHSV = 4000 h ⁻¹ and C:O = 8:3)	67
Figure 3.9	Effect of C:O ratio over the catalytic activity of 10 wt% molybdenum supported on SBA-15 (Temperature = 450 °C, GHSV = 4000 h ⁻¹)	71
Figure 3.10	Effect of GHSV on <i>n</i> -octane conversion with 10 wt% molybdenum supported on SBA-15 (Temperature = 450 °C and C:O = 8:3)	72
Figure 3.11	Effect of GHSV on selectivity to different products on 10 wt% molybdenum supported on SBA-15 (Temperature = 450 °C and C:O = 8:3)	73
Figure 4.1	XRD of the NiMoO ₄ and NiMoO ₄ /SBA-15 catalysts	82
Figure 4.2	(A) and (B) SEM images, where (C) and (D) TEM images of unsupported NiMoO ₄ and NiMoO ₄ /SBA-15	83
Figure 4.3	TPR of NiMoO ₄ and NiMoO ₄ supported on SBA-15 (NM = NiMoO ₄)	85

	Page No.	
Figure 4.4	Blank reaction results with a carborundum packed reactor tube at a C:O ratio of 8:3 with a GHSV of 4000 h ⁻¹	86
Figure 4.5	Effect of C:O ratio on conversion of <i>n</i> -octane over unsupported NiMoO ₄ at a GHSV of 4000 h ⁻¹ .	87
Figure 4.6	Oxygen conversion at varying C:O ratios over unsupported α-NiMoO ₄ at a GHSV of 4000 h ⁻¹	88
Figure 4.7	Octene (A), aromatics (B), CO _x (C), cracked (D) and cracked aromatics (E) products at different C:O ratios as a function of temperature over unsupported α-NiMoO ₄	89
Figure 4.8	CO and CO ₂ selectivity at different C:O ratios at a GHSV of 4000 h ⁻¹ over α-NiMoO ₄ catalyst as a function of temperature	90
Figure 4.9	Conversion of <i>n</i> -octane over different catalysts at a C:O ratio of 8:1 at a GHSV of 4000 h ⁻¹	91
Figure 4.10	Product distribution at isoconversion (A) different products selectivity (B) octenes breakdown (C) Aromatics breakdown	95

LIST OF TABLES

		Page No.
Table 1.1	Results for the oxidative dehydrogenation of propane over various metal molybdates	12
Table 2.1	Different planes of α -MoO ₃ with 2θ value and Full Width and Half Maximum	37
Table 2.2	Conversion and products selectivity for the non-catalytic reactions in a 24 grit carborundum packed reactor tube at a fixed GHSV of 4000 h ⁻¹	39
Table 2.3	Catalytic activity of the MoO ₃ under different C:O ratios at a GHSV of 4000 h ⁻¹	41
Table 2.4	Rietveld refinement table for used catalysts	45
Table 3.1	Physical properties of the different weight loadings of molybdenum supported on SBA-15	59
Table 3.2	Yields of octenes and aromatic products (Temperature = 450 °C, GHSV 4000 h ⁻¹ and C:O = 8:3)	69
Table 3.3	<i>n</i> -Octane conversion and product selectivity of the 10 wt% molybdenum supported on SBA-15 as a function of temperature (C:O = 8:3, GHSV = 4000 h ⁻¹)	70
Table 4.1	Effect of NiMoO ₄ loadings over the surface area and pore volume on SBA-15	84
Table 4.2	Catalytic testing of the catalysts at a C:O ratio of 8:1 and at a GHSV of 4000 h ⁻¹	93

LIST OF ABBREVIATIONS

BET	:	Brunauer-Emmett-Teller
DH	:	Dehydrogenation
EDX	:	Energy Dispersive X-ray Spectroscopy
EM	:	Electron Microscopy
FID	:	Flame Ionization Detector
FTIR	:	Fourier Transform Infrared
GC	:	Gas Chromatography
GC-MS	:	Gas Chromatography-Mass Spectrometry
GHSV	:	Gas Hourly Space Velocity
GTL	:	Gas To Liquid
HPLC	:	High Performance Liquid Chromatography
ICP-OES	:	Inductively Coupled Plasma – Optical Emission Spectroscopy
JCPDS	:	Joint Committee on Powder Diffraction Standards
MCM-41	:	Mobile Composition of Matter No. 41
MCM-48	:	Mobile Composition of Matter No. 48
NM	:	Nickel molybdate
ODH	:	Oxidative dehydrogenation
SEM	:	Scanning Electron Microscopy
TCD	:	Thermal Conductivity Detector
TEM	:	Transmission Electron Microscopy
TPD	:	Temperature Programmed Desorption
TPR	:	Temperature Programmed Reduction
SiC	:	Silicon Carbide/ Carborundum
SBA-15	:	Santa Barbara Amorphous type material 15
SAPO	:	Silico Alumino Phosphate Molecular sieves
VPO	:	Vanadium Phosphorus Oxide
XAS	:	X-ray Absorption Spectroscopy
XAFS	:	X-ray Absorption Fine Structure

Chapter 1

Introduction and Literature Survey

The international chemical growth rate is expected to rise this year (2014) from 2.4% to 3.8%, as the organic commodity chemicals recorded an increasing demand worldwide in recent years [1]. These commodity chemicals are being used for the production of a variety of high valued products due to several processes that are available to functionalise them. The commodity chemicals used extensively include olefins and aromatics, obtained primarily from crude oil either by steam cracking or fluid catalytic cracking of the petroleum fractions. However, these processes to produce olefins suffer some disadvantages, namely high energy and fuel demand, catalyst regeneration and coke formation [1, 2]. To make any industrial process cost effective, it is thus necessary to find alternative sources as starting materials or different processes to synthesise these chemicals.

Feedstocks replacing olefins include alkanes, which can be obtained from crude oil and the many gas to liquid plants worldwide. Alkanes are far less reactive than olefins since all the carbon atoms are saturated and exist in the stable sp^3 hybridised state. However, they can be converted to value added products by using oxidation or ammoxidation processes, typically at high temperatures ($> 450\text{ }^\circ\text{C}$) [3, 4]. Despite having good activity in liquid phase reactions, the high operational temperatures limit the use of homogeneous catalysis in alkane transformations. Therefore, the heterogeneous approach is preferred. In addition, it is preferred due to its ease of separation of product and reactant from the catalyst and it can be scaled up with fewer complications. Heterogeneous catalytic oxidation is an important field and currently, more than 60% of chemicals and organic intermediates are produced by heterogeneous processes [5]. Over the last few decades, a great deal of effort has been utilized in studying the oxidative transformation of alkanes. Short chain alkanes have been studied extensively by using vanadium and molybdenum and recently, more attention is afforded to longer chains in the C_6 - C_{10} range using vanadium supported on different materials [6-11].

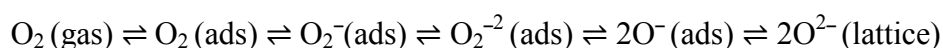
One of the goals set by many researchers in the recent past is to develop expertise in the area of oxidation catalysis to transform much of the available alkanes. Although this has proved to be a difficult task, some success in this efforts has materialized, e.g. the conversion of *n*-

butane to good yields of maleic anhydride [5]. Extensive research continues and efforts to contribute to the oxidation of alkanes are presented.

1.1 Oxidation

Oxidation is known to be one of the key technologies to convert petroleum based feedstocks to a variety of chemicals [12]. In addition, oxidation processes are being used in the preparation of basic chemicals such as H_2SO_4 , NH_3 , CH_3OH , and organic intermediates such as olefins, epoxides, hydroperoxides, alcohols, aldehydes, ketones, phenols, esters, lactones, oximes, and sulfoxides [5]. The choice of oxidant and oxygen species plays a major role in obtaining an acceptable yield to the desired product and it should possess an ability to limit unwanted or undesired reactions during the catalytic process, i.e. it should be active, but more selective towards the target product. Molecular oxygen is a preferred oxidant over other oxidants, due to environmental as well as economic reasons [13, 14]. CO_2 is also used as an oxidant and in one case for the oxidative dehydrogenation (ODH) of ethyl benzene to styrene [15]. However, the major drawback of this oxidant is the production of CO , which is environmentally unfriendly.

When a gaseous oxygen interacts with the surface of the catalyst, different oxygen species are formed, which remain in equilibrium with the gaseous oxygen as shown below [16]:



An important consideration in this scheme is the relationship that exists between the molecular oxygen, adsorbed oxygen and the lattice oxygen of the catalyst. The removal of an oxygen atom (lattice oxygen) from the catalyst during the activation of the alkane creates a vacancy that is filled by the equilibrium process shown. This process can continue in a catalytic redox cycle.

The process of oxygen adsorption on the catalyst surface changes the nature of the oxygen species from electrophilic (O_2^-) to nucleophilic (O^{2-}) [14]. Among the various oxygen species, the O^- , O_2^- (superoxide) and O_2^{2-} (peroxide), as the electrophilic oxygen species, are known to be responsible for the deep oxidation of the hydrocarbon, whereas the nucleophilic, electron rich, O^{2-} (lattice oxygen) species are thought to be involved in the partial oxidation reactions. This nucleophilic species reacts with the hydrocarbon molecule at the electron deficient site [14]. The catalytic oxidation of lower alkanes is widely studied using bulk and supported metal based catalysts which showed good activity for alkane oxidation with a good selectivity to the desired product such as olefins and oxygenates [17, 18]. However, with

most paraffinic substrates, the contribution of non-catalytic reactions was found to be significant, when compared to the catalytic activity [19, 20]

1.1.1 Non-catalytic oxidation of alkanes

The oxidation that takes place in the absence of a catalyst is considered as non-catalytic oxidation. Non-catalytic oxidation can be carried out by using an empty reactor tube or by filling the reactor tube with an inert material such as quartz chips or carborundum powder (SiC), however, the extent of these reactions vary considerably under these two reactor configurations. In an empty reactor tube, the alkane undergoes pyrolysis and conversion is achieved through significant gas phase radical reactions, whereas, in the presence of the inert material, the radicals are quenched resulting in low conversions [7, 19, 20]. With the inert material, the homogeneous reactions proceed through the available void space in between the inert material and results in the formation of targeted as well as unwanted products. It was found that, in the absence of any catalyst, under optimised conditions, slightly higher conversions with good selectivity towards the desired product was obtained by adjusting the hydrocarbon to oxygen ratio and residence time [19]. There are some cases reported where the non-catalytic reactions showed better activity than the catalytic reactions, e.g. ethane oxidation was carried out in an empty reactor with hydrocarbon to oxygen molar ratios of 1:1, 1:2 and 1:3. Conversion was shown to decrease with an increase in the hydrocarbon concentration and the products obtained were ethene and CO. The optimum ethane to oxygen ratio of 1:2 gave ethene selectivity of 74% with a conversion of 45% at 600 °C. With the reactor tube packed with inert SiC, the conversion decreased due to the quenching of the free radicals [19]. Catalytic studies carried out using Li-MgO under similar conditions, gave a yield of 12% to ethene, whereas, for the non-catalytic reaction, the yield was 33%. Similar observations were noted with propane, where the non-catalytic oxidation reaction was more efficient in terms of conversion and selectivity compared to when V/MgO was used as the catalyst [6]. Lemonidou *et al.* [21] studied the non-catalytic activation of *n*-butane and showed that the conversion of *n*-butane increased with an increase in temperature from 0.5% (550 °C) to 5.08% (610 °C), whereas the butene selectivity decreased from 15% (550 °C) to 4% (610 °C). In this reaction, *n*-butane underwent pyrolysis in an empty reactor tube and produced propylene (50%) and ethylene (22%) as the major products, with a butene selectivity of only 4% at 610 °C. They observed that, with equimolar ratios of *n*-butane and oxygen, conversion increased to 62% with increasing temperature, however, the selectivity to butene decreased from 50% to 12%, due to cracking of butenes to produce lower alkenes.

They also studied the effect of residence time on butane ODH and showed that the higher residence time led to higher conversion but lower butene selectivity. The highest conversion of 90% was observed with a residence time of 1.8 s and a C₂-C₄ alkene selectivity of 55%. The formation of the C₂ and C₃ products was explained by the decomposition of the *n*-butane as shown in the following equations (Equation 1-3) [21]:



The effect of void spaces at different positions in the reactor tube was investigated by Friedrich *et al.* [7] during the non-oxidative transformation of *n*-hexane. The effect of packing the catalyst at different positions in the reactor tube was probed in the temperature range of 300 to 500 °C. The experiments were carried out using an empty reactor tube and a reactor tube packed with carborundum. In the empty reactor tube, significant *n*-hexane conversion was noted with a high selectivity toward the C₃-C₄ cracked products. However, conversion decreased when reactions were carried out with the carborundum packed reactor tube due to the quenching of the free radicals over carborundum. The reaction was also carried out with a conventionally packed reactor tube, where the catalyst was placed at the hotspot, as well as at different positions in the tube to establish the extent of the non-catalytic reactions in the catalytic process. It was concluded that at a temperature of 400 °C, where the carborundum packed reactor tube exhibited no conversion, the conversion (47%) displayed by the conventionally packed reactor tube was solely related to the catalyst. However, when the catalyst was packed at the exit of the reactor tube, a similar activity to the carborundum packed reactor tube was observed. When the catalyst was placed at the entrance of the reactor tube, the behaviour observed was different from that of the set up involving placing the catalyst at the exit. The conversion achieved over this type of configuration was higher and it was attributed to the activation of feed over the catalyst, whilst the formation of final products was achieved in the intergranular space of the carborundum powder. It was also reported that the conversion decreased with a smaller sized carborundum powder (24 to 80

grit). In addition, it was shown that the formation of benzene was favoured over the various types of packing configurations with a significant decrease in CO_x . In other experiments, where the catalyst was either diluted with the carborundum in a fixed volume (1mL v/v), or distributed in the entire tube and was then compared, a similar conversion with high selectivities to benzene was observed. However, when the catalyst was diluted and packed along the length of the entire tube, a decrease in selectivity to CO_x was observed. It was concluded that the conversion essentially takes place in the presence of oxygen and the formation of CO_x takes place in the void spaces of the carborundum.

Friedrich and Mahomed [9] carried out the non-catalytic oxidation of *n*-octane in the presence and absence of carborundum powder with a feed consisting of 7% by volume of *n*-octane in air. The conversion of *n*-octane was significant (57% at 500 °C) in an empty reactor tube, however, the conversion was suppressed with carborundum (SiC) powder and gave only 6% conversion at the same temperature. The products observed were octenes, cracked alkenes, aromatics, oxygenates, CO and CO_2 . The octenes and oxygenates showed a decreasing trend, while CO_x (CO and CO_2) showed an increasing trend with an increase in temperature. The formation of octenes, aromatics and oxygenates, in this case, was claimed to form *via* the thermal route. The major oxygenated products observed were cyclic ethers and ketones. The formation of these oxygenated products was initiated by the activated peroxy species (O_2^{2-}) as described by Stoylkova *et al.* [22] for *n*-heptane oxidation and is shown in Figure 1.1. The cleavage of the peroxy complex can lead either to ketones or ethers.

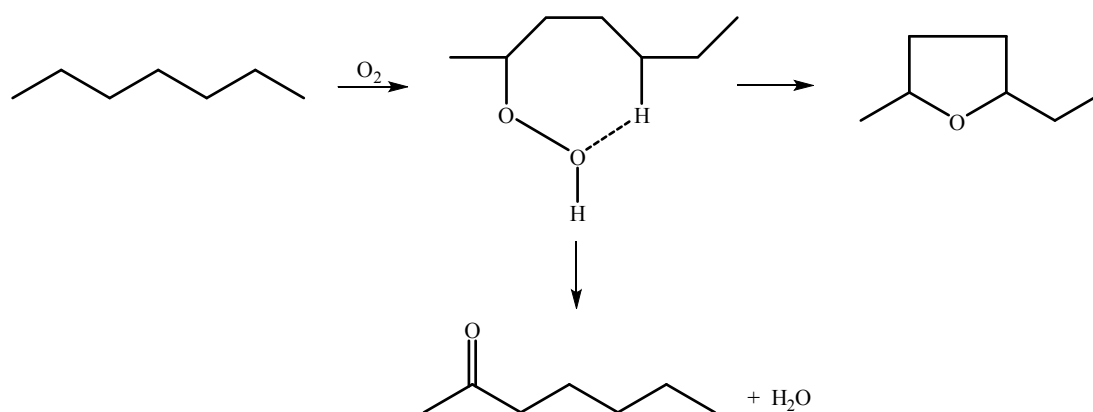


Figure 1.1 Formation of cyclic ethers and ketones by the gaseous oxygen (Redrawn with permission from Elsevier Copyright © 2014) [22].

It can be concluded from the studies carried out for the non-catalytic activation of ethane, propane and *n*-butane, that the gas phase radical chemistry gives significant selectivity to the desired product, however, for the longer chains, this is not necessarily the case. Although the non-catalytic reaction can give the same products as the catalytic reactions in the case of some alkanes, yield of these products can vary considerably [7]. For longer chain alkanes, the non-catalytic and catalytic reactions can be significantly different with respect to conversion as well as selectivity [9].

1.1.2 Catalytic oxidation of alkanes

Catalytic oxidation can be categorized into selective or partial oxidation, oxidative dehydrogenation (ODH) and total oxidation. Selective or partial oxidation and oxidative dehydrogenation are of interest to the researcher, whereas total oxidation is undesirable.

1.1.2.1 Selective or partial oxidation of alkanes

Methane, ethane, and propane are generally considered as lower alkanes. These lower alkanes have considerable importance in the chemical industry as they can be used as sources for a variety of commodity chemicals. Methane has been partially oxidised to formaldehyde by using bulk MoO₃, V₂O₅ with MoO₃ and V₂O₅ supported on silica, as shown in the study by Parmalianal *et al.* [23]. In this work, the catalyst loadings of 5, 10, 15 and 20 wt% for V and 4 and 7 wt% for Mo were investigated. When these bulk oxides were supported on silica, it showed an improved catalytic activity in comparison with bulk V₂O₅ and MoO₃. However, it was claimed that, at the lower loading, the activation of methane occurs through surface activation of the molecular O₂, whereas, with higher loadings of vanadium and bulk V₂O₅ and MoO₃ catalysts, it occurs through a redox mechanism. The supported V₂O₅ catalysts were found to be more active than the supported MoO₃ catalysts. The V₂O₅ catalyst over fumed silica was found to be more active than V₂O₅ supported on precipitated silica. The higher activity of the former catalyst was attributed to the weaker interaction of V₂O₅ with fumed silica. With the supported MoO₃ catalysts, the addition of MoO₃ over fumed silica exhibited higher conversion rates ($13.65 \times 10^{-7} \text{ g}^{-1} \cdot \text{s}^{-1}$) with a selectivity of 86% to formaldehyde, compared to the precipitated silica which gave a conversion rate of $10.50 \times 10^{-7} \text{ g}^{-1} \cdot \text{s}^{-1}$ and selectivity of 70% [23].

In the oxidation of ethane, Mo and V mixed metal oxides were investigated by Thorsteinson *et al.* [24]. The selective oxidation of ethane to ethene was carried out with a Mo_{0.73}V_{0.18}Nb_{0.09}O_x catalyst to give a conversion of 58% and a selectivity of 65% at a

temperature of 350 °C. Other catalysts reported for the oxidation of ethane were vanadium based and polyoxometallate complexes over TiO₂ [25, 26] and ZrO₂ [27]. With vanadium phosphorous oxide (VPO) and VO_x supported over TiO₂, the formation of acetic acid occurred at 180-250 °C, whereas, the formation of ethene was favoured temperatures >250 °C. The mixed metal oxide Mo₆V₃NbO catalyst was also studied in the conversion of ethane to ethene by Lopez Nieto and co-workers [28]. The catalyst was synthesized hydrothermally by heat treatment in the temperature range of 600-700 °C under a nitrogen stream. The resultant catalyst gave a yield of 75% with a selectivity of 82% to ethene.

Propane oxidation was widely studied, as acrolin, acetonitrile and acrylic acid are obtained by oxidising propane in a two-step process, i.e. propane to propene and propene to the required chemicals [29-31]. Bettahar *et al.* [31] reviewed the oxidation of propane and propylene over various mixed metal oxides which included VPO, VMgO, BiMo(V)O and VSbO. Summarizing their results, the VMgO catalyst gave 15% conversion with 65% selectivity to propylene. For the BiMo(V)O catalyst, a 15% conversion was observed with 65% selectivity to acrolin and the VSbO catalyst achieved a 40% propane conversion with 80% selectivity to acrylonitrile [31]. Propane oxidation was also studied over vanadium-phosphorus (V-P) catalysts [32, 33], metal-phosphines [34] and Bi-V-Mo oxides catalysts [35, 36]. None of these catalysts showed a yield of more than 10% to acrylic acid. However, T. Ushikubo and co-workers from Mitsubishi Corporation (Japan) [37] claimed that a yield of 48% to acrylic acid can be obtained over a MoV_{0.3}Te_{0.23}Nb_{0.12}O_x catalyst. The VPO catalyst which was used for the commercial *n*-butane oxidation to maleic anhydride was also used for propane oxidation to acrylic acid and showed a 23% conversion with a 48% selectivity to acrylic acid, corresponding to a 11.2% yield [38]. Wang *et al.* [39] studied the effect of promoting VPO catalysts with Co, Bi, Te, Nb, Mo and B, however, incorporation of these elements showed no improvement to the acrylic acid selectivity. With 0.01 % ceria doped VPO catalysts, the yield towards acrylic acid was increased to 18.7%, which is the highest among all the VPO based catalysts [38, 40]. Recently, Ovsitser *et al.* [41] used VO_x species supported over SiO₂, MCM-41 and SBA-15 for propane dehydrogenation in oxygen free and oxygen lean condition. A propene selectivity above 80% was obtained with a conversion more than 45% over all these catalysts in the temperature range of 550-570 °C.

The most successful commercialized example of a selective oxidation process is *n*-butane oxidation to maleic anhydride using the VPO catalyst. In this process, a maximum conversion of 85% was obtained with almost 70% selectivity towards maleic anhydride [42].

Mesoporous silica (SBA-15 and MCM-41) and fumed SiO₂ supported VPO catalysts were also employed to increase the yield of maleic anhydride, but only SiO₂ supported VPO catalysts exhibited higher conversion (96% at 400 °C) with 55% yield to maleic anhydride [43]. A MoV type mixed metal oxides catalytic systems, also reported for the oxidation of *n*-butane, showed lower selectivity to maleic anhydride than VPO catalyst [44].

In the oxidation of *n*-pentane, VPO catalysts have been used to produce maleic anhydride and phthalic anhydride [5, 13]. Zazhigolav and co-workers [45] carried out a mechanistic investigation of *n*-pentane oxidation to maleic and phthalic anhydride as showed in Figure 1.2. They proposed that adsorption of *n*-pentane takes place on basic sites, while the acidic sites are responsible for isomerisation followed by unsaturation and then insertion of oxygen to give maleic anhydride. The formed maleic anhydride undergoes a Diels-Alder reaction to give rise to phthalic anhydride [45]

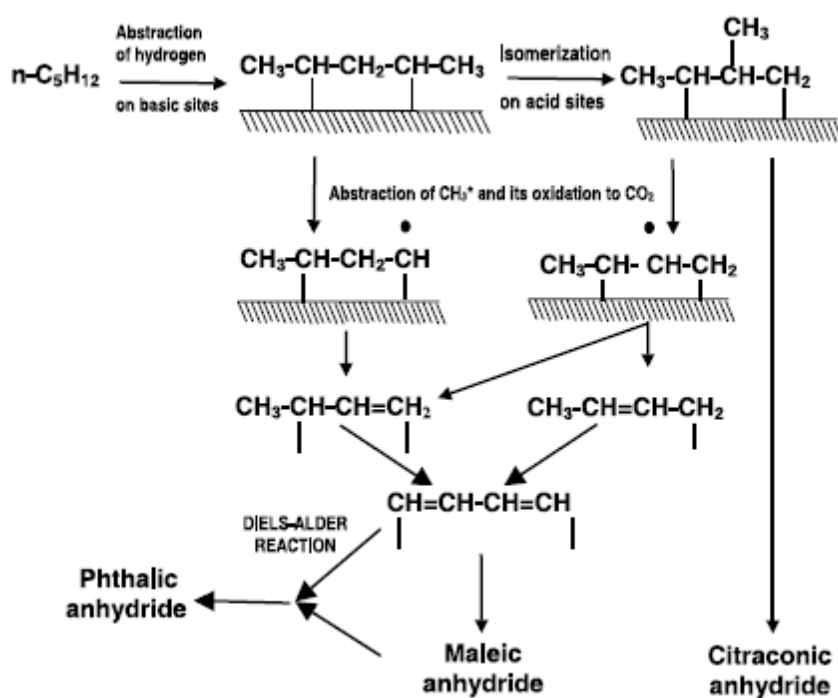


Figure 1.2 Mechanism of oxidation of *n*-pentane over VPO catalyst [45].

In the catalytic study of *n*-pentane oxidation by Singh *et al.* [46], vanadium pentoxide supported hydroxyapatites were used as catalysts. The catalysts were prepared by varying the

wt% of V₂O₅ from 2.5 to 15 on hydroxyapatite. The catalyst with 7.5 wt% V₂O₅ showed the highest yield towards maleic anhydride formation at a conversion of 65%.

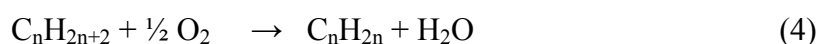
The oxidation of *n*-hexane to C₆ oxygenates using Titanium-silica (TS) with H₂O₂ as oxidant is an important transformation, however under these reaction conditions, the catalysts were found less effective and even in presence of ample amount of H₂O₂ lower conversion of *n*-hexane were reported [47-49]. Halasz and co-workers [50], synthesized TS-1 catalysts with Si/Ti molar ratios of 55, 82 and 66 and the activity of these catalysts was compared with the previous report. The TS-1 catalyst with Si/Ti molar ratio of 55 showed a highest *n*-hexane turnover rate and H₂O₂ efficiency (amount of H₂O₂ used for the monofunctional product formation) at 55 °C, which was far higher than the previous attempts of *n*-hexane oxidation by various researchers [47-49]. However in these studies, the improved activity of the catalyst is claimed to the availability of tetrahedral and non-tetrahedral titanium defects sites, which acts as an induced active sites, which were absent in the pure TS-1 catalysts. The addition of the vanadium in the silica matrix was carried out by Ramaswamy and Sivasanker [51]. The catalyst showed the formation of deeper oxidation products such as aldehyde, ketones and lactones, whereas with the TS catalysts alone showed significant amounts of alcohols and ketones.

Boyadjian *et al.* [52] studied the oxidative cracking of *n*-hexane over a Li-MgO catalyst to produce lower alkenes such as ethylene, propene and butenes. The high yield of these lower olefins was attributed to the greater concentration of Li-O⁻ on the catalyst surface which initiates the reaction by abstracting hydrogen radicals to create hexyl radicals, which further undergo a series of complex reactions to yield these alkenes. However, when the catalyst was promoted with Mo and Bi, an improved yield to the C₂-C₄ was observed. The O⁻ species was claimed to be very selective toward the formation of the lower alkenes.

1.1.2.2 Oxidative dehydrogenation of alkanes

Currently, expensive alkenes (olefins) are used as starting materials for the manufacture of a large number of valuable chemicals. This drawback can be averted by catalytically activating the abundant, inexpensive alkanes to alkenes. To produce alkenes from alkanes, two methods can be employed, viz. dehydrogenation (DH) and oxidative dehydrogenation (ODH). Dehydrogenation methods are commercially well-established and have been used since the 1930s. During World War II, the need for high octane aviation fuel was fulfilled by dehydrogenating butane over chromia-alumina catalysts to butene followed by dimerization to give octenes, then hydrogenated to yield high-octane aviation fuel [53]. In the 1970s,

continuous catalytic regeneration (CCR) technology was used for the production of light olefins and the technology was known as UOP OleflexTM with a production capacity of 900 000 metric tons per annum [53]. Later in the 1980s, the chromia-alumina catalysts were used for propane and isobutane activation to yield corresponding alkenes and this process was known as the CatofinTM process [53]. All these commercial processes work on dehydrogenation of alkanes and these processes give good yields toward olefins. However, the dehydrogenation reaction has several drawbacks. Continuous operation causes deactivation of the catalyst which requires frequent regeneration, resulting in the shutdown of the reactor. The endothermic nature of the reaction requires high operating temperatures, i.e. 600-800 °C making the reaction energy intensive [54]. In spite of operating at such high temperatures, the conversion obtained in these processes are limited, due to the equilibrium attained at such high temperatures between the reactant and products [55]. In addition to this, coking is also a major issue in these dehydrogenation reactions. The limitations posed by dehydrogenation processes are overcome by employing oxidative dehydrogenation (ODH) processes. The deactivation and reactor shutdown issues are omitted due to a continuous regeneration of the active phase of the catalysts by passing oxygen through it and coking is also avoided. In the presence of oxygen, high conversions are achieved at low temperatures due to the oxidation of the formed hydrogen to water, thus reducing its energy requirements as shown in Equation 4 [53].



ODH also has some disadvantages, such as over oxidation of the formed products to carbon oxides.

Mixed metal oxides such as MoVP were efficient in the ODH of ethane to ethene. Here, the selectivity to ethene increased at the expense of CO_x by addition of V to MoO_x and then P. When the MoO_x was tested, it showed poor activity (4.6%) with high CO_x selectivity (89%). The effect of doping the MoO_x based catalyst with vanadium showed an increase in conversion (8.7%) as well as selectivity towards ethene (53%). Furthermore, with the addition of phosphorus, the ethene selectivity was increased to 68% with a conversion of 14.3%. The improvement in the conversion and selectivity was due to the formation of the (Mo-V)₅O₁₄ phase. The addition of the phosphate group was claimed to be controlling the domain size of MoO_x as well as the interaction of Mo and V with ethane [56]. Martínez-Huerta *et al.* [57] supported vanadium oxide over Al₂O₃ for the ODH of ethane. They observed that the conversion of ethane, as well as selectivity to ethene increased with an

increase in V loading, but then decreased above a loading of 20 wt%. The decrease in the activity was ascribed to the polymerisation of V species on the surface of the catalysts.

The effect of Mo supported over Al₂O₃, SiO₂, TiO₂(anatase) and ZrO₂(Monoclinic) was investigated by Tsilomelekis *et al.* [58] for oxidative dehydrogenation of ethane to ethene. At lower loadings, the molybdenum exists as the monomeric MoO_x species, whereas with an increase in the molybdenum loading, polymeric Mo-O-Mo species are formed. The Mo-O-support bond and the nature of the support have a significant influence on the catalytic activity. As a result, the low cation electronegativity of the support causes an increase in the electron density at the oxygen site of the Mo-O-support anchoring bond. The increased electron density further causes an increase in the activity of the redox processes. The dependence of the reactivity on the support was found in the order, ZrO₂ > Al₂O₃ > TiO₂ > SiO₂, while the energy of activation for the ethane activation was found in the reverse order. A significant selectivity to ethene was observed with Mo supported on Al₂O₃, followed by ZrO₂, TiO₂, and SiO₂. Another study that examined ethane oxidation over MoO_x supported on SiO₂ was carried out by Erd"ohelyi *et al.* [59]. In their work, the active site was Mo⁺⁵, which adsorbed oxygen to create O⁻ species. The O⁻ species was characterised using Electron Spin Resonance (ESR). Ethane oxidation was initiated by the formation of an ethyl radical by abstraction of a hydrogen atom by the O⁻ species formed on the Mo⁺⁵ as shown below (Equation 5):



The ethyl radical then reacts with O⁻ (Equation 6) to form an ethoxide ion, which decomposes to ethene (Equation 7).



Oxidative dehydrogenation of propane to propene is also well studied by various researchers [17, 34, 60, 61]. The propane oxidation over various MMoO₄ was studied by Yoon *et al.* [17], where M= Mg, Ni, Co, Cu, Zn, Ca, Sr, Ba, La, Sm, Al and Cr . The results of the catalytic testing are shown in Table 1.1.

Table 1.1 Results for the oxidative dehydrogenation of propane over various metal molybdates [17].

Catalyst	Temperature °C	Propane conversion (%)	Propene selectivity (%)	Yield (%)
MgMoO ₄	500	8.9	67	5.96
CaMoO ₄	500	1.6	83	0.87
SrMoO ₄	500	1.0	62	0.62
BaMoO ₄	500	0.7	78	0.54
ZnMoO ₄	500	0.2	100	0.20
CoMoO ₄	500	9.3	63	5.85
NiMoO ₄	432	12.4	35	4.37
MnMoO ₄	500	1.4	49	0.68
CuMoO ₄	500	3.9	17	0.67
La ₂ Mo ₃ O ₁₂	500	6.3	57	3.59
Sm ₂ Mo ₃ O ₁₂	500	5.9	73	4.30
Al ₂ Mo ₃ O ₁₂	500	10.5	26	2.73
Cr ₂ Mo ₃ O ₁₂	476	12.3	14	1.72

(Note: Reprinted with permission from Elsevier Copyright © 2014)

Under the reaction conditions, the NiMoO₄ was found to be most active but gave a relatively low selectivity to propene. On the other hand, ZnMoO₄ showed the lowest conversion but was only selective to propene. The basic metal oxides presented good selectivity towards propene but they were less active than the Cr, Co and Al molybdates.

In another study for propane oxidation to propene using V-Mo/TiO₂ catalysts, the addition of the Mo to the V/TiO₂ catalyst showed an increase in the propene yield [61]. The catalyst with the lowest Mo content (0.6 wt%) with an optimum loading of vanadium (3.2wt%) over TiO₂ gave the best results. The improved activity of the catalyst was credited to the synergetic effect exerted at the Mo and V oxide interface.

The effect of the different oxidants on propane oxidation over V/MCM-41 was investigated by Kondratenko *et al.* [62]. They found that the activity was higher when O₂ was used as an oxidant as it can re-oxidise the reduced species, however, an improved selectivity towards propene was observed with N₂O as the oxidant. Zhang and co-workers [63] prepared an isolated V-Sb-O catalyst along with VO_x/SiO₂ and SbO_x/SiO₂. The catalysts were prepared by the wet impregnation method. The V-Sb-O catalyst gave the highest conversion and selectivity to propene compared to the other catalysts with a propene yield of 26%.

Oxidative dehydrogenation of *n*-butane to butene and butadiene was achieved over VO_x/SBA-15 catalysts with V loadings ranging from 2 to 28 wt% by Liu and co-workers

[64]. The butene selectivity increased gradually with V loading up to 9 wt%. A maximum selectivity of 27% at a 55% conversion was achieved with a V loading of 9 wt%. Further increase in the V loadings gave selectivity to CO_x of greater than 80%. A 9 wt% of V impregnated on SiO₂ catalyst gave a 47% conversion with a selectivity of 16% to butenes, resulting in a lower yield than that achieved over 9V/SBA-15 [64].

Vanadium supported on hexagonal mesoporous silica (HMS) was investigated for *n*-butane oxidation by Setnička *et al.* [65]. The effect of the preparation methods, i.e. wet impregnation and direct synthesis was examined. The V loadings were in the range from 1.2 to 15 wt%. At lower loadings, the preparatory method did not show any major difference in the structure of the catalyst, forming only monomeric VO_x species. However, with the direct synthesis method, monomeric VO_x species were present even at higher loadings. The increase in the V loading caused the formation of polymeric and 3D octahedral V species. The butene selectivity increased with an increase in V loadings. The catalyst prepared by the direct synthesis method exhibited an overall butene selectivity of 65 % and selectivity towards 1, 3-butadiene of 30%. This was 10% greater than the catalysts prepared by wet impregnation [65].

Bulanek *et al.* [66], studied the activation of *n*-butane over V supported on different mesoporous silica such as HMS, SBA- 15, SBA-16 and MCM-41 with a loading of 3 and 9 wt%. The 3 wt% V supported on SBA-15 showed the highest selectivity of 60% towards butene. Raju and co-workers [67] studied the ODH of *n*-butane over V supported Ce-Zr and Ti-Zr mixed oxide supports. CO₂ was used as a soft oxidant in this study. The V/Ce-Zr catalyst was more active than V/Ti-Zr due to the facile oxygen transport from Ce, which prevents deactivation of the catalyst [67]. The V/Ce-Zr catalyst displayed higher selectivity to butenes (45%) than V/Ti-Zr and Ce-Zr (18% and 10% respectively).

The oxidative dehydrogenation of *n*-pentane was studied by Korili and co-workers [68] over magnesium vanadate catalysts. Although similar conversions were obtained over the pyrovanadate (Mg₂V₂O₇) and orthovanadate (Mg₃V₂O₈) phases, high selectivity towards pentenes was obtained with the orthovanadate phase. The pentenes observed were 1-pentene together with *trans* and *cis* 2-pentene. The addition of a dopant, Sb₂O₅, resulted in an increase in the production of 1- and 2-pentene [68]. Valenzuela *et al.* [69] studied the ODH of isopentane using a series of catalysts such as ZnFe₂O₄ and MgFe₂O₄, V/MgO, Mo/MgO, MgCr₂O₄, MgO, Li/MgO, Li-Sn/MgO, Mg(P₂O₇), CrVO₄ and Cr₂(P₂O₇)₃. The 15 wt% V/MgO catalyst gave promising results with 70% selectivity to ODH products at a conversion of 10%. Further, the effect of residence time, temperature, and oxygen partial

pressure was investigated on the V/MgO catalyst. It was concluded that the conversion increased with the increase in residence time and oxygen content in the gaseous feed, however, the temperature increase caused an increase in the selectivity to mono-olefins and isoprene at low conversion only. The selectivity to the olefins decreased with an increase in the oxygen partial pressure.

V/MgO catalysts were used for *n*-hexane oxidation and in the same study, the effects of voids in the reactor was investigated [7]. It was observed that the formation of benzene was due to both a catalytic and non-catalytic contribution. When the catalyst was packed at the entrance of the tube and the void space was filled with carborundum, a selectivity of 19% and a conversion of 50% was found. The non-catalytic contribution obtained over a carborundum packed reactor tube to benzene was 14% selectivity with on *n*-hexane conversion of 40%. The oxidation of *n*-hexane was also carried out by using NiMoO₄ catalysts by Pillay *et al.* [70]. The contributions from its individual metal oxides (NiO and MoO₃) were also investigated and compared. The α -NiMoO₄ with excess MoO₃ gave good selectivity to C₆ cyclic compounds, whereas MoO₃ gave good selectivity towards cyclopentane. On the other hand, β -NiMoO₄ produced hexenes as the dominant products and NiO produced mainly carbon oxides.

The oxidation of *n*-heptane is not well explored compared to other alkanes. Dasireddy *et al.* [71] carried out the ODH of *n*-heptane over VMgO catalysts and investigated the effect of the orthovanadate phase of vanadium on the catalytic activity. The MgO, itself, was found to be non-selective to heptenes and produced CO_x as the dominant product. However, in the presence of vanadium, the formation of heptenes, aromatics compounds and oxygenates was favoured. The favoured aromatic product was toluene, whereas the dominant oxygenated product was 2-heptanol. Other investigations in heptane activation were mainly focussed on cracking and isomerisation. Pant and Kunzru [72] investigated the cracking of *n*-heptane over K promoted calcium aluminate to produce lower alkenes. The unpromoted catalyst gave higher yields to lower alkenes, but a significant amount of coke was formed during this transformation. It was shown that the addition of K to the calcium aluminate decreased the coke formation on the catalyst. When *n*-heptane was oxidised over alumina silicate (SAPO-5 and 11, BEA and MCM-41), partially oxidised products were formed, including 2, 3 and 4-heptanones, cyclic compounds and 1-hepten 4-ol [22].

Catalytic oxidation of *n*-octane was investigated over hydrotalcites incorporating different ratios of V and Mg. The product profile displayed a high selectivity to octenes with low selectivity to aromatics, in which styrene was the dominant aromatic product [9]. In another

study [73], also involving the oxidation of *n*-octane, VMgO was used as a catalyst with vanadium loadings of 5, 15, 25 and 50 wt% over MgO. The 15 wt% V on MgO showed the highest selectivity to 1-octene among the octene isomers, however, for the other weight loadings of V, the dominant isomer was 2-octene. Vanadium pentoxide supported over hydroxyapatite was also used as a catalyst for the activation of *n*-octane. Two main phases were observed at higher loadings, namely vanadium pentoxide and the pyrovanadate phase. It was concluded that the vanadium pentoxide phase was responsible for the formation of octenes at lower loadings, while the pyrovanadate phase that existed at higher loadings was responsible for the formation of aromatics [74]. Further to this study, the different octenes were fed to the reactor to study the activation and cyclisation mechanism of octenes to various products (aromatics, oxygenates, cracked and CO_x). The study was carried out using different hydroxyapatites incorporating Ba, Mg, Sr and Ca. The alkaline earth hydroxyapatites were further used as supports to impregnate 2.5 wt% and 10 wt% vanadium. When the 1-octene was fed over the catalyst, the 2.5 wt% vanadium pentoxide supported over Sr-Hap gave greater than 50% selectivity towards C₈ products (aromatics and oxygenates) at a conversion of 27%. The effect of hydrocarbon to oxygen ratio was also investigated on these prepared catalysts. The lowest oxygen ratio favoured the formation of aromatics and oxygenates, while the higher oxygen ratios favoured the formation of CO_x [75]. Recently, ceria based catalysts were studied for *n*-octane oxidation with cobalt substitution in the ceria lattice giving good yields towards value added products such as octenes, aromatics and C₈ oxygenates, with low selectivity toward CO_x [76].

In summary, the ODH of alkanes is an important route to produce alkenes with some advantages and disadvantages. The major disadvantage of the ODH route is the fact that products are more reactive than the starting material, which often leads to the formation of significant amounts of CO_x. Different catalytic systems have been developed and tested to achieve high yields of ODH products and subsequently suppress the production of CO_x. However, it is important to mention that the nature of the reaction becomes more complex with an increase in the carbon number. As the carbon number increases, so do the side reactions, which results in lowering the yields of the ODH products. The complexity of the reaction can be reduced by altering parameters such as oxygen source, different species of the active metal, different supports and obviously the reaction parameters, such as contact time, GHSV and oxygen concentration.

Extensive work has been carried out in the ODH of lower alkanes and it is still progressing with new and innovative ideas. In comparison, the chemistry behind the ODH of longer

chain alkanes is not well explored, although some attempts have been made to explore the ODH of *n*-hexane [6], *n*-heptane [71] and *n*-octane [9, 73-76]. With the *n*-octane ODH studies, the catalysts used were mainly V based, however, in the case of lower alkane ODH, most of these catalysts are V or Mo based catalysts. The different V based catalysts have been well established for the ODH of *n*-octane, however, Mo based catalytic systems still remain to be investigated further.

1.2 Catalytic Systems

1.2.1 MoO₃ and MoO_x supported catalysts

MoO₃ is extensively studied for oxidation reactions due to its ability to undergo reduction by oxidising the substrate. MoO₃ exists mainly in two phases, α - and β -MoO₃. The α -MoO₃ phase is thermodynamically stable with tetrahedral geometry (Fig. 1.2A) and exists between 20 and 600 °C. β -MoO₃ is a metastable phase possessing an octahedral geometry (Fig. 1.2B) and only exists up to 300 °C. Further heating of this phase will result in the formation of the thermodynamically stable α -phase [77]. β -MoO₃ has a surface area at least 1.5 times greater than α -MoO₃ as a result of the difference in geometry. However, use of the β -MoO₃ phase is limited to lower temperatures due to its phase change.

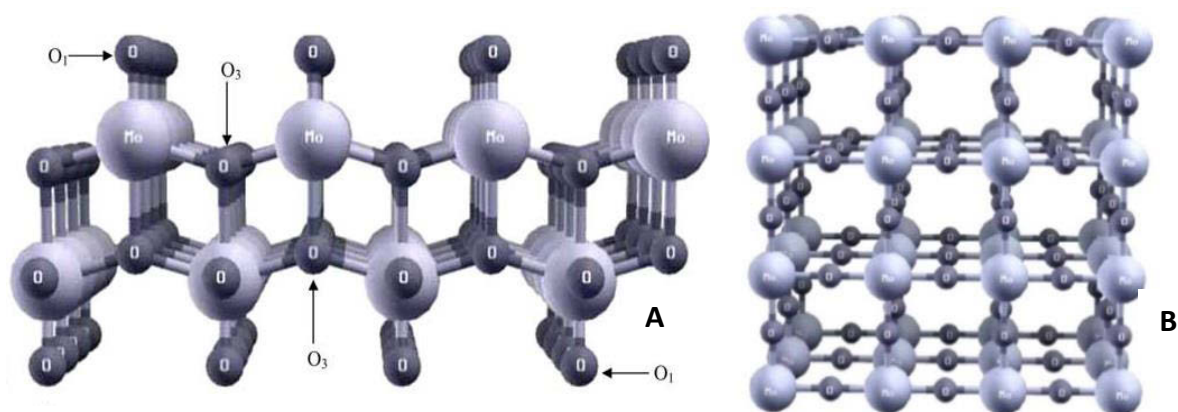
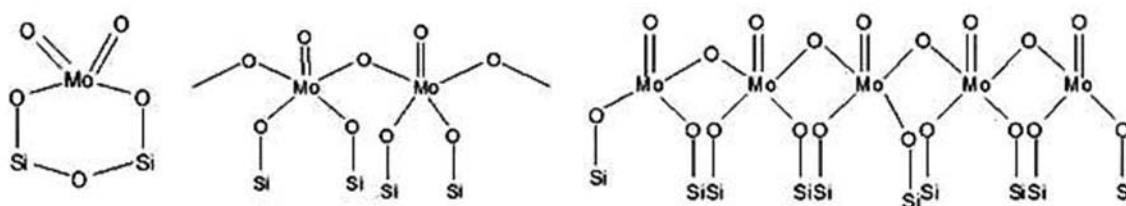


Figure 1.3 Crystal structures of (A) α -MoO₃ and (B) β -MoO₃ [78] (Redrawn with permission from Elsevier Copyright © 2014).

The catalytic oxidation of methanol to formaldehyde was carried out over α -MoO₃ where moderate yields towards formaldehyde was achieved, whereas with the β -MoO₃, a higher yield (22%) was achieved at 250 °C [77]. Alkane oxidation generally takes place between

300-450 °C and at this high temperature range, β -MoO₃ changes to α -MoO₃. Therefore, most of the work reported in literature focuses mainly on the α -MoO₃ phase. Redox studies of the α -MoO₃ were also investigated in order to understand the reduction and oxidation behaviour of the catalyst. Under reducing conditions, MoO₃ undergoes reduction to MoO₂ due to the stripping of lattice oxygen via the sub-oxide formation [79]. The sub-oxides observed during the reduction of MoO₃ were Mo₁₈O₅₂, Mo₁₇O₄₇, Mo₉O₂₆, Mo₈O₂₃ and Mo₅O₁₄ [80, 81]. The formation of the sub-oxides are temperature dependent and they only form at temperatures > 450 °C [80]. At temperatures < 450 °C, a single step reduction of MoO₃ to MoO₂ was reported [80]. The formation of this sub-oxide was proved by using advanced techniques such as XAS and XAFS. Propane oxidation was also carried out using MoO₃ and Ga₂O₃ and a physical mixture of both oxides. Results indicated that the activation ability of the catalyst is mainly due to Ga₂O₃, while the selectivity to the desired product is due to MoO₃ [60]. Since MoO₃ was found to be selective and not active, it was necessary to activate it, either by adding additional metal centres to produce metal molybdates or fixing it on an active support. The resultant catalysts showed far better performance towards the activation of lower alkanes [17, 18].

Various supports such as ZrO₂, Al₂O₃, TiO₂ and SiO₂ were used to improve the conversion as well as the selectivity to ODH products [18, 82-84]. Smith *et al.* [85] showed that when (NH₄)₆Mo₇O₂₄·H₂O, is impregnated on SiO₂ at different pH, it forms different species over the support. At a pH between 7 and 12, MoO₄²⁻ forms, whereas at a pH between 3 and 6 and below 2, Mo₈O₂₆⁶⁻ and Mo₇O₂₄⁶⁻ form respectively [86]. Generally, the wet impregnation method employed for the catalyst preparation leads to the formation of Mo₇O₂₄⁶⁻ over the support. The Mo species formed also depends upon the weight loadings of molybdenum oxide over the support. With SiO₂, generally at lower loadings, monomeric MoO_x species are observed, whereas, with an increase in the weight loadings, polymeric MoO_x species form. With loadings greater than 15 wt%, the crystalline MoO₃ phase over the support is formed [18]. The structure of monomeric, dimeric, and polymeric MoO_x species are shown in Figure 1.4.



Monomeric MoO_x

(pH =7-12)

Dimeric MoO_x

(pH=3-6)

Polymeric MoO_x

Figure 1.4 MoO_x structures observed over SiO₂ at different pH values [87].

The species present over the surface of the catalyst varies with the support employed. In the case of ZrO₂, only polymeric species exist [82], but with silica, the presence of three types of species, as shown in Figure 1.4, are evident [87]. Raman spectroscopy is an important tool for the identification of the different species of molybdenum, as this technique is very sensitive and gives unique and accurate information about the environment around the Mo species. The monomeric MoO_x species possesses a M=O stretch at ~970 cm⁻¹ [18]. The presence of the Mo-O-Mo bridging in the polymeric and dimeric MoO_x species can be confirmed by the appearance of the peak at ~820 cm⁻¹, which corresponds to the asymmetric stretch of bridging oxygen, whereas the symmetric stretch can be observed at 666 cm⁻¹ [77]. The crystalline MoO₃ species possesses strong peaks for MoO₃ at 991, 820 and 666 cm⁻¹. However, due to the high dispersion of molybdenum oxide over the support, the XRD peaks responsible for the monomeric MoO_x species cannot be seen, but as it reaches monolayer coverage, the formation of polymeric MoO_x species occurs on the surface of the support and displays the characteristic peaks for the molybdenum oxide.

MoO₃ supported over ZrO₂ catalysts were used for propane ODH studies [82]. XRD characterisation of the ZrO₂ alone displayed the existence of monoclinic and tetragonal phases. However, with the addition of MoO_x, the ZrO₂ showed a higher proportion of the tetragonal phase than the monoclinic phase. The presence of polymeric and crystalline MoO_x species was verified by Raman spectroscopy. It was showed that the propane ODH rates are strongly dependant on the species present on the support. The rates decreased with increasing molybdenum loadings and were due to the decreasing accessibility of the Mo-O species, since the molybdenum domain size increased with increasing molybdenum content, this was also reflected in the vibrational energy of M=O in Raman spectra, which found

increased with an increasing molybdenum loadings.. The apparent decrease in the catalytic activity was attributed to the formation of two dimensional polymolybdate species and three dimensional MoO_x crystallites over the support. It was concluded that the presence of the polymolybdates species is very important in order to achieve high catalytic activity [82].

The effect of alkali dopants such as Li, K and Cs was also investigated over a $\text{MoO}_x/\text{ZrO}_2$ catalyst for ODH of propane. However, the doped catalysts showed a decrease in activity as the addition of these dopants caused a decrease in the reducibility of the Mo species [88]. In another study carried out by the same authors using a MoO_x supported Al_2O_3 catalyst for the ODH of propane, a decrease in the rates of propane consumption was noted over the $\text{MoO}_x/\text{Al}_2\text{O}_3$ catalysts with increase in the domain size of MoO_x species. The species found in this case, at lower and moderate Mo loadings, were 2D oligomeric MoO_x species, whilst at higher loadings, MoO_3 crystallites were observed [83, 89]. The propane consumption rates increased with an increase in the two dimensional domain sizes; however, a decrease was noted with the crystalline MoO_3 species.

$\text{MoO}_3/\text{SiO}_2$ catalysts were studied for the oxidation of methane to formaldehyde. It was observed that the catalysts with lower loadings provided acceptable yields towards formaldehyde, whereas CO and CO_2 formed predominantly when catalysts with higher loadings were used. [85, 90].

1.2.2 Supported NiMoO_4 and NiMoO_4 catalysts

In the oxidation of alkanes, MoO_3 was found to be selective but not very active; therefore, an additional metal centre was required to increase the activity. Metal molybdates have considerable importance in the activation of lower alkanes due to their activity and selectivity to the desired products. Molybdates belong to the group of minerals consisting of a molybdate anion and a metal ion centre [91]. The minerals of this class exist as two iso-structural groups, viz. scheelites and wolframites. The scheelite structure forms under normal conditions, whereas the wolframites form under high pressure [92].

NiMoO_4 belongs to the AMoO_4 group, where A is a divalent cationic metal centre with a coordination number of eight, while the molybdenum is tetrahedrally co-ordinated to oxygen. NiMoO_4 exists in two phases, namely α - NiMoO_4 and β - NiMoO_4 , where α - NiMoO_4 is the thermodynamically stable phase at room temperature. This phase converts to β - NiMoO_4 when heated to 720 °C and remains stable when cooled to 200 °C. When the temperature is decreased to below 200 °C, it reverts to α - NiMoO_4 [93]. These transitions from the α - to β -

and β - to α -phases were validated by Kaddouri *et al.* [94] employing DTA. Figure 1.5 shows the two transitions of NiMoO_4 , where the endotherm shows conversion of the α -phase to β -phase at 720 °C, whereas the exotherm shows the transition of the β -phase to the α -phase below 200 °C.

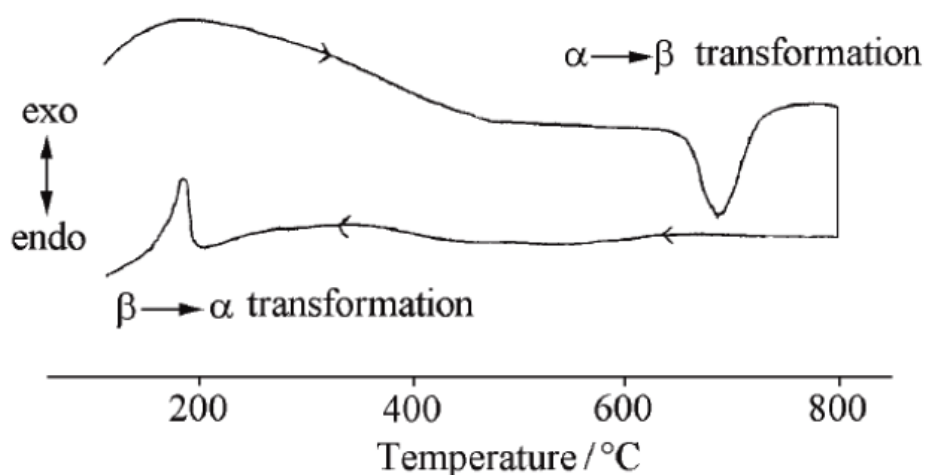


Figure 1.5 DTA cycle of stoichiometric NiMoO_4 phase transitions [94]. (Redrawn with permission from Springer Copyright © 2014))

The α - NiMoO_4 crystallizes in a $C2/m$ monoclinic space group in which the Ni and Mo ions are localized in the oxygen octahedral chains parallel to the $C2$ axis as shown in Figure 1.6.

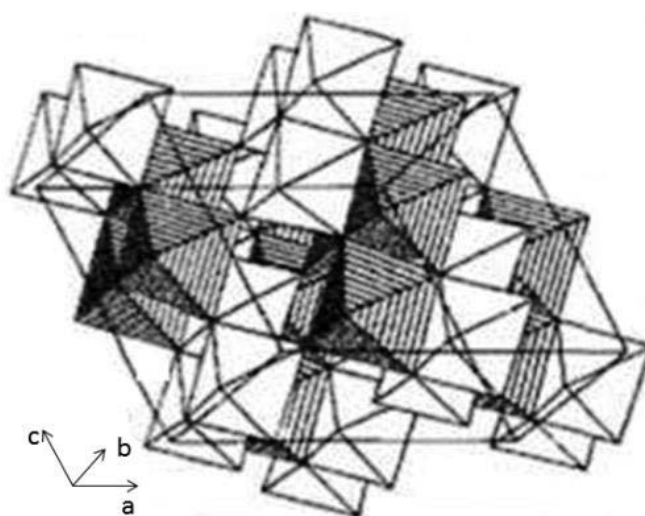


Figure 1.6 Arrangement of the oxygen octahedral in α - NiMoO_4 . The octahedral containing Ni (Mo) ions are shaded by line [95]. (Redrawn with permission from Elsevier Copyright © 2014)

The synthesis of NiMoO₄ is complex, as various factors simultaneously play roles in its formation. Generally, the co-precipitation method is used to synthesise NiMoO₄ [14]. Several factors need to be considered during the preparation of NiMoO₄, viz. pH, chemical phase and composition, aging time, temperature of preparation and filtration [6, 14]. Altering the specific conditions could lead to formation of a range of minerals with the general formula $x\text{NiO } y\text{MoO}_3 \cdot n\text{H}_2\text{O } m\text{NH}_3$ [6, 96]. When stoichiometric amounts of Ni and Mo salt solutions are mixed at a pH of 5.6, followed by heating of the solution at 85 °C, a solid precipitate forms. Hot filtration, followed by drying at 120 °C for 5 h and calcination of the powder at 550 °C, yields NiMoO₄ as a yellow powder.

In a study of propane oxidation with various metal molybdates, high selectivity to propene was observed at lower temperatures, whereas increased temperatures resulted in increased CO_x formation. The activity of the catalyst depends on the metal centre used. From all the catalysts prepared, it was shown that NiMoO₄ was the most active catalyst for propane ODH. It was also noted that the catalysts prepared to give Sr, Mg, Ca, Ba, La, Zn and Sm molybdates were highly selective, but gave poor conversions. On the other hand, molybdates prepared using Al and Cr were more active catalysts, but still showed lower conversion than NiMoO₄. However, they were not selective towards propene [17].

Metal molybdates generally exist in stoichiometric ratio of the metal to molybdenum but a slight excess of the MoO₃ was shown to improve the catalytic performance of both NiMoO₄ and CoMoO₄, due to a synergistic effect exerted by the metal oxide phases [97, 98]. The metal oxide phases, when tested separately, displayed low activities. Pure NiMoO₄ exhibited high selectivity to butadiene from 1-butene, due to the Ni-O-Mo sites [99]. During the synthesis, a slight excess of molybdenum resulted in formation of MoO₃ after calcination. An excess of MoO₃ was shown to be beneficial in the oxidation of propene to produce acrylic acid with good yields. This activity was credited to excess MoO₃ as it increased the superficial acidity and thus allowed product formation. β-NiMoO₄ is active in the oxidation of propene to acrylic acid, and it also oxidises acrolein to acrylic acid. However, α-NiMoO₄ was not active for such transformations [100]. Although the addition of MoO₃ was responsible for activating alkane molecules, the performance was totally dependent on the preparation conditions as physical mixtures will have different properties than catalysts prepared by the co-precipitation method [101].

For propane and isobutane oxidation with NiMoO₄ catalysts, K, Ca, and P were used as promoters. These promoters showed an increase in the formation of propene, however, for isobutane oxidation, only the K promoted catalyst showed high selectivity to isobutene [102]. Generally, metal oxides and metal molybdates are used independently as catalysts. However, with supported catalysts, improvement in the catalytic activity can be observed and it also eliminates some of the problems associated with bulk phases. These catalysts help to remove the heat of reaction from the active sites and thus stabilize the desired phase [103].

When NiMoO₄ was precipitated over SiO₂, stabilisation of small amounts of the high temperature β-NiMoO₄ phase at room temperature was observed along with the presence of the α-NiMoO₄ phase. This catalyst showed better catalytic activity than bulk β-NiMoO₄ which was stabilized by an excess of NiO [103]. There are also reports for the synthesis of the NiMoO₄ by the sol-gel method in which the catalysts were prepared by using different silica sources which showed increased selectivity towards isobutene [104]. Zavoianu *et al.* [105] studied the catalytic activity of NiMoO₄ and NiMoO₄/TiO₂ for isobutane ODH. The results of this study showed that the TiO₂ support also stabilises the β-NiMoO₄ phase at room temperature. The catalytic testing of these catalysts revealed that the supported catalysts exhibited different products when compared to the bulk product profile, however, lower CO_x and improved selectivity to the isobutene was observed with the supported catalysts.

Pillay *et al.* [106] claimed that higher selectivity to hexene can be obtained over β-NiMoO₄ than α-NiMoO₄. In this study, reaction parameters such as contact time and feed concentration were varied to get the optimum condition to produce hexenes. The 1-hexene selectivity reported in this work was 27.4%, which was higher than the selectivity of the thermodynamically more stable isomer, viz. *trans* 2-hexene (25%). Although both phases of NiMoO₄ are active and selective for the ODH of lower alkanes, they differ significantly in terms of activity and selectivity. The α-phase is active and selective towards olefins as well as CO_x, whereas the β-NiMoO₄ phase is less active but more selective to olefins. However, both the bulk phases possess a common disadvantage, which is coking. The coking of the catalysts could be overcome by supporting these active phases over a suitable support. Supporting these phases improves their surface area, removes heat rapidly from the active site of the catalyst and stabilises the desired phase [103]. Mesoporous silica provides an alternative support, since it possesses a definite structure and higher surface area than the traditional supports such as SiO₂, ZrO₂, Al₂O₃ and TiO₂. For oxidative transformations, a support that has been used to great effect is SBA-15, which has numerous other applications in the field of catalysis, separation technologies, electronic engineering and optical devices

[107]. The versatile nature of the support was the basis of further investigation for *n*-octane oxidation.

1.2.3 SBA-15

The synthesis of mesoporous material was first reported in 1970 and later patented. In early 90's Japanese scientists and Mobil's scientists separately reported synthesis of mesoporous silica materials, named M41S mesoporous silicate. However, these materials were synthesized using cationic type surfactants, which are known to be toxic and expensive. In 1998 Zao *et al.* discovered the synthesis of SBA-15 using non-ionic co-block polymer. This synthetic method became popular in recent years because the surfactants are biodegradable, cheap and non-toxic compared to the method reported previously. SBA-15 has been used as a catalyst support due to promising features such as high surface area $\sim 700 \text{ m}^2/\text{g}$ and tunable pore diameter (6 to 30 nm). In addition, it possesses thicker silica walls and has relatively high hydrothermal stability [108]. A TEM image of SBA-15 and its mesopore structure is shown in Figure 1.7.

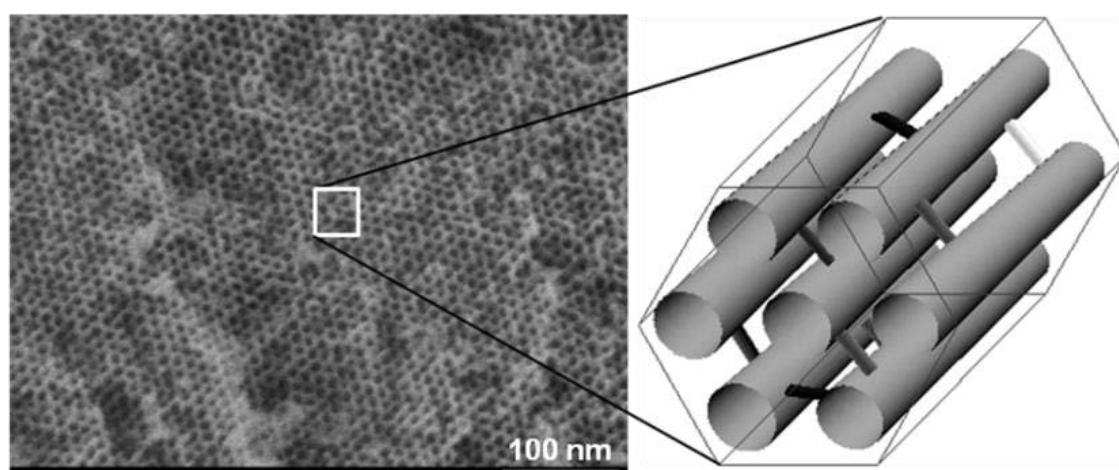


Figure 1.7 TEM image and pore structure of SBA-15 [109]. (Redrawn with permission of author © 2014)

SBA-15 was first synthesized by Zhao and co-workers [110] in 1998. SBA-15 possesses well-ordered 2D hexagonal mesoporous channels with uniform pore sizes up to approximately 300 \AA (30 nm). Recently, Cao *et al.* [111] showed that it is possible to tune the pore size of SBA-15 from 3-30 nm by using different micelle expanders such as 1, 3, 5-trimethyl benzene tri-iso propyl benzene (TIPB), triethyl benzene (TEB) and alkanes (pentane to decane). TIPB was shown to be the best micelle expander resulting in a pore size of 26 nm. They also inferred that the pore size of the SBA-15 can be increased to 70 nm, but

this leads to the loss of the 2D hexagonal ordering. Supported SBA-15 catalysts were found to be useful in hydrodesulphurisation [112-115], epoxidation [116], FT synthesis [117], biodiesel production [118] and methane reforming [119].

The MoO_x/SBA-15 catalyst was used to activate methane to formaldehyde where different weight loadings of molybdenum oxide and the kinetics associated with these reactions were studied by Lou *et al.* [120]. It was shown that the isolated MoO_x species were less reactive than the polymeric MoO_x species. At lower MoO₃ loadings, isolated (mono-oxo or di-oxo) species formed on the support and an increase in MoO₃ loading resulted in the formation of polymeric MoO_x species. It was concluded that the oxidation of methane over monomeric MoO_x species follows first order reaction kinetics, whereas the polymeric MoO_x species follow higher order reaction kinetics. The 20 wt% MoO_x/SBA-15 gave a formaldehyde yield of 1.4% at 500 °C. In addition, vanadium oxide was added to obtain Mo-V-O to the 20 wt% MoO_x/SBA-15, but the resultant catalyst gave lower yields (1%) towards formaldehyde. Further, it was concluded that a higher activity of the polymeric species was due to Mo species surrounding the active molybdenum centre, which shows that the relationship between the adjacent Mo centres is one of the key factors in controlling the activity.

Lou *et al.* [18] also studied the activation of ethane by using different weight loadings of MoO_x on SBA-15. At lower weight loadings, i.e. at 2.9 and 4.7 wt%, molybdenum oxide existed as isolated monomeric MoO_x species, whereas with higher molybdenum loadings, i.e. 7, 10, 15 and 20 wt%, it existed as polymeric MoO_x species and crystalline MoO_x species. The isolated MoO_x species were less reactive than polymeric MoO_x species and favoured the formation of acetaldehyde, whereas formaldehyde was formed over polymeric MoO_x species. The lower selectivity to acetaldehyde and high selectivity to formaldehyde was due to the consecutive oxidation of the acetaldehyde over higher weight loadings of molybdenum.

Ethane oxidation was carried out with a framework which incorporated Mo-SBA-15 and a K doped Mo-SBA-15 [121]. In this study, the structural regularity of the mesoporous material decreased with an increase in molybdenum loading, with the maximum being 12 wt% of molybdenum. Further increase in the molybdenum content resulted in the destruction of the mesopore ordering. Upon addition of 0.05 % K to Mo-SBA-15, an increase in the selectivity towards acetaldehyde was observed, giving a yield of 10 %.

The research conducted by Orlov *et al.* [124], who investigated the oxidation of propene using MnO₂ supported on SBA-15 as catalysts, showed that the use of different metal precursors for the preparation of the catalysts affected the activity of the final catalyst. When Mn₂(CO)₁₀ was the precursor for the oxide phase, a conversion of 94% of propene was

obtained, compared to a 57% propene conversion using $\text{Mn}(\text{OAc})_2$ as the precursor. This high conversion of propane was attributed to the higher Mn content in the $\text{Mn}_2(\text{CO})_{10}$ [122]. Zhang *et al.* [123] reported on the ODH of propane using chromium oxide supported on SBA-15 in non-oxidative and oxidative systems. The catalysts used in this study were $\text{Cr}_2\text{O}_3/\text{ZrO}_2$, $\text{Cr}_2\text{O}_3/\gamma\text{-Al}_2\text{O}_3$, and $\text{Cr}_2\text{O}_3/\text{SBA-15}$. Modification of the support was also carried out by introducing zirconia during the synthesis to prepare a $\text{Cr}_2\text{O}_3\text{-ZrO}_2/\text{SBA-15}$ catalyst. In the non-oxidative study, the $\text{Cr}_2\text{O}_3\text{-ZrO}_2/\text{SBA-15}$ was shown to be the most selective system (98% to propene) and most resistant to coking compared to the other two catalysts, whereas in oxidative dehydrogenation, $\text{Cr}_2\text{O}_3/\text{SBA-15}$ displayed lower CO_x selectivity (85%) compared to $\text{Cr}_2\text{O}_3/\text{ZrO}_2$ and $\text{Cr}_2\text{O}_3/\gamma\text{-Al}_2\text{O}_3$, which gave selectivities greater than 90%. When CO_2 was used as the oxidant a considerable drop in CO_x selectivity was observed. The most active catalyst was again $\text{Cr}_2\text{O}_3/\text{SBA-15}$ with 85% propene selectivity and 10% selectivity to CO_x , the rest of the products being cracked products.

A comparative study of the partial oxidation of *n*-butane and *n*-propane over VPO supported on SiO_2 , MCM-41 and SBA-15 was undertaken by Li *et al.* [124]. They found that MCM-41 and SBA-15 gave a high degree of VPO dispersion due to the high surface area of these materials compared to SiO_2 . However, for *n*-butane oxidation, the 45 wt% VPO/ SiO_2 catalyst produced significantly more maleic anhydride compared to VPO supported on MCM-41 or SBA-15. These results were attributed to the lattice oxygen reactivity and structural disorder of the VPO component in fumed SiO_2 , creating more lattice defects that resulted in the higher activity. In the case of propane, the 45 wt% VPO/SBA-15 catalyst again showed the highest activity, but it was less selective to acrylic acid than VPO supported on SiO_2 and MCM-41 [43].

Huang *et al.* [125] studied Pt-Sn/SBA-15 and Pt-Sn/ $\text{Al}_2\text{O}_3\text{-SBA-15}$ catalysts for propane dehydrogenation. In this study, the activity of the catalyst for propane dehydrogenation was correlated with the H_2 uptake by the catalysts. In terms of catalytic activity, the Pt-Sn supported on $\text{Al}_2\text{O}_3\text{-SBA-15}$ exhibited higher activity compared to a Pt-Sn/SBA-15. The decreased activity of Pt-Sn/SBA-15 was claimed to be due to the formation of a Pt-Sn alloy on the surface of SBA-15. However, the modification of the Pt-Sn/SBA-15 with alumina was claimed to enhance the interaction between Sn and SBA-15 and thus giving high propane dehydrogenation activity.

Reddy *et al.* [126] investigated the oxidation of cyclohexane to cyclohexanone and cyclohexanol using cobalt supported on SBA-15. A 9.4% conversion and 78% selectivity towards cyclohexanone was obtained. Recently, Mishra *et al.* [127] developed a catalyst for

the oxidation of *n*-pentane and *n*-hexanes. Rhenium was grafted over SBA-15 by using surface modification by reacting with a rhenium complex. High selectivity toward oxygenates were observed for both the alkanes. The C₅ products were pentane 2-one and pentane 2-ol and the C₆ products were hexane 2-one and hexane 2-ol with selectivities greater than 90%. A small amount of C₅ and C₆ acids was also reported to have formed.

1.3 Objective of this study

MoO₃, being an important metal oxide has been used for the oxidation of lower alkanes either in bulk form, supported, or in the form of mixed metal oxides. Their application for the oxidation of higher alkanes has not been reported extensively. Its use as a catalyst for *n*-octane oxidation is being reported for the first time. From the various studies, MoO₃ itself was shown to be less active, thus it was always used with an additional metal centre such as with metal molybdate or supported over an active support such as alumina, zirconia or silica. SBA-15, which is a high surface area material was found useful for the oxidation of alkanes using molybdenum, chromium and tin. In addition to the above, enhancement of the catalytic activity of MoO₃ will be studied by the addition of Ni as an active metal centre. Thus the aims of this study include,

- The catalytic activity of MoO₃ being evaluated under different strength of the oxidising environment in the presence of *n*-octane.
- The effect of different species of molybdenum on the catalytic activity will also be studied by supporting MoO_x on SBA-15.
- The catalytic activity of NiMoO₄ will be studied in oxygen lean and rich environment for oxidative dehydrogenation. In addition, the effect of the different bulk and supported α and β phases on the product profile will also be investigated.

References

- [1] http://www.chemweek.com/lab/Outlook-2014-Looking-forward_57898.html. (Date of Access 9th Oct. 2014).
- [2] T. Ren, M. Patel, K. Blok, *Energy*. 31 (2006) 425-451.
- [3] G. Franz, R.A. Sheldon, *Ullmann's Encyclopedia of Industrial Chemistry*, Wiley-VCH Verlag GmbH & Co. KGaA, 2000.
- [4] R.K. Grasselli, *Catal. Today*. 49 (1999) 141-153.
- [5] B.K. Hodnett, *Heterogeneous Catalytic Oxidation: Fundamental and Technological Aspects of the Selective and Total Oxidation of Organic Compounds*, John Wiley & Sons, Inc., 2000.
- [6] H.B. Friedrich, N. Govender, M.R. Mathebula, *Appl. Catal. A: Gen.* 297 (2006) 81-89.
- [7] H.B. Friedrich, A.S. Mahomed, *Appl. Catal. A: Gen.* 347 (2008) 11-22.
- [8] T. Komatsu, H. Ishihara, Y. Fukui, T. Yashima, *Appl. Catal. A: Gen.* 214 (2001) 103-109.
- [9] B. Pillay, Ph D Thesis, University of KwaZulu Natal (2009).
- [10] S. Pradhan, J.K. Bartley, D. Bethell, A.F. Carley, M. Conte, S. Golunski, M.P. House, R.L. Jenkins, R. Lloyd, G.J. Hutchings, *Nat. Chem.* 4 (2012) 134-139.
- [11] R. Schlögl, *Modern Heterogeneous Oxidation Catalysis*, Wiley-VCH Verlag GmbH & Co. KGaA, 2009, pp. 1-42.
- [12] T. Punniyamurthy, S. Velusamy, J. Iqbal, *Chem. Rev.* 105 (2005) 2329-2364.
- [13] G. Centi, F. Cavani, F. Trifiro, Editors, *Selective Oxidation by Heterogeneous Catalysis*, Kluwer/Plenum Publ, 2001.
- [14] L.M. Madeira, M.F. Portela, *Catal. Rev.* 44 (2002) 247-286.
- [15] A. Burri, N. Jiang, M. Ji, S.-E. Park, Y. Khalid, *Top. Catal.* 56 (2013) 1724-1730.
- [16] G.K. Borekov, in: J. Anderson, M. Boudart (Eds.), *Catalysis*, Springer Berlin Heidelberg, 1982, pp. 39-137.
- [17] Y. Lou, H. Wang, Q. Zhang, Y. Wang, *J. Catal.* 247 (2007) 245-255.
- [18] Y.S. Yoon, N. Fujikawa, W. Ueda, Y. Moro-oka, K.W. Lee, *Catal. Today*. 24 (1995) 327-333.
- [19] R. Burch, E.M. Crabb, *Appl. Catal. A: Gen.* 97 (1993) 49-65.
- [20] R. Burch, E.M. Crabb, *Appl. Catal. A: Gen.* 100 (1993) 111-130.
- [21] A.A. Lemonidou, A.E. Stambouli, *Appl. Catal. A: Gen.* 171 (1998) 325-332.

- [22] T.Y. Stoylkova, C.D. Chanev, H.T. Lechert, C.P. Bezouhanova, *Appl. Catal. A: Gen.* 203 (2000) 121-126.
- [23] A. Parmalianal, V. Sokolovskii, M.S. Scurrrell, D. Miceli, F. Arena, F. Frusteri, in: H.E. Curry-Hyde, R.F. Howe (Eds.), *Stud. Surf. Sci. Catal.*, Elsevier, 1994, pp. 491-496.
- [24] E.M. Thorsteinson, T.P. Wilson, F.G. Young, P.H. Kasai, *J. Catal.* 52 (1978) 116-132.
- [25] M. Roy, H. Ponceblanc, J.C. Volta, *Top. Catal.* 11-12 (2000) 101-109.
- [26] L. Tessier, E. Bordes, M. Gubelmann-Bonneau, *Catal. Today.* 24 (1995) 335-340.
- [27] D.I. Enache, E. Bordes-Richard, A. Ensuque, F. Bozon-Verduraz, *Appl. Catal. A: Gen.* 278 (2004) 93-102.
- [28] J.M.L. Nieto, P. Botella, M.I. Vazquez, A. Dejoz, *Chem. Comm.* (2002) 1906-1907.
- [29] C.R. Adams, T.J. Jennings, *J. Catal.* 3 (1964) 549-558.
- [30] M. Allen, R. Betteley, M. Bowker, G.J. Hutchings, *Catal. Today.* 9 (1991) 97-104.
- [31] M.M. Bettahar, G. Costentin, L. Savary, J.C. Lavalley, *Appl. Catal. A: Gen.* 145 (1996) 1-48.
- [32] M. Ai, *Catal. Today.* 13 (1992) 679-684.
- [33] G. Landi, L. Lisi, J.C. Volta, *J. Mol. Catal. A: Chem.* 222 (2004) 175-181.
- [34] Y. Takita, H. Yamashita, K. Moritaka, *Chem. Lett.* 18 (1989) 1733-1736.
- [35] Y.C. Kim, W. Ueda, Y. Moro-ok, *Catal. Today.* 13 (1992) 673-678.
- [36] W. Ueda, K. Oshihara, *Appl. Catal. A: Gen.* 200 (2000) 135-143.
- [37] T. Ushikubo, H. Nakamura, Y. Koyasu, S. Wajiki, Mitsubishi Kasei Corp., Japan . 1994, p. 9.
- [38] M.M. Lin, *Appl. Catal. A: Gen.* 207 (2001) 1-16.
- [39] W.W. Z. Wang, G. Liu, G. Mao, D. Kuang, *Acta. Petrol. Sin.* 14 (1998) 21.
- [40] Y.H. H. Cheng, H. Wang, *Shiyu Huagong (chinese).* 28 (1999) 803.
- [41] O. Ovsitser, R. Schomaecker, E.V. Kondratenko, T. Wolfram, A. Trunschke, *Catal. Today.* 192 (2012) 16-19.
- [42] N. Ballarini, F. Cavani, C. Cortelli, S. Ligi, F. Pierelli, F. Trifirò, C. Fumagalli, G. Mazzoni, T. Monti, *Top. Catal.* 38 (2006) 147-156.
- [43] X.-K. Li, W.-J. Ji, J. Zhao, Z. Zhang, C.-T. Au, *Appl. Catal. A: Gen.* 306 (2006) 8-16.
- [44] B. Solsona, F. Ivars, P. Concepción, J.M. López Nieto, *J. Catal.* 250 (2007) 128-138.
- [45] V.A. Zazhigalov, J. Haber, J. Stoch, E.V. Cheburakova, *Catal. Comm.* 2 (2001) 375-378.
- [46] S. Singh, S. Jonnalagadda, *Catal. Lett.* 126 (2008) 200-206.

- [47] M. G. Clerici, *Appl. Catal.* 68 (1991) 249-261.
- [48] T. Tatsumi, K. Asano, K. Yanagisawa, in: J. Weitkamp, W. Hölderich (Eds.), *Stud. Surf. Sci. Catal.*, Elsevier, 1994, pp. 1861-1868.
- [49] M.A. Uguina, G. Ovejero, R. Van Grieken, D.P. Serrano, M. Camacho, *Chemical Communications* (1994) 27-28.
- [50] I. Halasz, M. Agarwal, E. Senderov, B. Marcus, *Appl. Catal. A: Gen.* 241 (2003) 167-184.
- [51] A.V. Ramaswamy, S. Sivasanker, *Catal. Lett.* 22 (1993) 239-249.
- [52] C. Boyadjian, B. van der Veer, I.V. Babich, L. Lefferts, K. Seshan, *Catal. Today.* 157 (2010) 345-350.
- [53] M.M. Bhasin, J.H. McCain, B.V. Vora, T. Imai, P.R. Pujadó, *Appl. Catal. A: Gen.* 221 (2001) 397-419.
- [54] B.M. Weckhuysen, R.A. Schoonheydt, *Catal. Today.* 51 (1999) 223-232.
- [55] F.E. Frey, W.F. Huppke, *Ind. Eng. Chem.* 25 (1933) 54-59.
- [56] N. Haddad, E. Bordes-Richard, A. Barama, *Catal. Today.* 142 (2009) 215-219.
- [57] M.V. Martínez-Huerta, X. Gao, H. Tian, I.E. Wachs, J.L.G. Fierro, M.A. Bañares, *Catal. Today.* 118 (2006) 279-287.
- [58] G. Tsilomelekis, A. Christodoulakis, S. Boghosian, *Catal. Today.* 127 (2007) 139-147.
- [59] A. Erd"ohelyi, F. Máté, F. Solymosi, *J. Catal.* 135 (1992) 563-575.
- [60] T. Davies, S.H. Taylor, *J. Mol. Catal. A: Chem.* 220 (2004) 77-84.
- [61] T.V. Malleswara Rao, E. Vico-Ruiz, M.A. Bañares, G. Deo, *J. Catal.* 258 (2008) 324-333.
- [62] E.V. Kondratenko, M. Cherian, M. Baerns, D. Su, R. Schlögl, X. Wang, I.E. Wachs, *J. Catal.* 234 (2005) 131-142.
- [63] H. Zhang, S. Cao, Y. Zou, Y.-M. Wang, X. Zhou, Y. Shen, X. Zheng, *Catal. Comm.* 45 (2014) 158-161.
- [64] W. Liu, S. Lai, H. Dai, S. Wang, H. Sun, C. Au, *Catal. Lett.* 113 (2007) 147-154.
- [65] M. Setnička, R. Bulánek, L. Čapek, P. Čičmanec, *J. Mol. Catal. A: Chem.* 344 (2011) 1-10.
- [66] R. Bulánek, A. Kalužová, M. Setnička, A. Zukal, P. Čičmanec, J. Mayerová, *Catal. Today.* 179 (2012) 149-158.
- [67] G. Raju, B.M. Reddy, S.-E. Park, *J. CO₂ Util.* 5 (2014) 41-46.
- [68] S.A. Korili, P. Ruiz, B. Delmon, *Catal. Today.* 32 (1996) 229-235.

- [69] R.X. Valenzuela, J.M. Muñoz Asperilla, V.C.s. Corberán, *Ind. Eng. Chem. Res.* 47 (2008) 8037-8042.
- [70] B. Pillay, M.R. Mathebula, H.B. Friedrich, *Appl. Catal. A: Gen.* 361 (2009) 57-64.
- [71] V.B.C. Dasireddy, F. Khan, S. Singh, H. Friedrich, *Catal. Lett.* 144 (2014) 590-597.
- [72] K.K. Pant, D. Kunzru, *Ind. Eng. Chem. Res.* 36 (1997) 2059-2065.
- [73] E.A. Elkhalfa, H.B. Friedrich, *Appl. Catal. A: Gen.* 373 (2010) 122-131.
- [74] V.D.B.C. Dasireddy, S. Singh, H.B. Friedrich, *Appl. Catal. A: Gen.* 421-422 (2012) 58-69.
- [75] V.D.B.C. Dasireddy, S. Singh, H.B. Friedrich, *Appl. Catal. A: Gen.* 456 (2013) 105-117.
- [76] M. Narayanappa, V.D.B.C. Dasireddy, H.B. Friedrich, *Appl. Catal. A: Gen.* 447-448 (2012) 135-143.
- [77] T. Mizushima, K. Fukushima, H. Ohkita, N. Kakuta, *Appl. Catal. A: Gen.* 326 (2007) 106-112.
- [78] A.D. Sayede, T. Amriou, M. Pernisek, B. Khelifa, C. Mathieu, *Chem. Phys.* 316 (2005) 72-82.
- [79] E. Lalik, *Catal. Today.* 169 (2011) 85-92.
- [80] T. Ressler, J. Wienold, Rolf E. Jentoft, F. Girgsdies, *Eur. J. Inorg. Chem.* 2003 (2003) 301-312.
- [81] T. Ressler, J. Wienold, R.E. Jentoft, T. Neisius, *J. Catal.* 210 (2002) 67-83.
- [82] K. Chen, S. Xie, E. Iglesia, A.T. Bell, *J. Catal.* 189 (2000) 421-430.
- [83] K. Chen, S. Xie, A.T. Bell, E. Iglesia, *J. Catal.* 198 (2001) 232-242.
- [84] R. Grabowski, B. Grzybowska, K. Samson, J. Słoczyński, J. Stoch, K. Wcisło, *Appl. Catal. A: Gen.* 125 (1995) 129-144.
- [85] M.R. Smith, L. Zhang, S.A. Driscoll, U.S. Ozkan, *Catal. Lett.* 19 (1993) 1-15.
- [86] M.G. C. V. Krishnan, B. Hsiao and B. Chu, *Int. J. Electrochem. Sci.* 2 (2007) 29-51.
- [87] G. Mestl, T.K.K. Srinivasan, *Catal. Rev.* 40 (1998) 451-570.
- [88] K. Chen, S. Xie, A.T. Bell, E. Iglesia, *J. Catal.* 195 (2000) 244-252.
- [89] K. Chen, E. Iglesia, A.T. Bell, in: J.J.S. E. Iglesia, T.H. Fleisch (Eds.), *Stud. Surf. Sci. Catal.*, Elsevier, 2001, pp. 507-512.
- [90] K. Suzuki, T. Hayakawa, M. Shimizu, K. Takehira, *Catal. Lett.* 30 (1994) 159-169.
- [91] <http://www.oxforddictionaries.com/definition/english/molybdate>. (Date of Access 9th Oct. 2014).
- [92] A. Sleight, *Acta. Crystal. B* 28 (1972) 2899-2902.

- [93] I.I. L. M. Plyasova, M. M. Andrushkevich, R. A. Buyanov, I. S. Itenberg, G. A. Khramova, L. G. Karakchiev, G. N. Kustova, G. A. Stepanov, A. L. Tsailingol'd and F. S. Philipenko, *Kinet. Catal.* 14 (1973) 823.
- [94] A. Kaddouri, R. Del Rosso, C. Mazzocchia, D. Fumagalli, *J. Therm. Anal. Calorim.* 63 (2001) 267-277.
- [95] H. Ehrenberg, I. Svoboda, G. Wltschek, M. Wiesmann, F. Trouw, H. Weitzel, H. Fuess, *J Magn. Magn. Mater.* 150 (1995) 371-376.
- [96] A. Kaddouri, R. Del Rosso, C. Mazzocchia, P. Gronchi, D. Fumagalli, *J. Therm. Anal. Calorim.* 66 (2001) 63-78.
- [97] U. Ozkan, G.L. Schrader, *J. Catal.* 95 (1985) 120-136.
- [98] U. Ozkan, G.L. Schrader, *Appl. Catal.* 23 (1986) 327-338.
- [99] L.M. Madeira, M.F. Portela, C. Mazzocchia, *Catal. Rev.* 46 (2004) 53-110.
- [100] Fourth International Conference on the Chemistry and Uses of Molybdenum, August 9-13, 1982, Golden, Colorado, USA, Climax Molybdenum Co. Mich., 1982.
- [101] C. Mazzocchia, *Reactivity of solids*, 1985, pp. 1061-1066.
- [102] A. Kaddouri, C. Mazzocchia, E. Tempesti, *Appl. Catal. A: Gen.* 169 (1998) L3-L7.
- [103] D. Cauzzi, M. Deltratti, G. Predieri, A. Tiripicchio, A. Kaddouri, C. Mazzocchia, E. Tempesti, A. Armigliato, C. Vignali, *Appl. Catal. A: Gen.* 182 (1999) 125-135.
- [104] E. Tempesti, A. Kaddouri, C. Mazzocchia, *Appl. Catal. A: Gen.* 166 (1998) L259-L261.
- [105] R. Zăvoianu, C.R. Dias, M. Farinha Portela, *Catal. Comm.* 2 (2001) 37-42.
- [106] B. Pillay, M. Mathebula, H. Friedrich, *Catal. Lett.* 141 (2011) 1297-1304.
- [107] S. Che, K. Lund, T. Tatsumi, S. Iijima, S.H. Joo, R. Ryoo, O. Terasaki, *Angew. Chem. Int. Ed.* 42 (2003) 2182-2185.
- [108] Y. Wan, Zhao, *Chem. Rev.* 107 (2007) 2821-2860.
- [109] <http://nano.uib.no/abstracts/kleitz.html> (Date of Access 9th Oct. 2014).
- [110] D. Zhao, J. Feng, Q. Huo, N. Melosh, G.H. Fredrickson, B.F. Chmelka, G.D. Stucky, *Science.* 279 (1998) 548-552.
- [111] L. Cao, T. Man, M. Kruk, *Chem. Mater.* 21 (2009) 1144-1153.
- [112] O.Y. Gutiérrez, F. Pérez, G.A. Fuentes, X. Bokhimi, T. Klimova, *Catal. Today.* 130 (2008) 292-301.
- [113] T.E. Klimova, D. Valencia, J.A. Mendoza-Nieto, P. Hernández-Hipólito, *J. Catal.* 304 (2013) 29-46.

- [114] T. Klimova, J. Reyes, O. Gutiérrez, L. Lizama, *Appl. Catal. A: Gen.* 335 (2008) 159-171.
- [115] A. Soriano, P. Roquero, T. Klimova, in: E.M. Gaigneaux, P. Ruiz (Eds.), *Stud. Surf. Sci. Catal.*, Elsevier, 2010, pp. 525-528.
- [116] H. Cui, Y. Zhang, Z. Qiu, L. Zhao, Y. Zhu, *Appl. Catal. B: Env.* 101 (2010) 45-53.
- [117] J.J. Rodrigues, F.A.N. Fernandes, M.G.F. Rodrigues, *Appl. Catal. A: Gen.* 468 (2013) 32-37.
- [118] S.-Y. Chen, T. Mochizuki, Y. Abe, M. Toba, Y. Yoshimura, *Catal. Comm.* 41 (2013) 136-139.
- [119] Z.-J. Zuo, C.-F. Shen, P.-J. Tan, W. Huang, *Catal. Comm.* 41 (2013) 132-135.
- [120] Y. Lou, Q. Tang, H. Wang, B. Chia, Y. Wang, Y. Yang, *Appl. Catal. A: Gen.* 350 (2008) 118-125.
- [121] J. Liu, L. Yu, Z. Zhao, Y. Chen, P. Zhu, C. Wang, Y. Luo, C. Xu, A. Duan, G. Jiang, *J. Catal.* 285 (2012) 134-144.
- [122] A. Orlov, J. Klinowski, *Chemosphere.* 74 (2009) 344-348.
- [123] X. Zhang, Y. Yue, Z. Gao, *Catal. Lett.* 83 (2002) 19-25.
- [124] J.-H. Li, C.-C. Wang, C.-J. Huang, Y.-F. Sun, W.-Z. Weng, H.-L. Wan, *Appl. Catal. A: Gen.* 382 (2010) 99-105.
- [125] L. Huang, B. Xu, L. Yang, Y. Fan, *Catal. Comm.* 9 (2008) 2593-2597.
- [126] S. Sreevardhan Reddy, B. David Raju, A.H. Padmasri, P.K. Sai Prakash, K.S. Rama Rao, *Catal. Today.* 141 (2009) 61-65.
- [127] G.S. Mishra, K. Machado, A. Kumar, *J. Ind. Eng. Chem.* 20 (2014) 2228-2235.

Chapter 2

A Study of α -MoO₃ in oxidative and non-oxidative conditions under *n*-octane

Abstract

Molybdenum trioxide was synthesized and characterized by XRD, SEM, and TEM. The thermodynamically stable phase, the α -MoO₃ phase, was studied in the activation of *n*-octane by varying the oxygen concentration in the feed as a function of temperature. Carbon to oxygen ratios of 8:0, 8:1, and 8:2 were investigated over a temperature range of 350 to 550 °C at a GHSV of 4000 h⁻¹. The conversion of *n*-octane increased with an increase in temperature; however, it was more significant with higher oxygen concentrations in the feed due to the operating redox cycle between MoO₃ and Mo₄O₁₁. The α -MoO₃ reduces to Mo₄O₁₁ under oxygen lean conditions and finally to MoO₂ with feed containing no oxygen. In an oxygen rich environment, α -MoO₃ partially reduced to Mo₄O₁₁ but the presence of “excess” oxygen in the feed inhibits the further reduction of Mo₄O₁₁ to MoO₂ by oxidizing it back to MoO₃. For C:O ratios of 8:0 and 8:1, dehydrogenation of *n*-octane occurs by MoO₂, as well as by ODH via the lattice oxygen of MoO₃ to produce octenes, whereas at the higher C:O ratio, i.e. 8:2, at the same temperature, the dominant products were CO_x. Contributions from non-catalytic reactions of *n*-octane were also studied over a carborundum packed reactor tube using the same ratios of carbon and O₂. The blank reactions showed an increase in conversion with temperature especially at the higher C:O ratio.

Keywords: MoO₃, Mo₄O₁₁, MoO₂, *n*-octane, redox cycle.

2.1 Introduction

The selective oxidation of alkanes has established itself as an important area of research in the last few decades due to their abundance and relatively low value [1]. Many of these alkanes are products and by-products of numerous petrochemical plants, which are operating worldwide. The conversion of these alkanes to value added products, such as olefins, is important in the chemical and pharmaceutical industries [1]. In the activation of *n*-octane, previous work has

shown that *n*-octane can be oxidatively dehydrogenated to form octenes, followed by dehydrocyclization of the octenes to C8 aromatics [2-5].

One of the aims of the heterogeneous catalysis is to make the process cost efficient and environmentally friendly with lower by-products selectivity. Thus, a systematic understanding of the catalytic behaviour is important. The selectivity and activity of the catalyst is claimed to be dependent on the size and nature of the hydrocarbon, surface structure and size of the active site [6]. Thus in the case of MoO₃ alone, in the oxidation of propene the (1 0 0) plane gives predominantly acrolien whereas the other planes (1 0-1), (1 0 1) and basal plane (0 1 0) are involved in the production of CO₂. However for isobutene, the plane responsible for the non-selective formation of propene was the (0 1 0) plane. However, this plane was found to be selective toward butadiene during the dehydrogenation of but-1-ene to butadiene. The (1 0 0) plane was claimed to be involved in the over oxidation of butadiene to methacrolien and CO_x. From these studies, it was hypothesised that the geometry as well as the atomic arrangements are important in the oxidation reaction [6-9]. Therefore, it is important to illustrate the catalytic behaviour of MoO₃ with respect to the longer chain paraffins. In literature, molybdenum has been used in oxidation reactions either as molybdates or in the form of molybdenum oxides [10, 11]. Metal molybdates such as NiMoO₄, CoMoO₄ and MgMoO₄ exhibited good activity for the oxidation of lower alkanes [10, 12-14]. In the case of higher alkanes, such as *n*-hexane, NiMoO₄ was shown to oxidise the substrate to form hexenes and benzene in relatively high selectivities [15, 16]. However, in addition to the molybdates, it has been shown that excess molybdenum has a beneficial effect on the catalytic activity of the molybdate catalyst [14]. The slight excess amount of molybdenum on the surface was found to act as an active site for propane oxidative dehydrogenation [14].

The MoO₃ is shown to be active in wide range of reactions such as isomerisation, cracking, oxygen insertion and in generation of an electrophilic oxygen species on its surface [17]. Also, Goguet and co-workers showed that MoO₃ has a high activity of isomerisation of *n*-butane [18]. In addition to that, the MoO₃ is shown to be more selective than V₂O₅ in the partial oxidation reactions of ethene, propene and isobutene to acetaldehyde, acrolein and methacrolein, respectively [19]. The methane oxidation to formaldehyde is another example where the improved selectivity to formaldehyde is credited to MoO₃ [20]. Ressler *et al.* [21] described the reaction between propane and MoO₃ at temperatures greater than 450 °C, where the allylic

species are formed by abstraction of a proton in the presence of molybdenum trioxide, followed by oxygen insertion to give acrolein. At temperatures greater than 450 °C, the MoO₃, under a reducing environment, was reported to form different crystallographic shear plane structures, known as sub-oxides, such as Mo₁₈O₅₂, Mo₄O₁₁, Mo₁₇O₄₇, Mo₉O₂₇, Mo₈O₂₃ and Mo₅O₁₄ [21]. These sub-oxides possess a valency in the range between +4 to +6 and their formation is explained on the basis of the defects in the structure of the catalyst [21, 22].

In this study, and continuing with the work already carried out on longer chain alkanes with metal molybdates by our group, it was deemed necessary to understand the role of MoO₃ alone in the ODH of *n*-octane [15, 23]. The oxidative dehydrogenation of *n*-octane over MoO₃ was carried out by investigating the effects of different concentrations of oxygen in the feed over the catalysts. The catalyst phases, which appeared during the reaction, are used to explain both the desired and undesired products formed. In addition, the reactions were carried out in the absence of the catalyst to evaluate the non-catalytic contributions as also described previously by other authors [24-26].

2.2. Experimental

2.2.1 Catalyst synthesis and characterisation

Molybdic acid (M and B Chemicals) was calcined at 550 °C for 5 h under positive airflow. The thermal decomposition of molybdic acid gave the thermodynamically stable α -MoO₃ phase. X-ray diffraction carried out with a Bruker D8 advance instrument was used to analyse the different phases of the metal oxide. For TEM, a Jeol TEM 1010 electron microscope was employed. The sample was suspended in acetone and loaded on a copper grid. Images were captured using iTEM software. The SEM images were recorded using a Zeiss Ultra Plus instrument. Prior to analysis, the samples were mounted on aluminium stubs using double-sided carbon tape and subsequently gold spluttered using a Polaron E5100 coating unit.

2.2.2 Catalytic testing

Gas-phase catalytic oxidation of *n*-octane over α -MoO₃ was carried out in a continuous flow fixed bed reactor (300 mm stainless steel tube, 10 mm I.D.) with the temperatures ranging from 350 to 550 °C. The hotspot of the reactor tube was located and the catalyst (mesh size 600-1000 μ m) was placed at the centre of the hotspot region. The empty spaces on either side of the

catalyst bed were filled with 24-grit carborundum and the ends plugged with glass wool. K-type thermocouples were used to monitor the temperature in the catalyst bed and in the reactor furnace. The thermocouples were controlled by CB-100 RK temperature control units. The feed was delivered into the reactor system using a high precision isocratic pump (Lab Alliance Series II) with flow rate of 0.05 mL/min. The reactor lines were maintained at 200 °C with the aid of heating tape.

The blank reactions were performed with a carborundum powder (24 grit) packed reactor tube to minimise the pyrolysis of the *n*-octane as well as to reduce the extent of homogeneous gas phase reactions. Catalytic tests were carried out at different carbon to oxygen molar ratios keeping the GHSV constant at 4000 h⁻¹ with a catalyst bed volume of 1 mL. The concentration of *n*-octane in the gaseous mixture was maintained at ~11.3 % (v/v) by adjusting the nitrogen flow. Air was used as an oxidant and nitrogen the diluent gas to achieve a total flow rate of 67 mL/min. The total volume of the gaseous products at the outlet was measured using a wet gas flow meter (Ritter Drum-Type Gas Meter). The products were analyzed using Perkin Elmer Clarus 400 FID and TCD gas chromatographs equipped with a SGE BP-PONA capillary column (0.25 mm I.D., 50 m length) and a SUPELCO Carboxen (0.53 mm I.D., 30 m length) column respectively. A Perkin Elmer Clarus 500 GC-MS was used to identify unknown products. The calculated carbon balance was between 98-102%.

2.3 Results and Discussion

2.3.1 Catalyst characterization

2.3.1.1 Powder X-ray diffraction

Figure 2.1 shows the X-ray diffractogram of α -MoO₃. The characteristic peaks for the alpha phase are found at 2θ values of 12.6, 23.5, 25.8 and 27.4 which are responsible for the planes (020), (110), (040) and (130) respectively [27]. The Full Width Half Maximum (FWHM) for all the indexed planes in Figure 2.1 were obtained from the instrument and is showed in Table 2.1

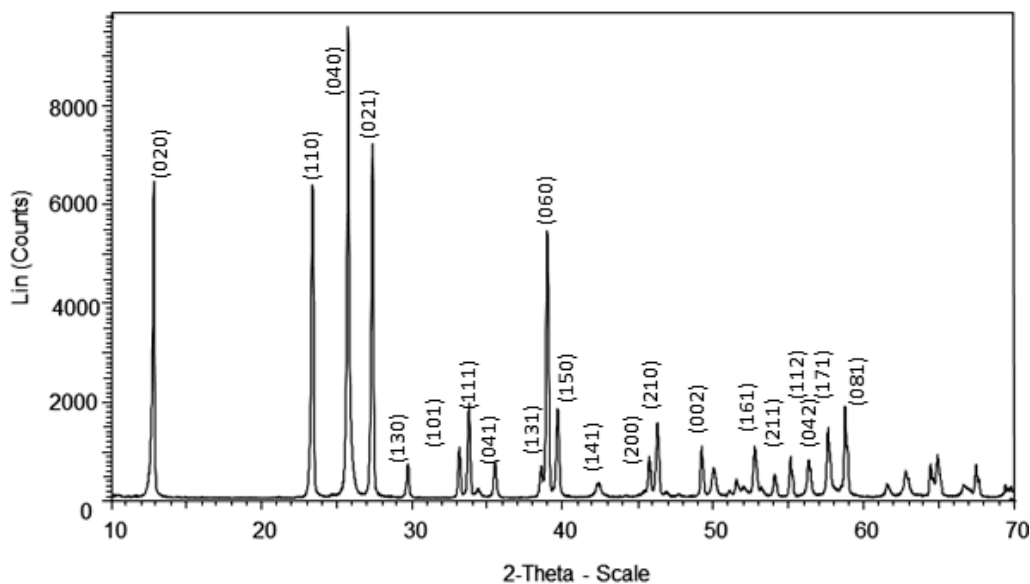


Figure 2.1 XRD diffractogram of α -MoO₃.

Table 2.1 Different planes of α -MoO₃ with 2θ value and Full Width and Half Maximum

2θ °	Planes	FWHM [2θ °]
12.70	(020)	0.1446
23.28	(110)	0.1653
25.59	(040)	0.1446
27.28	(021)	0.1653
29.60	(130)	0.2066
33.09	(101)	0.1653
33.71	(111)	0.2066
35.39	(041)	0.186
38.49	(131)	0.0827
38.80	(060)	0.186
39.57	(150)	0.248
42.35	(141)	0.248
45.69	(200)	0.1653
46.16	(210)	0.1446
49.22	(002)	0.1653
50.02	(230)	0.2893
52.73	(161)	0.186
54.06	(211)	0.186
55.15	(112)	0.124
56.31	(042)	0.124
58.62	(171)	0.1512

2.3.1.2 Scanning and transmission electron microscopy

The morphology of α -MoO₃ studied by scanning electron microscopy showed a plate-like structure with plate lengths of 2-4 μm (Figure 2.2A). This plate-like structure of α -MoO₃ has been well documented [28]. The TEM image of α -MoO₃ is shown in Fig. 2.2B.

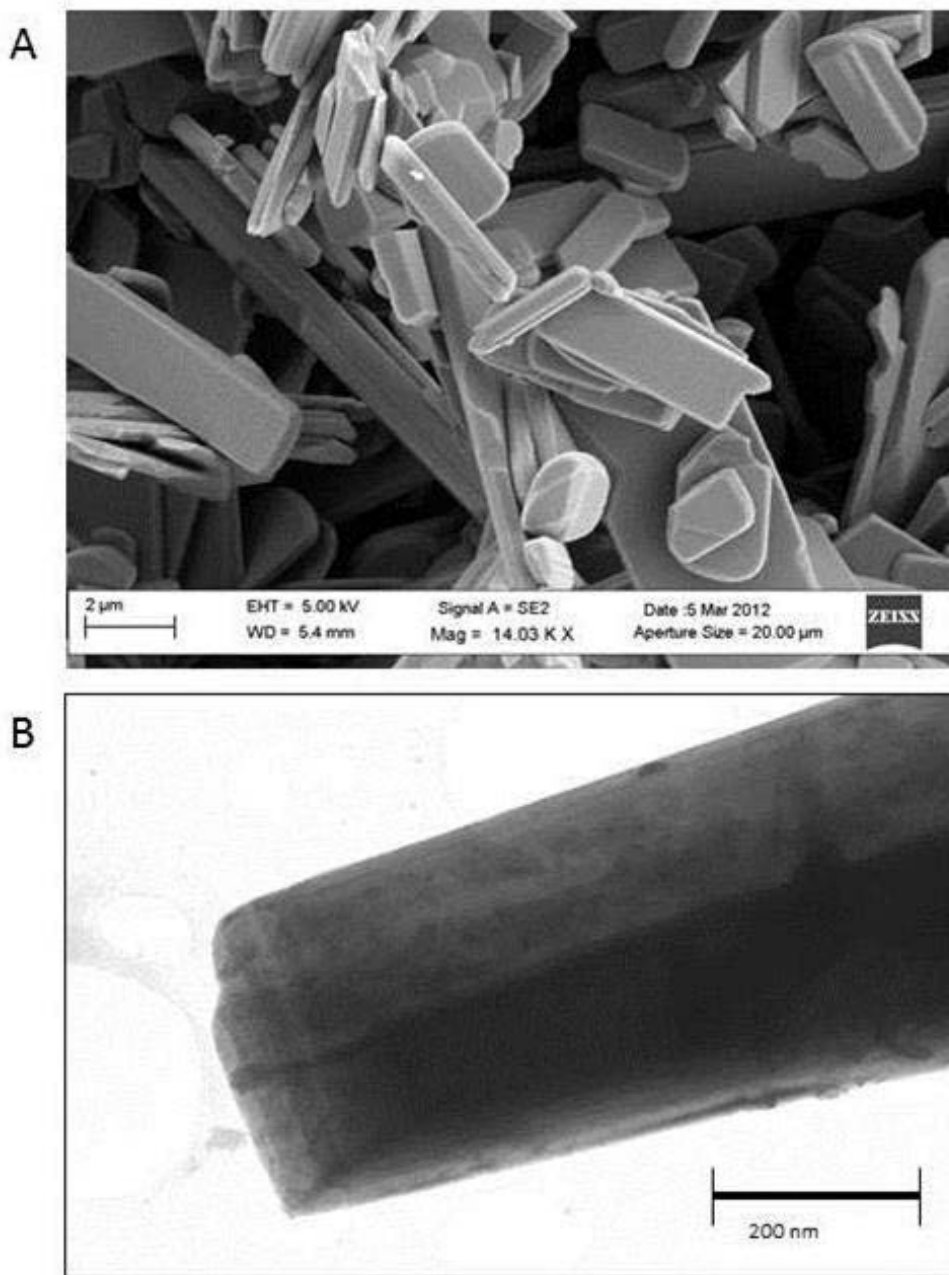


Figure 2.2 SEM (A) and TEM (B) micrographs of α -MoO₃.

A layered structure of α -MoO₃ is observed which is similar to the observation made by Routray *et al.* [29], who stated that α -MoO₃ is composed of well stacked thin layers held together by van der Waals forces.

2.3.2 Catalytic Testing

2.3.2.1 Effect of variation of oxygen

2.3.2.1.1 Blank reaction results

The conversion and product selectivity of the blank reactions for C:O ratios of 8:0 to 8:2 is shown in Table 2.2.

Table 2.2 Conversion and products selectivity for the non-catalytic reactions in a 24 grit carborundum packed reactor tube at a fixed GHSV of 4000 h⁻¹.

C:O ratio	Temperature °C	Conversion %	Octenes %	Aromatics %	Cracked %	COx %	Dienes %
(8:0)	350	0.0	0	0	0	0	0
	400	0.0	0	0	0	0	0
	450	0.0	0	0	0	0	0
	500	0.4	0	0	100	0	0
	550	0.7	0	0	100	0	0
(8:1)	350	0.3	0	0	0	0	0
	400	0.7	55.3	0	0	44.7	0
	450	0.8	52.1	0	0.7	47.2	0
	500	2.0	37.8	4.3	20.3	37.6	0
	550	2.3	36.2	6.4	21.5	34.8	1.3
(8:2)	350	0.0	0	0	0	100	0
	400	0.5	27.2	0	5	67.8	0
	450	1.4	42.8	0	17.4	39.8	0
	500	3.6	36	3.5	25.6	35.1	0
	550	5.3	32.2	8.7	29.8	26.8	2.6

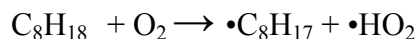
At the C:O ratio of 8:0, no conversion was observed between 350 and 450 °C, with a slight increase in conversion being observed at 500 and 550 °C, but it was below 1%. Under these conditions, the activation of the *n*-octane occurs thermally forming cracked products via the formation of free radicals. The *n*-octane undergoes thermal decomposition, as shown below, to

produce ethyl and hexyl radicals or pentyl and propyl radicals (Appendix-1, Table A1.2.1), or it can undergo symmetric decomposition to produce two butyl radicals [26].



These radicals undergo a loss of hydrogen to produce the corresponding alkenes. The non-catalytic reactions in the presence of oxygen were carried out at C:O ratios of 8:1 and 8:2. The effect of oxygen concentration on the conversion is given in Table 2.1. The conversion of *n*-octane increased with increasing temperature and oxygen concentration in the feed. In the presence of oxygen, the energy of activation is lowered, as oxygen participates in the initiation as well as propagation steps of the reaction [24-26].

The conversion was observed to be similar for both the ratios at the lower temperatures (350 to 450 °C) but then showed an increase for the C:O of 8:2 at higher temperatures (500 and 550 °C). At 350 °C, no conversion was observed for the anaerobic conditions and the ratio of 8:1 and thus only the selectivity for the higher temperatures is reported. However, at the ratio of 8:2, a very low conversion was observed. The products formed under these conditions, that is, at the higher temperatures, were octenes, aromatics, cracked products, and CO_x. The activation of *n*-octane taking place in the presence of oxygen is via the formation of the octyl radical, in a similar manner to that found with other paraffins [26, 30].



The formed octyl radical can further undergo removal of hydrogen to form octenes or it can undergo secondary oxidation with the oxygen to form aromatics, cracked products, and CO_x. With respect to selectivity, the introduction of oxygen resulted in the formation of octenes, which were found to be absent at a ratio of 8:0. Further, octenes selectivity decreased with increasing oxygen concentration in the feed. Interestingly, octenes selectivity reached a maximum for each ratio of carbon and O₂, with the maxima shifting to higher temperatures as the feed became more oxygen rich. This is possibly due to the stabilisation of the octyl free radical at higher

concentrations of oxygen followed by its subsequent decomposition to octenes. The decrease in octenes selectivity with increasing temperature was most pronounced for the ratio of 8:1. The decrease in the octenes selectivity was accompanied by an increase in the selectivity of secondary oxidation products, primarily CO_x, followed by cracked products and then aromatics. With the increase in O₂ a decrease was noted in the octenes selectivity after 450°C with subsequent rise in aromatic and cracked products. The CO_x selectivity also showed a decreasing trend at the higher temperature.

2.3.2.1.2 Catalytic testing of α -MoO₃

Catalytic testing of α -MoO₃ was conducted at carbon to oxygen (C:O) ratios of 8:0, 8:1, and 8:2 with the GHSV fixed at 4000 h⁻¹. The effect of increasing the oxygen concentration on *n*-octane conversion with varying temperature is shown in Table 2.3.

Table 2.3 Catalytic activity of the MoO₃ under different C:O ratios at a GHSV of 4000 h⁻¹.

C:O ratio	Temperature °C	Conversion %	Octenes %	Aromatics %	Aromatics <8 %	Cracked %	CO _x %	Dienes %	Oxygenates %
(8:0)	350	0.0	0	0	0	0	0	0	0
	400	0.1	65	0	0	0	35	0	0
	450	0.1	69	0	0	7	24	0	0
	500	1.1	89	0	0	11	0	0	0
	550	0.7	0	0	0	100	0	0	0
(8:1)	350	0.1	0	0	0	0	0	0	0
	400	0.2	62	0	0	0	38	0	0
	450	1.2	52	0	0	0	47	0	0
	500	2.5	61	3	0	8	26	1	0
	550	3.4	54	10	1	7	25	2	0
(8:2)	350	0.5	100	0	0	0	0	0	0
	400	0.9	48	4	0	9	30	0	8
	450	2.0	48	3	0	7	43	0	0
	500	3.1	31	6	1	12	50	0	0
	550	7.5	22	9	2	23	42	0	1

Conversion increased with an increase in the temperature and with an increase in the oxygen content in the feed. The low conversion achieved at temperatures ranging from 350 °C to 450 °C at all ratios in this study, could be due to the lattice oxygen of α -MoO₃ being insufficiently labile in this temperature range, giving almost similar conversions independent of carbon to oxygen

ratios [21]. According to Ressler *et al.* [21], the lattice oxygen becomes more labile above 450 °C, and the catalyst either undergoes reduction via the sub-oxide (Mo_4O_{11}) to MoO_2 or it is reoxidized to $\alpha\text{-MoO}_3$ depending upon the strength of the oxidizing environment. Marin and Ha [31] carried out partial oxidation of gasoline over MoO_2 , and showed the generation of hydrogen in the absence of steam over the surface of MoO_2 . The generation of hydrogen takes place on the metallic site of MoO_2 [32]. Thus, it was important to establish the contribution of the lattice oxygen as well as the extent of dehydrogenation when working at a ratio of 8:0. The result of this time on line (TOL) experiment, carried out at 550 °C, is shown in Figures 2.3A and 2.3B.

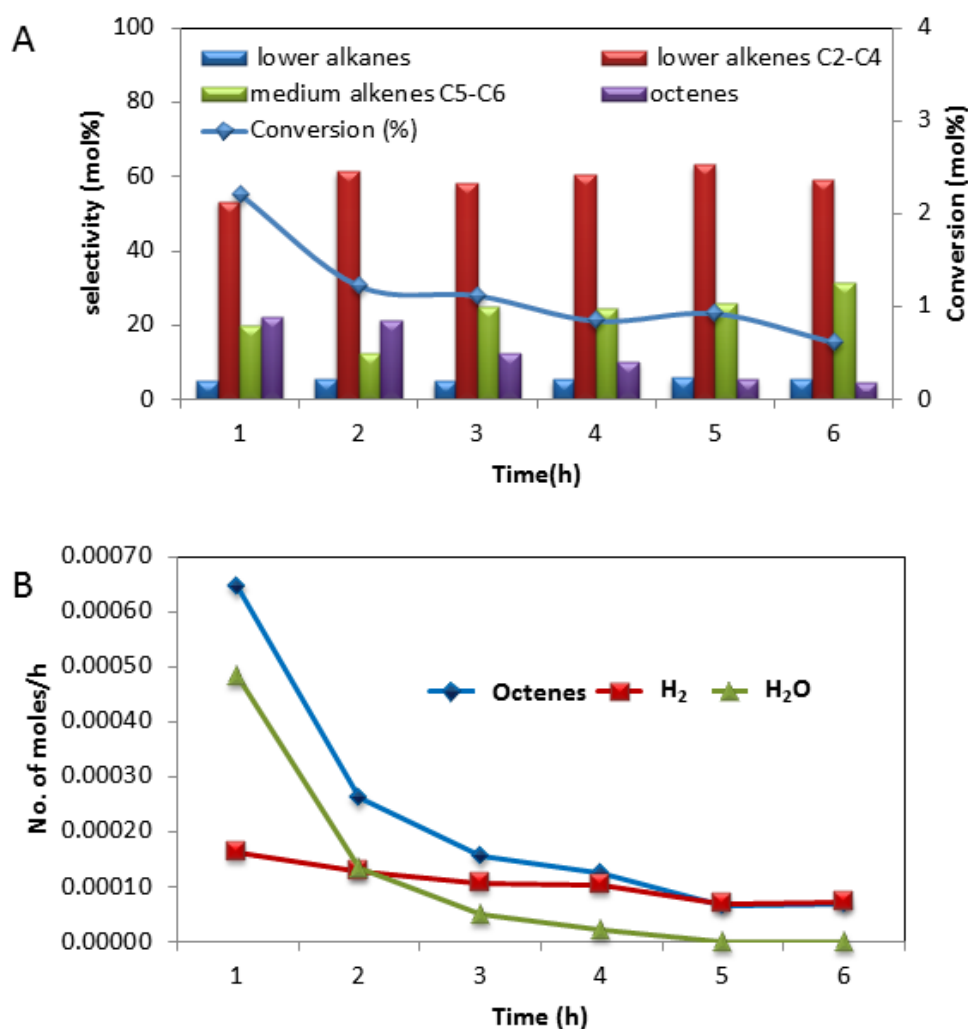


Figure 2.3 Time on line experiment at 550 °C without oxygen with MoO_3 at a GHSV of 4000 h^{-1} (A) *n*-octane conversion and product selectivity (B) formation of octenes, hydrogen, and water as a function of time on line.

The conversion (Figure 2.3A) showed a decreasing trend with time due to two factors; firstly, stripping of lattice oxygen and secondly, coking of the catalyst. The products formed were octenes and cracked products from C1 to C6, mainly olefins. Small amounts of water were also detected in the product mixture. This suggests that both oxidative dehydrogenation as well as dehydrogenation was taking place simultaneously over the catalyst, at least in the early stages of the testing. This is evident from both the water and hydrogen analysis as a function of octene formation shown in Figure 2.3B. The octene formation rate decreases with time accompanied by a decreasing rate of water formation. At the same time, hydrogen is detected in the product stream, which also decreases steadily with time, but not to the same extent as water and octenes. After about 4 hours, the water content in the product becomes negligible and the formation of octenes is thus ascribed to dehydrogenation only as shown by the continued formation of hydrogen in equimolar ratio to the octenes. The cracking of the *n*-octane, evident by the short chain olefins in the product stream, could be due to the reaction of MoO₂ surface oxygens with hydrogen to give Brønsted Mo-OH species, which are known for the isomerisation as well as cracking of hydrocarbon [17, 32]. The absence of CO and CO₂ in the product spectrum suggests that the lattice oxygen, under these conditions, does not participate in either deep oxidation to CO₂ or consecutive oxidation reactions of the octane. The X-ray diffractogram of the used catalyst shown in Figure 2.4A, shows peaks associated only with the MoO₂ phase. This shows the complete reduction of the trioxide phase under the conditions tested. No further reduction to the metal was observed.

When α -MoO₃ was tested at 550 °C using a feed with low oxygen content (C:O = 8:1), a lower conversion was observed as compared to the oxygen rich feed (C:O = 8:2). The reactions were repeated at 550 °C, and after 5 h the air and *n*-octane flow were halted and the catalysts were cooled down under positive nitrogen flow. From XRD analysis of the material, used under oxygen deficient conditions (8:1), strong peaks for MoO₂, Mo₄O₁₁ and weak peaks for MoO₃ were observed (Figure 2.4B). The oxidizing environment at this ratio was thus not strong enough to oxidize the Mo₄O₁₁ effectively back to α -MoO₃, which resulted in the further reduction of Mo₄O₁₁ to MoO₂. However, the reduction was not complete, giving a composition that contained both oxidised and reduced phases of the MoO₃. In the case of the used catalyst, under the oxygen rich environment (8:2), the presence of the α -MoO₃ and Mo₄O₁₁ phases can be clearly seen (Figure 2.4C). Thus, the redox cycle of α -MoO₃ to Mo₄O₁₁ and Mo₄O₁₁ to α -MoO₃

was maintained, resulting in higher conversion. The percentage of each phase, which was calculated from Rietveld refinement, for the used catalysts is shown in Table 2.3.

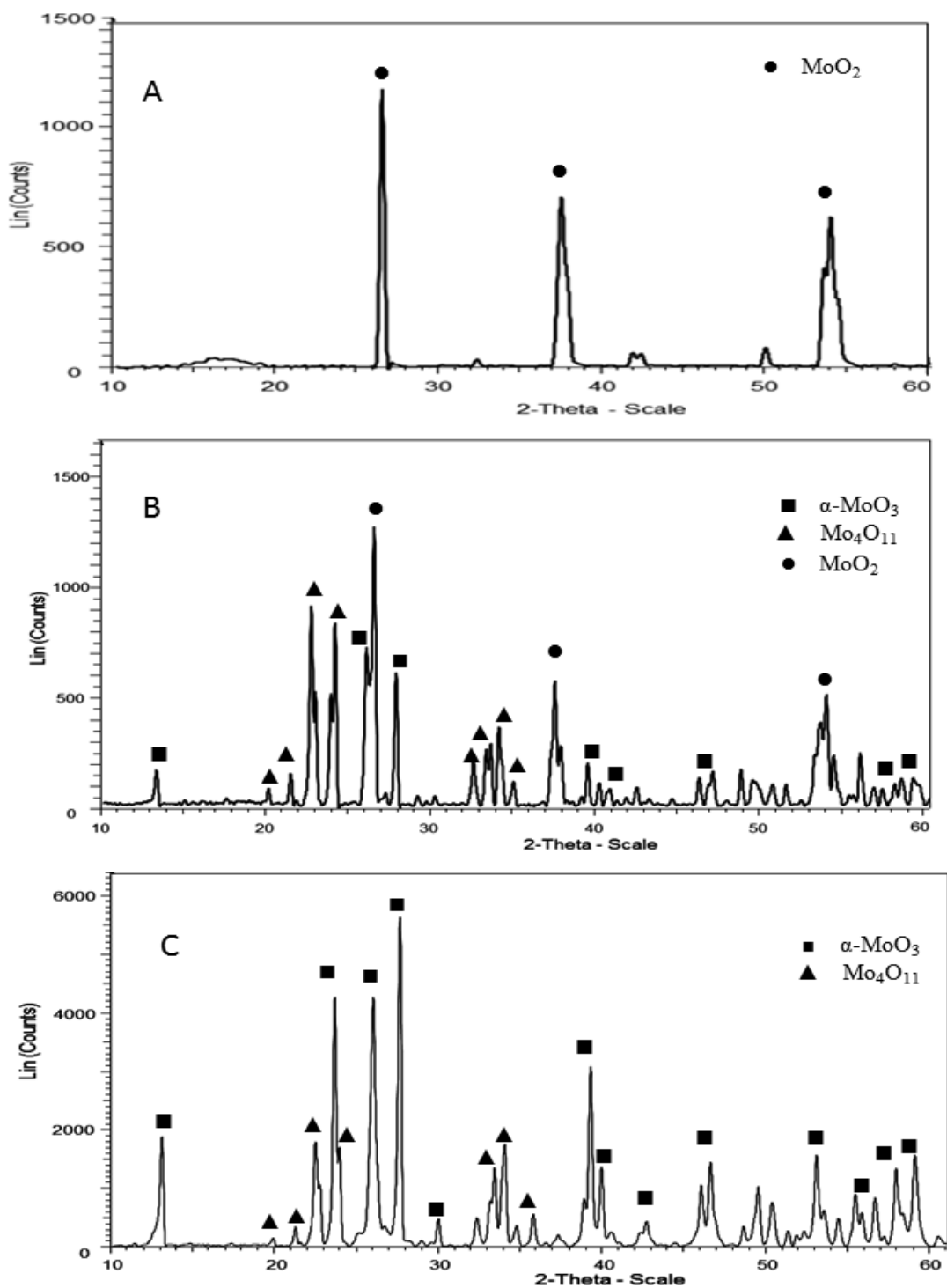


Figure 2.4 XRD diffractograms of the used catalysts after reaction with n-octane of C: O ratio of 8:0 (A), 8:1(B), and 8:2 (C).

Table 2.4 Retvield refinement table for used catalysts

C:O ratio	Phases	Percent (%)
(8:0)	Suboxide,	0
	MoO ₃	0
	MoO ₂	100
(8:1)	Suboxide,	48
	MoO ₃	18.7
	MoO ₂	33.3
(8:2)	Suboxide,	24.8
	MoO ₃	75.2
	MoO ₂	0

The molecular oxygen flowing through the reaction in an oxygen rich environment easily replenishes the lattice oxygen deficiency created during the redox mechanism. To achieve a higher efficiency of the catalyst, it is necessary to keep the molybdenum at a higher oxidation state, between Mo⁺⁴ and Mo⁺⁶. The oxygen dependency of α -MoO₃, as well as the corresponding pathways, namely ODH or DH, in this study can be explained using the schematic diagram shown in Figure 2.5.

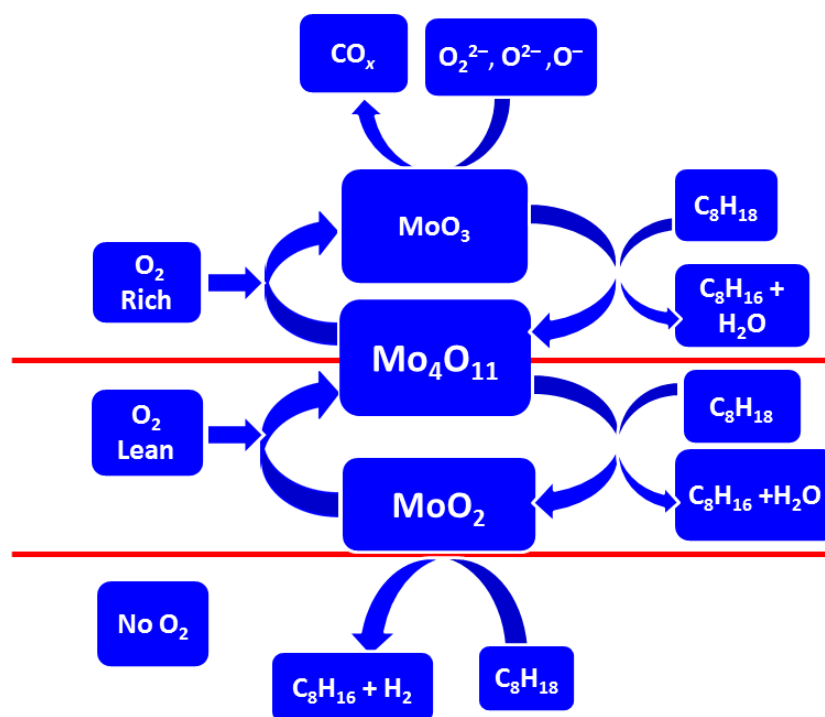


Figure 2.5 Schematic representation of α -MoO₃ reduction/oxidation via Mo₄O₁₁ under *n*-octane.

Here, molybdenum, which is in the +6 oxidation state, will oxidatively dehydrogenate *n*-octane to give octenes, while at the same time being reduced to the sub-oxide phase, Mo₄O₁₁. This phase, depending upon the strength of the oxidizing environment, will follow one of two pathways. It can undergo partial reduction to form MoO₂ in an oxygen deficient feed or in an oxygen rich feed, it can be re-oxidized to α-MoO₃. The evidence of both DH as well as ODH taking place simultaneously under these conditions, was confirmed from GC analyses which showed the presence of both water and hydrogen under steady state conditions. Finally, the partially reduced Mo₄O₁₁ can be reduced completely to form MoO₂ in the absence of O₂. During the presence of this phase, only dehydrogenation of *n*-octane takes place.

Haber and Lalik, when looking at the catalytic properties of MoO₃, mention that the gaseous oxygen when physisorbed over the catalyst gets activated to O₂⁻, O₂²⁻, O⁻ and these activated species are capable of oxidising the alkane molecule to CO₂, while at the same time maintaining an equilibrium with the lattice oxygen in the catalyst [17]. They further go on to explain that the surface hydroxyl groups of MoO₃ possess Brønsted acidity, which can easily transfer hydrogen, from an adsorbed olefin and in the process, generate a carbocation. The resultant carbocation may undergo cracking or isomerisation to form the associated reaction products. These arguments, coupled with the characterisation evidence, were used to explain the selectivity of the products at the different conditions used.

2.3.2.1.3 Product selectivity with MoO₃

The product selectivities at the various C:O ratios as well as temperatures are shown in Table 2.2. Dehydrogenation as well as ODH is favoured at C:O ratios of 8:0 and 8:1 because re-oxidation of the sub-oxide, Mo₄O₁₁, is slow. In fact, these ratios further contribute to form MoO₂. However, in the presence of higher concentration of oxygen, the re-oxidation of the sub-oxide to α-MoO₃ occurs. Thus at a C:O ratio of 8:2, the oxidative dehydrogenation pathway is followed.

Under anaerobic conditions, the catalyst shows no conversion at 350 °C. However, with an increase in temperature, the formation of octenes was observed with selectivity peaking at 500 °C but with a further increase in temperature to 550 °C, only cracked products were observed, which is likely due to the complete loss of lattice oxygen. This observation is attributed to the formation of MoO₂, which favours the formation of cracked products and agrees with those of Wehrer *et al.* [33] who observed similar behaviour for the oxidation of *n*-hexane over MoO₂. It

is important to note that the exclusive formation of cracked products at 550 °C was achieved at steady state conditions as opposed to the initial formation of octenes as shown in Figure 2.3.

At a ratio of 8:1, a slightly lower selectivity towards octenes was observed with a subsequent rise in CO_x products. A further increase in the oxidizing environment to 8:2 resulted in a decrease in the octenes selectivity. This is in accordance with previous research which showed that when the feed is rich with *n*-octane, the main products are octenes and when the feed is enriched with oxygen, the occurrence of secondary reactions results in a decrease in selectivity toward octenes [4]. The different octene selectivities at 550 °C among all ratios tested are shown in Figure 2.6.

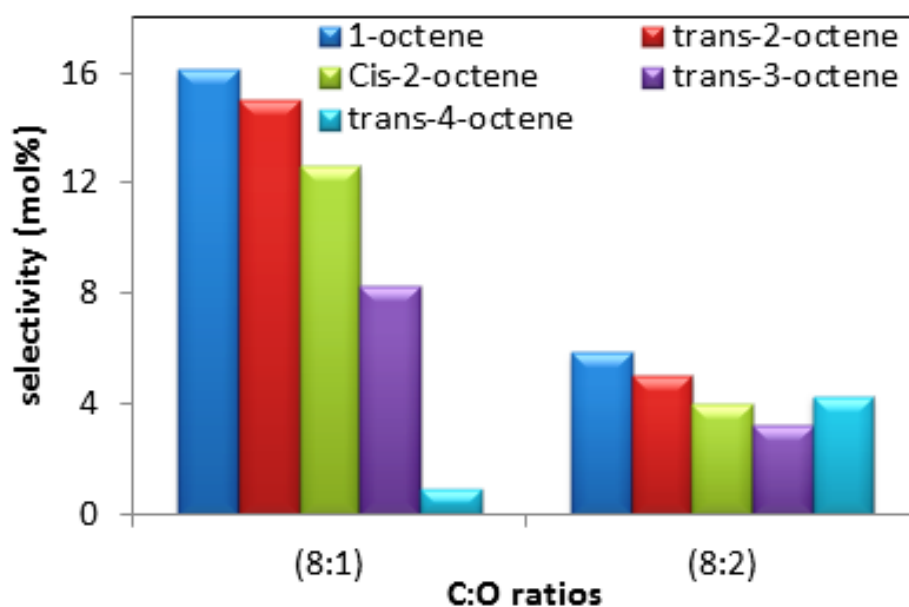


Figure 2.6 Effect of oxygen content over octenes isomers at 550 °C (at carbon to oxygen ratio of 8:1 and 8:2 with a GHSV of 4000 h⁻¹).

The selectivity order was 1-octene > *trans* 2-octene > *cis* 2- octene > *trans* 3-octene > *trans* 4-octene > *cis* 4-octene. In addition to octenes and CO_x, cracked products as well as aromatics became more pronounced at the higher temperatures and at higher C:O ratios. In addition to the ODH products and cracked products formed, it was observed that at the ratio of 8:2, oxygenates were forming, although not at all the temperatures tested. The highest selectivity was observed at 400 °C. The oxygenates were identified as furans and ketones as described by Friedrich and Mahomed [34].

By altering the strength of the oxidation environment, it is possible to tailor the selectivities to desired products, i.e. limiting the amount of oxygen in the feed leads to the formation of octenes, whereas in a strong oxidizing environment, octenes that are formed are converted to aromatic compounds or to carbon oxides. The highest aromatics selectivity (10%) was observed at 550 °C at a C:O ratio of 8:1. The selectivity toward the different aromatic compounds at 550 °C for tested C:O ratios is shown in Figure 2.7.

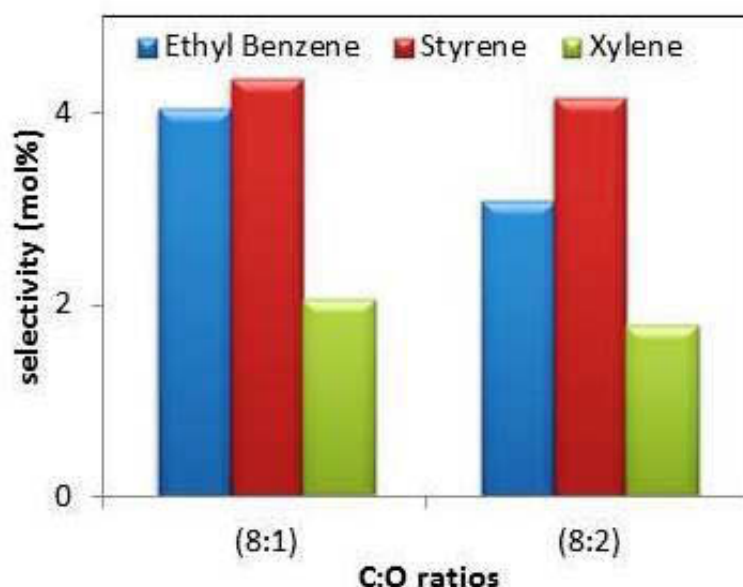


Figure 2.7 Aromatics breakdown at C:O ratio of 8:1 and 8:2 with a GHSV of 4000 h⁻¹.

The formed ethyl benzene undergoes further oxidative dehydrogenation to produce styrene. The *trans*-2-octene acts as a precursor for *o*-xylene formation by C2-C7 cyclization [35]. A further increase in oxygen content in the feed results in a decrease in aromatics selectivity, which is compensated by an increase in the selectivity toward cracked products and CO_x. The cracked products start appearing at 450 °C at a C:O ratio of 8:0 and were the only products formed at 550 °C. The cracked product selectivity under oxidative environments was less significant due to the secondary oxidation of octenes or aromatics. Thus at low C:O ratio, cracking is likely occurring thermally, whilst at the high C:O ratio, both thermal as well as oxidative cracking is taking place. CO_x selectivity was found to be dominant at the highest oxygen content in the feed, whilst in the absence of gas phase oxygen, CO_x was only formed at the lower temperatures. In the presence of

gas phase oxygen, CO_x formation is governed by the presence of physisorbed oxygen derived from the gas, while in the absence of gas phase oxygen, the lattice oxygen is involved in the formation of CO_x [17, 36].

2.3.3 SEM analysis of the used catalysts

In addition to the XRD analysis of the used catalysts, SEM images were obtained and the results explained by comparison with the XRD data. Figure 2.8 provides the SEM images for the fresh MoO_3 catalyst (Figure 2.8A) as well as the used catalysts at the different C:O ratios.

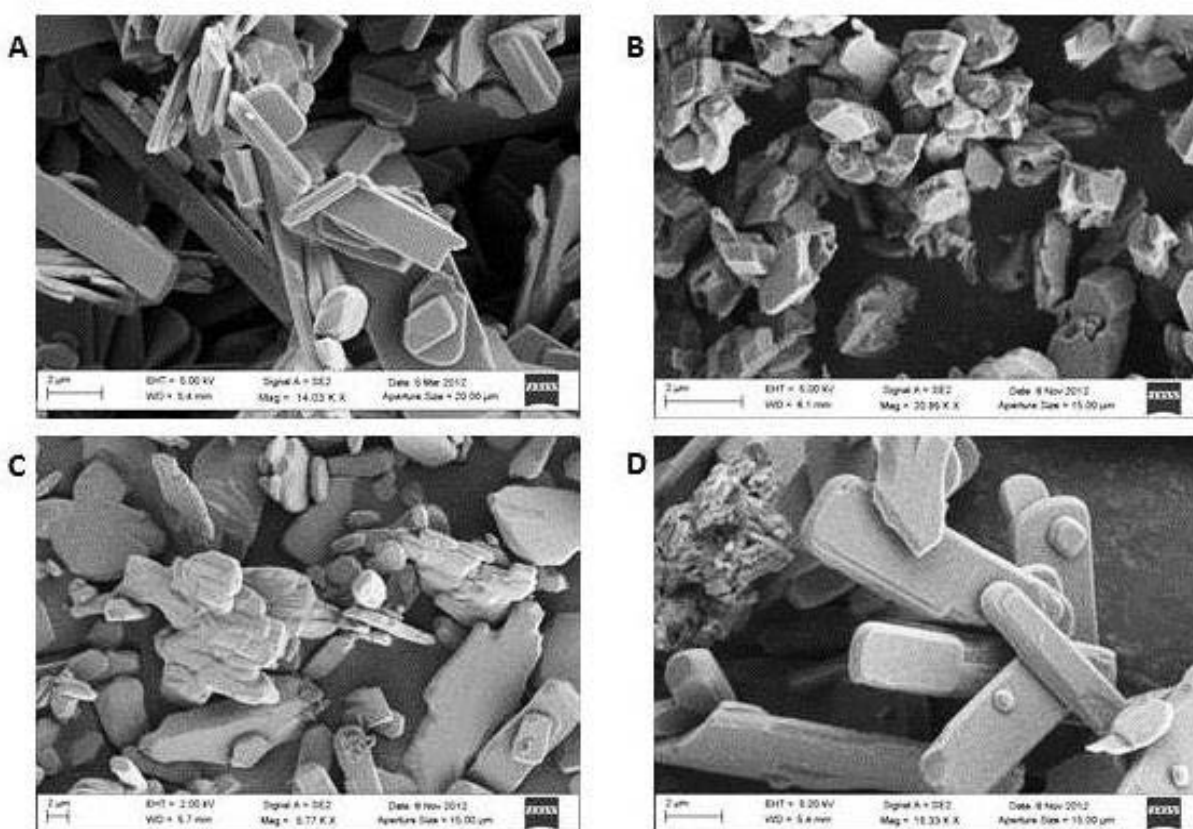


Figure 2.8 SEM images of fresh catalyst (A) and used catalysts at C:O ratios of 8:0 (B), 8:1 (C) and 8:2 (D).

The fresh catalyst shows the typical plate-like crystals associated with MoO_3 . Before analysis, the catalyst tested under dehydrogenation conditions was heated at 500 °C under flowing nitrogen for several hours to desorb the coke formed during the reaction. The SEM image of this catalyst clearly shows the disappearance of the plate-like morphology of MoO_3 and showed the cubic and more faceted morphology of MoO_2 (Figure 2.8B). This is verified by the XRD

analysis as shown in Figure 4A. In the case of the other used catalysts, the increasing oxygen content in the feed was responsible for the re-oxidation of the sub-oxide to the α -MoO₃ phase. However, for the C:O ratio of 8:1, MoO₂ also formed and gave a mixed phase system. This is evident when examining the SEM image, (Figure 2.8C), where both the plate like crystals of MoO₃ as well as the more irregular cube forms of MoO₂ are present. With a further increase in the oxygen content, the XRD peaks for α -MoO₃ become more prominent, underlining the effect of oxygen in the system. The SEM images of this catalyst (Figure 2.8D) showed a higher extent of regeneration of the reduced phases by the dominance of the plate-like crystals of MoO₃. Again, this was verified when compared to the X-ray analysis (Figure 2.4C). Thus, although regeneration of the α -MoO₃ phase was achieved in all cases where oxygen was present, the dominance of the phase was clearly dependent on the amount of oxygen present in the feed.

2.4. Conclusions

The non-catalytic as well as catalytic oxidation of *n*-octane was evaluated using MoO₃ as catalyst. For the non-catalytic reactions and in the absence of O₂, only cracked products were observed. As the O₂ content was increased in the feed, conversion increased with the appearance of olefins and aromatics as well as total oxidation and cracked products. The selectivity towards the various products was dependent on the ratio of carbon to oxygen and the temperature of the reaction. For the catalytic transformation of *n*-octane, in the absence of oxygen, both the ODH and DH pathways gave octenes initially, until complete reduction of MoO₃ had taken place after which, only DH of *n*-octane occurred and finally cracking at the highest extreme of investigated temperature. The introduction of O₂ into the feed improved the conversion of *n*-octane, whilst at the same time changing the selectivity profile, which was once again controlled by the oxygen content in the feed as well as temperature. During oxygen lean conditions, octenes selectivity was found to be generally higher, whilst during oxygen rich conditions, CO_x was found to dominate. Aromatics were observed to form at lower temperature in the feed containing a higher concentration of oxygen. The selectivity of the catalysts were explained by the redox behaviour in the presence of oxygen and complete reduction in the absence of oxygen. During the reaction, the reduction of α -MoO₃ and its re-oxidation takes place via a sub-oxide phase, Mo₄O₁₁ depending on the strength of the oxygen environment. Dehydrogenation conditions and oxygen lean conditions led to the formation of MoO₂, whereas in an oxygen rich environment, the sub-

oxide is re-oxidized to α -MoO₃. The dominant isomer among the octenes was 1-octene, while styrene was the most favoured aromatic product.

Acknowledgements

This work was financially supported by SASOL, THRIP and the NRF. We also thank the electron microscope unit, UKZN, for microscopic work.

References

- [1] T. Blasco, J.M. Lopez Nieto, *Appl. Catal. A: Gen.* 157 (1997) 117-142.
- [2] V.D.B.C. Dasireddy, S. Singh, H.B. Friedrich, *Appl. Catal. A: Gen.* 456 (2013) 105-117.
- [3] M. Narayanappa, V.D.B.C. Dasireddy, H.B. Friedrich, *Appl. Catal. A: Gen.* 447–448 (2012) 135-143.
- [4] E.A. Elkhalfa, H.B. Friedrich, *Catal. Lett.* 141 (2011) 554-564.
- [5] E.A. Elkhalfa, H.B. Friedrich, *Appl. Catal. A: Gen.* 373 (2010) 122-131.
- [6] J.C. Védrine, *Appl. Catal. A: Gen.* 474 (2014) 40-50.
- [7] J.C. Volta, J.L. Portefaix, *Appl. Catal.* 18 (1985) 1-32.
- [8] F. Bertinchamps, E.M. Gaigneaux, *Catal. Today* 91–92 (2004) 105-110.
- [9] E.M. Gaigneaux, P. Ruiz, B. Delmon, *Catal. Today* 32 (1996) 37-46.
- [10] Y.S. Yoon, N. Fujikawa, W. Ueda, Y. Moro-oka, K.W. Lee, *Catal. Today* 24 (1995) 327-333.
- [11] T. Davies, S.H. Taylor, *J. Mol. Catal. A: Chem.* 220 (2004) 77-84.
- [12] M. Chen, J.-L. Wu, Y.-M. Liu, Y. Cao, L. Guo, H.-Y. He, K.-N. Fan, *J. Solid State Chem.* 184 (2011) 3357-3363.
- [13] D. Cauzzi, M. Deltratti, G. Predieri, A. Tiripicchio, A. Kaddouri, C. Mazzocchia, E. Tempesti, A. Armigliato, C. Vignali, *Appl. Catal. A: Gen.* 182 (1999) 125-135.
- [14] W. Ueda, K.H. Lee, Y.S. Yoon, Y. Moro-oka, *Catal. Today* 44 (1998) 199-203.
- [15] B. Pillay, M.R. Mathebula, H.B. Friedrich, *Appl. Catal. A: Gen.* 361 (2009) 57-64.
- [16] B. Pillay, M.R. Mathebula, H.B. Friedrich, *Catal. Lett.* 141 (2011) 1297-1304.
- [17] J. Haber, E. Lalik, *Catal. Today* 33 (1997) 119-137.

- [18] A. Goguet, S. Shekhtman, F. Cavallaro, C. Hardacre, F.C. Meunier, *Appl. Catal. A: Gen.* 344 (2008) 30-35.
- [19] K. Takehira, T. Komatsu, N. Sakai, H. Kajioka, S. Hamakawa, T. Shishido, T. Kawabata, K. Takaki, *Appl. Catal. A: Gen.* 273 (2004) 133-141.
- [20] T. Takemoto, K. Tabata, Y. Teng, L.-X. Dai, E. Suzuki, *Catal. Today* 71 (2001) 47-53.
- [21] T. Ressler, J. Wienold, Rolf E. Jentoft, F. Girgsdies, *Eur. J. Inorg. Chem.* 2003 (2003) 301-312.
- [22] T. Ressler, R.E. Jentoft, J. Wienold, M.M. Günter, O. Timpe, *J. of Phys. Chem. B* 104 (2000) 6360-6370.
- [23] M.I. Fadlalla, H.B. Friedrich, *Catal. Sci. Tech.* 4 (2014) 4378-4385.
- [24] R. Burch, E.M. Crabb, *Appl. Catal. A: Gen.* 97 (1993) 49-65.
- [25] R. Burch, E.M. Crabb, *Appl. Catal. A: Gen.* 100 (1993) 111-130.
- [26] A.A. Lemonidou, A.E. Stambouli, *Appl. Catal. A: Gen.* 171 (1998) 325-332.
- [27] L. Seguin, M. Figlarz, R. Cavagnat, J.C. Lassègues, *Spectrochim Acta A* 51 (1995) 1323-1344.
- [28] E. Söderhjelm, M. House, N. Cruise, J. Holmberg, M. Bowker, J.-O. Bovin, A. Andersson, *Top. Catal.* 50 (2008) 145-155.
- [29] K. Routray, W. Zhou, C.J. Kiely, W. Grünert, I.E. Wachs, *J. Catal.* 275 (2010) 84-98.
- [30] W.J. Pitz, C.K. Westbrook, *Combust. Flame* 63 (1986) 113-133.
- [31] O.G. Marin Flores, S. Ha, *Appl. Catal. A: Gen.* 352 (2009) 124-132.
- [32] H. Al-Kandari, F. Al-Khorafi, H. Belatel, A. Katrib, *Catal. Comm.* 5 (2004) 225-229.
- [33] P. Wehrer, C. Bigey, L. Hilaire, *Appl. Catal. A: Gen.* 243 (2003) 109-119.
- [34] H.B. Friedrich, A.S. Mahomed, *Appl. Catal. A: Gen.* 347 (2008) 11-22.
- [35] E.A. Elkhalfa, H.B. Friedrich, *J. Mol. Catal. A: Chem.* 392 (2014) 22-30.
- [36] L.M. Madeira, M.F. Portela, *Appl. Catal. A: Gen.* 281 (2005) 179-189.

Chapter 3

Effect of different weight loadings of Mo/SBA-15 on the oxidative dehydrogenation of *n*-octane

Abstract

In this study, the effect of different weight loadings of molybdenum supported on SBA-15 for the oxidative dehydrogenation of *n*-octane was investigated. The wet impregnation method was used to load 4, 7, 10 and 18 wt% of molybdenum on SBA-15 and the resultant materials were characterised by ICP-OES, BET physisorption studies, XRD, Raman spectroscopy, TEM and SEM. Results from Raman spectroscopy showed the presence of monomeric and a small amount of polymeric MoO_x species for the 4 wt% catalyst. For the 7 wt% molybdenum loading, along with the monomeric and polymeric MoO_x species, formation of MoO₃ crystallites was also seen. With an increase in the molybdenum loading to 10 wt%, the co-existence of MoO₃ crystallites and polymeric MoO_x species was present, whereas only crystalline MoO₃ was present at a loading of 18 wt%. The catalytic results showed that SBA-15 is active but selective to cracked products (33%) and CO_x (32%), whereas the loaded catalysts produced octenes and C8 aromatics. Conversion of *n*-octane increased with the molybdenum loading, which was accompanied by a decrease in octene selectivity due to secondary oxidation of octenes to aromatics, cracked products and CO_x. The yields to octenes were higher over the 4 wt% catalyst, whereas the activation of *n*-octane over the 10 wt% molybdenum catalyst showed an enhanced yield to aromatics. When the 10 wt% catalyst was tested over the temperature range of 350 to 550 °C, the *n*-octane conversion and selectivity towards aromatics increased. Also, the extent of non-selective oxidation increased with an increase in the oxygen content in the feed. A variable GHSV study revealed that the octenes, cracked products and CO₂ are the primary products of the reaction.

Keywords: SBA-15, monomeric, polymeric, crystalline MoO₃, *n*-octane, ODH.

3.1 Introduction

The oxidation of alkanes is rapidly obtaining importance in heterogeneous catalysis, since alkanes, which are abundant due to many gas to liquid plants operating worldwide, have the potential to replace the traditional feedstocks such as alkenes and aromatics to produce value added products [1, 2]. Alkanes can be converted into alkenes traditionally by dehydrogenation. However, this method has several drawbacks, such as the reaction being endothermic, coking of catalysts, low conversions and high operational temperatures, usually higher than 500 °C [3, 4]. Some of these drawbacks are overcome by oxidative dehydrogenation (ODH). ODH favours the formation of products with improved yield, since the reaction operates under non-equilibrium conditions. In addition, the catalytically active sites can be maintained with the continuous supply of oxygen contained in the feed, thus avoiding the formation of coke [5].

Molybdenum oxides are useful in the oxidation of alkanes, alcohols and alkenes [6-9]. The catalytic performance of molybdenum oxides is enhanced when placed on the surface of a support and is effective in the presence of molecular oxygen for the oxidation of methanol, methane, ethane, propane to propene, dimethyl ether to formaldehyde and the epoxidation of propylene [10-15].

Previous reports on supported molybdenum oxide based catalysts showed that its catalytic performance was largely affected by the nature of the molybdenum species present on the support [14, 16, 17]. However, the types of molybdenum species present on the support are dependent on the molybdenum weight loading, nature of the support, pH during the catalyst synthesis and the pre-treatment of the catalysts [18-20]. Silica is a preferred support for molybdenum compared to other supports, due to its irreducibility and weak interaction with molybdenum oxide species [20]. Molybdenum oxides supported on silica showed efficiency in the oxidation of lower alkanes to targeted products such as formaldehyde, acetaldehyde and acrolein [21-23]. Another study involved the oxidation of ethane using molybdenum oxide supported on silica and silica-titania forming ethylene, acetaldehyde, CO and CO₂. The ethylene yield was higher over the silica-titania support compared to the silica alone, which was attributed to a more equal distribution of the MoO_x species between the silica and titania domains [24]. Catalysts prepared by Lou *et al.* [25] showed the presence of monomeric species at low loadings, but polymeric MoO_x and crystalline MoO₃ were present at higher loadings.

When these catalysts were tested for ethane oxidation, ethylene, acetaldehyde and formaldehyde were produced. The catalyst with monomeric MoO_x species was selective towards ethylene and acetaldehyde, whereas the catalyst containing polymeric MoO_x species and crystalline MoO₃ displayed high selectivity to formaldehyde.

Earlier, Chen *et al.* [26, 27] studied the oxidative dehydrogenation of propane as a function of molybdenum loadings with Al₂O₃ and ZrO₂ as supports. The lower weight loading catalysts, up to 5 wt%, indicated the presence of polymeric MoO_x species, whereas at higher loadings, crystalline MoO₃ was present. Over both the supports, higher feed consumption rates were noted at the lower loadings and ascribed to the presence of 2-dimensional polymeric MoO_x species compared to when crystalline MoO₃ was present on the supports. The lower feed consumption rates over the catalysts which contained 3-dimensional MoO₃ crystallites, were ascribed to the decreased feed accessibility to the reactive 2-dimensional polymolybdate species, which are embedded in a 3-dimensional MoO₃ crystallite structure.

Extensive work has been carried out on the ODH of lower alkanes to generate a conceptual understanding of the structure and activity relationship of lower alkanes over these catalytic systems. However, it is important to extend the application of these catalysts to ODH of longer chain alkanes. Previous work based on vanadia catalysts for the ODH of *n*-octane showed that octenes and C₈ aromatics could be obtained with considerable yields [28-31]. In this study, the effect of different species of molybdenum oxide, brought about by changing the weight loading of molybdenum, on SBA-15 was investigated for the ODH of *n*-octane. SBA-15 was used as a support, owing to its properties such as high surface area with a definite 2D structure, a larger pore volume, tunable pore diameter (up to 30 nm) and thermal stability [32].

3.2 Experimental

3.2.1 Preparation of catalysts

3.2.1.1 Synthesis of SBA-15

SBA-15 was synthesized using the method proposed by Cao *et al.* [33]. Tetraethyl ortho-silicate (TEOS) (Aldrich) was used as the silica source and Pluronic P123 (PEP-PPO-PPE) (EO₂₀-PO₂₀-EO₂₀, Mol. Wt - 5800, Aldrich) as the organic polymer. In a typical synthesis, 14.6 g of Pluronic P123 and 0.161 g of the NH₄F were dissolved in 540 mL of 1.3 M HCl. The mixture was stirred for 1 h. After complete dissolution of the polymer, 30 mL of TEOS was added drop-wise and the resultant gel was stirred for 24 h. The gel was then transferred to a

closed vessel and treated hydrothermally at 100 °C for 24 h. The material was filtered under vacuum, washed several times with deionised water and dried at room temperature. The white powder obtained was then calcined at 550 °C for 5 h to remove the organic polymer template.

3.2.1.2 Synthesis of molybdenum supported on SBA-15 catalysts

Catalysts were prepared using the wet impregnation method. Ammonium heptamolybdate tetrahydrate ($\text{NH}_4\text{Mo}_7\text{O}_{24}\cdot 4\text{H}_2\text{O}$, Merck) was used as a molybdenum precursor. For a 4 wt% molybdenum loading, 0.061 g of ammonium heptamolybdate was dissolved in 50 mL of water and stirred for 30 minutes. The calculated amount of SBA-15 was then immersed in the aqueous solution of molybdenum precursor and the resultant slurry was stirred at room temperature for 6 h and subsequently heated to 100 °C to remove water. The material was then placed in an oven (at 135 °C) for a further 6 h and calcined in air at 550 °C for 5 h. The 7, 10 and 18 wt% Mo catalysts were prepared using the method described above.

3.2.2 Characterization of catalysts

The diffractogram of SBA-15 was obtained using a Small Angle X-Ray Scattering (Anton Parr SAXS) instrument. The Cu source ($\lambda = 1.5406 \text{ \AA}$) was used with a PAN analytical X-Ray PW3830 generator operating at a voltage of 40 kV and a current of 50 mA. The phases of the metal oxide present on the SBA-15 support were analysed using a Bruker D8 Advance instrument equipped with an Anton Parr XRD 900 reaction chamber with a Cu source. A temperature control unit, TCU 750 was employed to control the temperature. The molybdenum content in the catalysts was obtained by ICP-OES using a Perkin Elmer Optima 5300 DV spectrometer. A Micromeritics Tristar II instrument was used for the determination of the surface area of the samples. The samples were degassed under vacuum at 90 °C for 1 h and then at 200 °C overnight. The surface area was calculated using the standard Brunauer-Emmett-Teller (BET) multipoint method from relative pressure ratios, p/p_0 ranging from 0.050 to 0.300. The pore volume of the SBA-15 was calculated by using the adsorption branch of the isotherm at $p/p_0 = 0.95$. Raman spectra of the samples were obtained using an Advantage 532 Series spectrometer equipped with Nuspec software. Transmission electron microscopy (TEM) was carried out on a Jeol TEM 1010 Electron Microscope. The samples were suspended in acetone and then sonicated for a few minutes before applying onto a Cu grid. TEM images

were captured using iTEM software. The surface morphology of all the catalysts were examined with a Zeiss Ultra Plus Scanning Electron Microscope.

3.2.3 Catalytic testing

Gas-phase catalytic oxidation of *n*-octane was carried out in a continuous flow fixed bed reactor at temperatures ranging from 350 to 550 °C at atmospheric pressure. A stainless steel reactor tube (10 mm I. D. and 300 mm L) was used in all the reactions. The catalyst with bed volume of 1 mL, in the form of pellets (600-1000 µm) was placed in the isothermal zone of the reactor tube. The empty spaces at either sides of catalysts were filled with 24-grit carborundum and the ends of the reactor tube were plugged with glass wool. K-type thermocouples controlled by temperature control units (CB-100 RK) were used to monitor the change in temperature at the catalyst bed and in the reactor furnace. The feed was delivered using a high precision isocratic pump (Lab Alliance Series II) with a flow rate of 0.05 mL/min. and reactor lines were heated to 200 °C.

The concentration of *n*-octane was maintained at 11.3% (v/v) and the GHSV fixed at 4000 h⁻¹ for all the reactions. The total volume of the gaseous products at the outlet was measured using a wet gas flow meter (Ritter Drum-Type Gas Meter). The products were analysed with a Perkin Elmer Clarus 400 FID and TCD gas chromatograph equipped with a SGE BP-Pona capillary column, (I.D. = 0.25 mm, L = 50 m) and a Supelco Carboxen column, (I.D. = 0.53 mm, L = 30 m) respectively. A Perkin Elmer Clarus 500 GC-MS was used to identify unknown products. The calculated carbon balance varied between 98-102% and data points were obtained in duplicate with an error of 2%.

3.3. Results and discussion

3.3.1 Characterisation of catalyst

3.3.1.1 ICP-OES

The ICP-OES results of the prepared catalysts are shown in Table 3.1. A very close correlation to the nominal value for molybdenum loadings was observed for the prepared catalysts, indicating that negligible loss of molybdenum had occurred during the synthesis.

3.3.1.2 BET analysis

The summary of physisorption characterisation of the support and the catalysts is presented in Table 3.1.

Table 3.1 Physical properties of the different weight loadings of Mo supported on SBA-15

Catalysts	ICP wt%	Surface area (m ² /g)	Average pore volume (cm ³ /g)	Average pore diameter (nm)	Average crystallite size (nm) ^a
SBA-15	-	772	1.30	6.7	-
4%	3.9	481	0.97	8.1	4.21
7%	7.1	395	0.94	8.9	4.62
10%	9.8	346	0.87	9.5	4.90
18%	17.6	212	0.56	11.6	5.75

^a Calculated by using Scherer's equation.

The surface area of the catalysts decreased gradually from 481 to 212 m²/g as the molybdenum loading increased from 4 to 18 wt%. The pore volume also recorded a decrease with an increase in molybdenum loading, indicating that the molybdenum oxide is not only located on the surface but also inside the pores of SBA-15. The crystallite size of the molybdenum oxide was also found to increase with an increase in the molybdenum loading. This suggests that, with an increase in the molybdenum loading, the MoO_x species are aggregating on the surface of SBA-15 to form MoO₃ crystallites. A significant decrease in pore volume was observed for the 18 wt% catalyst, probably due to the loss of mesoporosity that is reflected in the capillary condensation step of this catalyst. The capillary condensation step was observed at a higher p/p_0 value of 0.64 in comparison to the other catalysts, whose capillary condensation step started at 0.59 (Figure 3.1) [25].

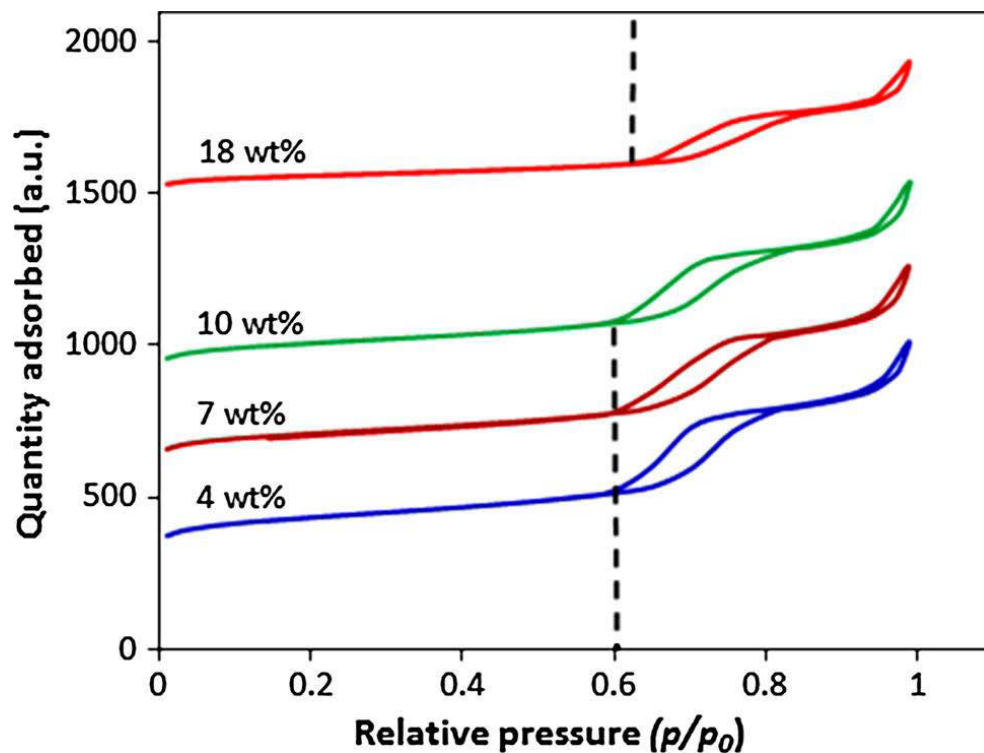


Figure 3.1 N₂ adsorption-desorption isotherms of different loadings of molybdenum supported on SBA-15 catalysts.

Although all of the prepared catalysts displayed the type IV isotherm and H1 type hysteresis, with cylindrical mesoporous channels, the decrease in the N₂ adsorption reflects a disturbance or collapse of the mesoporosity of the sample, as the pore diameter of the sample was found to increase for the 18 wt% catalyst [25].

3.3.1.3 Powder X-Ray Diffraction

The Small Angle X-ray Scattering (SAXS) diffraction pattern of the SBA-15, shown in the Appendix 1(A1.3.1), displayed three characteristics peaks between 2θ values of 0 to 2.

An intense peak corresponding to the (100) plane is observed with minor reflections corresponding to the (110) and (200) planes, which relates to a $p6mm$ hexagonal symmetry [33, 34]. The XRD patterns of the catalysts and the bare SBA-15 are shown in Figure 3.2.

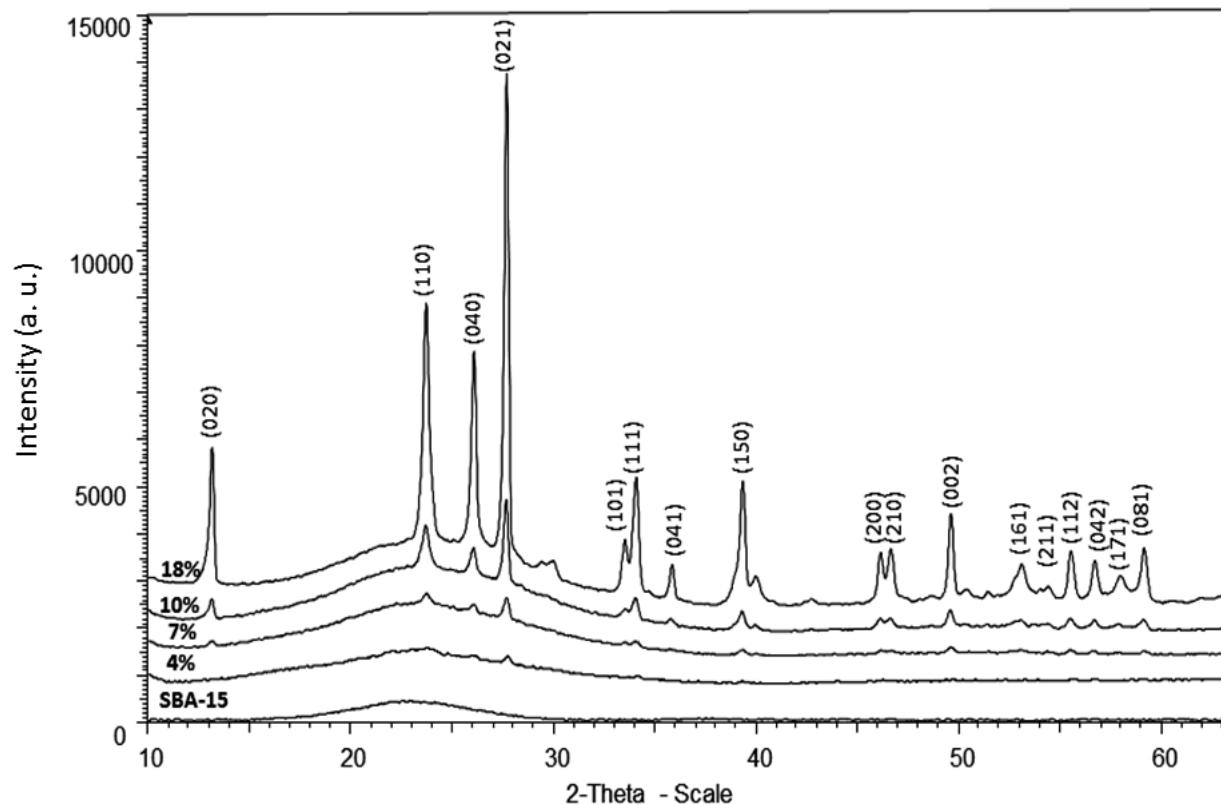


Figure 3.2 XRD diffractograms of catalysts with varying loadings of molybdenum on SBA-15 and SBA-15 support.

The bare support displayed a single broad reflection in the 2θ range of 20 to 30°, representative of amorphous silica [35]. The catalyst with the lowest loading of molybdenum (4 wt%) does not exhibit any characteristic peaks of MoO_3 , probably due to the high dispersion of the metal oxide over the high surface area SBA-15 support [25]. Peaks related to the (110), (040), (021) and (111) planes are just visible. These peaks are more pronounced for the 7 wt% catalyst and many of the other peaks associated with MoO_3 also appeared. These peaks matched by the data contained in JCPDS file No. 05-0508 for $\alpha\text{-MoO}_3$. The intensity of these lines increased with an increase in the metal loading, as can be observed for the 10 and 18 wt% catalysts. The more intense peaks observed for the 18 wt% catalyst were ascribed to the crystalline MoO_3 phase [25].

3.3.1.4 Raman spectroscopy

Raman spectra of the catalysts with 4, 7 and 10 wt% are shown in Figure 3.3 whilst Figure 3.4 shows the Raman spectrum of the 18 wt% catalyst.

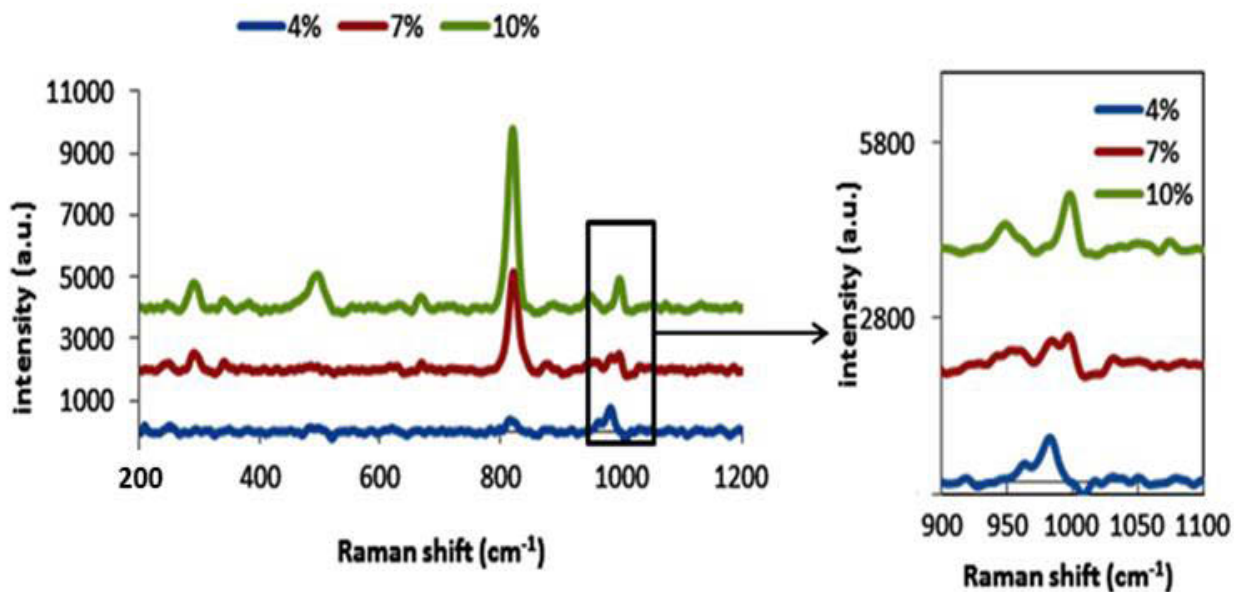


Figure 3.3 Raman spectra of the catalysts with 4, 7, and 10 wt% molybdenum supported on SBA-15.

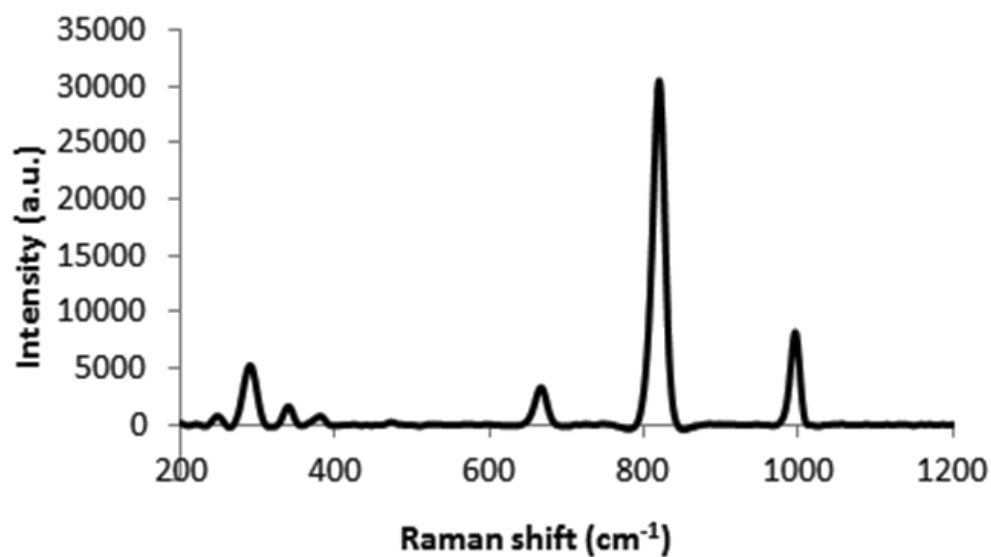


Figure 3.4 Raman spectrum of 18% molybdenum on SBA-15.

For the 4 wt% catalyst, the peak at 982 cm^{-1} is assigned to the Mo=O bond, whereas the peak at 961 cm^{-1} could be attributed to the Mo-O-Si bond [25]. The peak at 815 cm^{-1} could be assigned to the Mo-O-Mo linkage, due to the spectra being recorded at ambient conditions [24]. Based on the peak intensities, at this loading, monomeric MoO_x species were found to be dominant. With the 7 wt% Mo catalyst, the formation of poorly dispersed crystalline MoO_x species were confirmed with the peaks present at 999 cm^{-1} , 833 cm^{-1} and 665 cm^{-1} . These peaks were assigned for the M=O stretch, Mo-O-Mo asymmetric and symmetric stretch respectively. In addition, peaks were observed at 981 cm^{-1} and 954 cm^{-1} , assigned to Si-O-Mo and polymolybdate species respectively [24]. These observations were found in accordance with the XRD data, as at this loading, three peaks for MoO_3 started appearing in the 2θ range of 20 to 30° . With a further increase in the Mo loading to 10 and 18 wt%, the peak at 822 cm^{-1} for Mo-O-Mo intensified, which would indicate the formation of MoO_3 crystallites on SBA-15. For the 10 wt% Mo loading, the intensity of the peak at 952 cm^{-1} was enhanced compared to the 7 wt% molybdenum loading, indicating a higher concentration of polymeric MoO_x species, whereas the peak for Mo-O-Si bonding is not visible due to the higher concentration of molybdenum. At the highest weight loading, peaks for crystalline MoO_3 were found as the most intense peaks (Figure 3.4), with no peaks being observed for the polymeric MoO_x species. The appearance of crystalline MoO_3 also resulted in the appearance of peaks in the lower region of the spectrum, at 463 cm^{-1} associated with the O-Mo-O stretching and bending, 357 cm^{-1} for the O-Mo-O scissor mode, 332 cm^{-1} for O-Mo-O bending and 285 cm^{-1} for the O=Mo=O wagging mode [36]. Thus, based on the above results, at lowest Mo loadings, the molybdenum species were shown to exist in the form of monomeric and to a minor extent, as polymeric MoO_x species; whereas with 7 wt% Mo loading, the co-existence of crystalline, monomeric and polymolybdate species was noted. With a further increase in molybdenum loadings to 10 wt%, an increased concentration of crystalline and polymeric MoO_x species was detected. On the other hand, only crystalline MoO_3 was identified at the highest loading.

3.3.1.5 SEM and TEM studies

A morphological investigation of the prepared catalysts was carried out using TEM and SEM. Figure 3.5a-d shows the TEM images and Figure 3.6a-d shows the SEM images of the 4, 7, 10 and 18 wt% molybdenum loaded catalysts supported on SBA-15. The TEM image of the SBA-

15 showed 2-dimensional ordering and hexagonal mesoporous channels (Appendix 1, A1.3.2). The 2-dimensional ordering of the mesoporous channels was maintained for 4, 7 and 10 wt% molybdenum loadings, which is consistent with the surface area and physisorption analyses, whereas for the 18 wt% catalyst, the 2-dimensional ordering is disrupted.

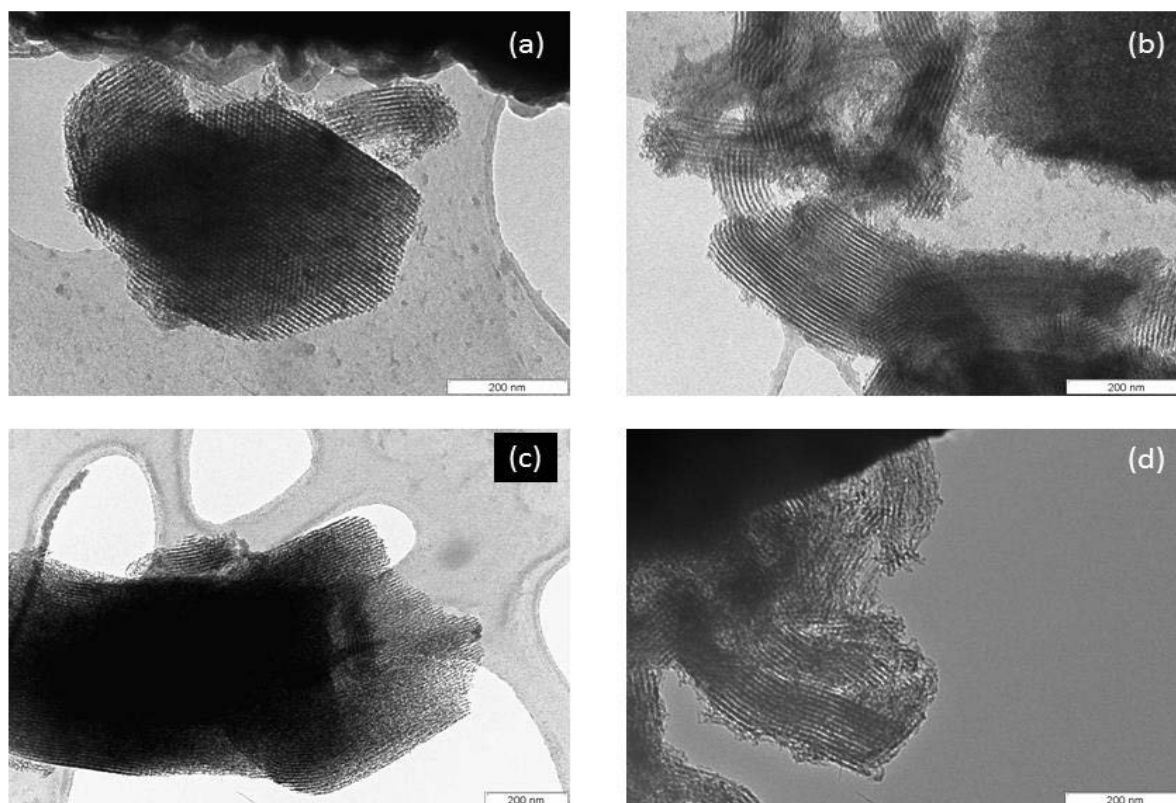


Figure 3.5 TEM images of 4 wt% (a), 7 wt% (b), 10 wt% (c) and 18 wt% (d) molybdenum supported on SBA-15 respectively.

The SEM image of SBA-15 displays a characteristic wheat like morphology of SBA-15 (Appendix 1, A1.3.3). Figure 3.6 shows the SEM images of the loaded catalysts. At lower Mo loadings (4 and 7 wt%), the SEM images of the catalysts (Figure 3.6a and 3.6b) showed no change in the morphology of SBA-15. This suggests that the MoO_x species are present in the form of very small MoO_x clusters or MoO_x nanoparticles. The catalyst with the 10 wt% Mo loading (Figure 3.6c) showed the presence of needle shaped particles on the wheat like morphology of SBA-15. A further increase in the Mo loading caused the appearance of MoO_3 crystallites on the surface of SBA-15, as observed in Figure 3.6d [25]. From EDS mapping, an

increase in molybdenum loading results in aggregation of the molybdenum species on the surface of SBA-15 (Appendix 1, A1.3.4)

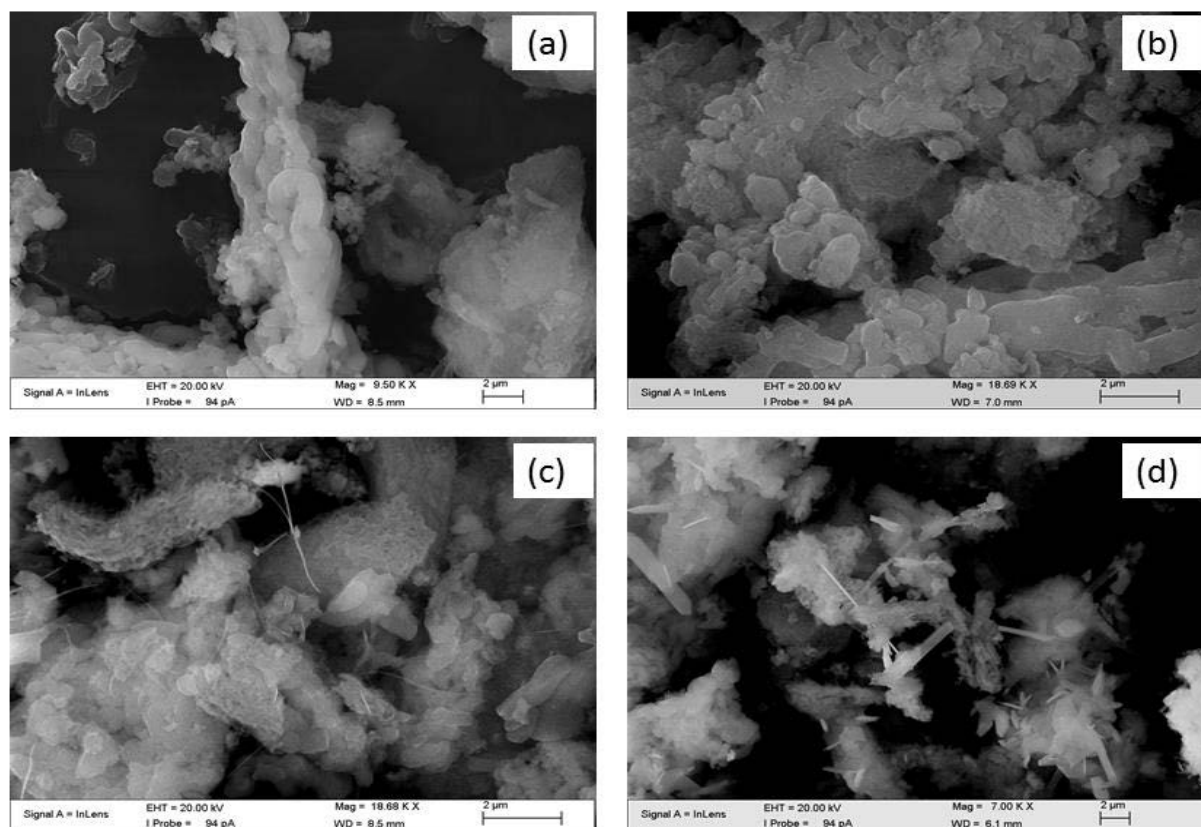


Figure 3.6 SEM images of 4 wt% (a), 7 wt% (b), 10 wt% (c) and 18 wt% (d) molybdenum supported on SBA-15 respectively.

3.3.2 Catalytic results

3.3.2.1 Catalytic testing of molybdenum supported on SBA-15

Figure 3.7 shows the effect of molybdenum loading on the conversion of *n*-octane at 450 °C, at a C:O ratio of 8:3 and a GHSV of 4000 h⁻¹. At the outset, the catalytic activity of the SBA-15 was assessed and was found to be active, but non-selective to C8 products, as it gives greater than 60% selectivity to cracked products and CO_x. The activation of *n*-octane occurs through the activated oxygen species and this is also supported by the complete oxygen conversion obtained over the SBA-15 support. Here, the gaseous oxygen adsorbs on the surface of SBA-15 and undergoes the formation of activated oxygen species, such as O₂²⁻, O₂⁻ and O⁻ species, which are responsible for the formation of carbon oxides and cracked products [37, 38].

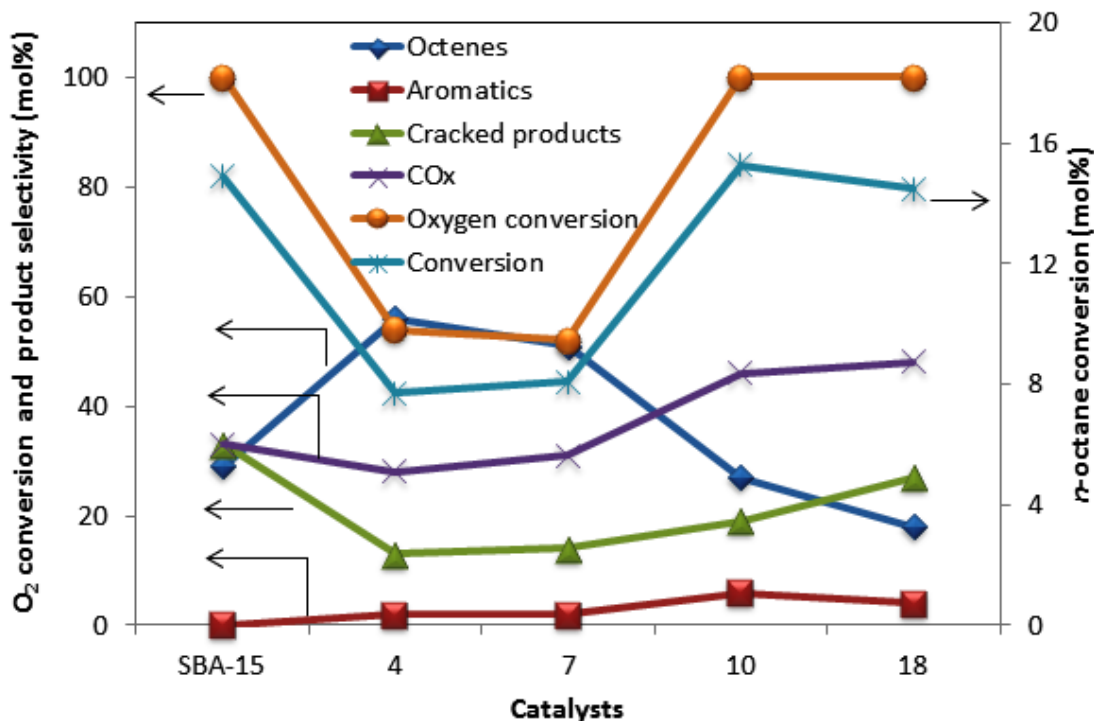


Figure 3.7 Conversion (oxygen and *n*-octane) and product selectivity as a function of weight loadings of molybdenum supported on SBA-15 (Temperature = 450 °C, GHSV = 4000 h⁻¹ and C:O = 8:3).

With the supported catalysts, no significant difference in the *n*-octane conversion is observed for the 4 and 7 wt% catalysts, suggesting the existence of similar species on the support surface. Although at 7 wt% Mo loading, a small amount of MoO₃ crystallites were also observed, together with the monomeric and polymeric MoO_x species, it appears that these MoO₃ crystallites did not affect the catalysis significantly. With the 10 wt% Mo catalyst, a significant rise in *n*-octane conversion was noted and it was also evident in the oxygen conversion. The increased *n*-octane conversion with this catalyst could be due to the activated oxygen species as a result of the aggregation of MoO_x species, forming MoO₃ crystallites, thus causing the gaseous oxygen to interact with an increased exposed surface area of the support and forming activated oxygen species. With the other two catalysts of lower loading, this was not the case, due to the high dispersion of the molybdenum oxide species preventing gaseous oxygen from interacting with the support surface. With a further increase in the molybdenum loading to 18 wt%, similar *n*-octane and oxygen conversion was recorded which emphasises that the

conversion over the catalyst with highest molybdenum loading is due mainly to adsorbed oxygen species.

The octenes selectivity was at its highest over the catalysts with low molybdenum content, that is for the 4 and 7 wt% catalysts. This suggests that for these systems, the presence of monomeric and polymeric MoO_x species, which arise from the low molybdenum loading, show high selectivity to the ODH of *n*-octane for the formation of olefins. This was also observed by Lou *et al.* [25] for ethane oxidation over MoO_x/SBA-15 to produce ethylene. The 10 and 18 wt% catalysts showed a decrease in the selectivity to octenes with a subsequent increase in CO_x and cracked product selectivity, which could be attributed to the non-selective activated oxygen species on the exposed support [37, 39]. A slight increase in the aromatic selectivity was observed for the 10 wt% catalyst due to the presence of polymeric MoO_x species, but it showed a decrease in selectivity over crystalline MoO₃ species present on the 18 wt% Mo catalyst. The formation of CO_x also increased over the 18 wt% catalyst, when compared to bare SBA-15, which could be attributed to the crystalline MoO₃ species on the support.

The *n*-octane consumption rate and ODH products formation rate is shown in Figure 3.8.

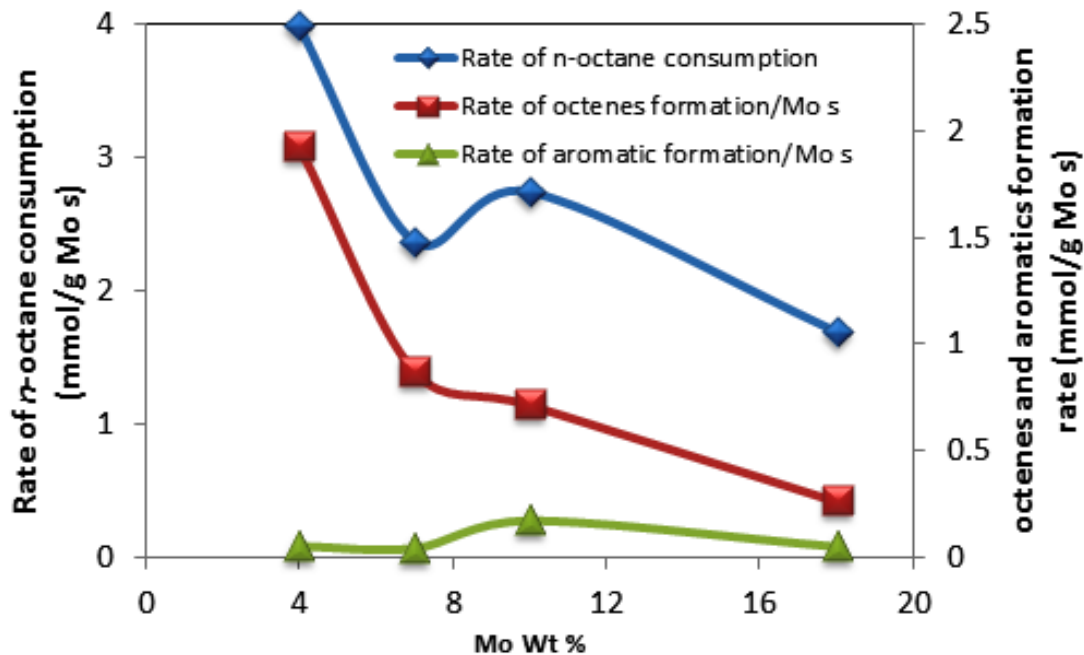


Figure 3.8 Rate of *n*-octane consumption and rate of formation of octenes and aromatics over the different wt% of molybdenum supported on SBA-15 (Temperature = 450 °C, GHSV = 4000 h⁻¹ and C:O = 8:3).

The catalyst with the lowest loading i.e. the catalyst with a higher proportion of monomeric species, showed a higher rate of *n*-octane consumption, as well as octenes formation, compared to the other catalysts. With an increase in molybdenum loading, the consumption rate decreased due to the presence of MoO₃ crystallites, however, the Raman peaks corresponding to polymeric MoO_x species displayed an increasing intensity up to 10 wt% Mo loading, implying that the concentration of polymeric MoO_x species was higher over this catalyst. The polymeric MoO_x species are reported to be active in the ODH of alkanes [40]. The increased formation rate of aromatic products could be related to presence of the polymeric MoO_x species. In the presence of crystalline MoO₃ species (18 wt% Mo/SBA-15), the *n*-octane conversion rate, as well as the ODH rate, decreased. This was accounted for by the lower accessibility to the polymeric MoO_x species which resulted in an increased formation of adsorbed oxygen species on the support [41].

The rate of alkane consumption is dependent on both the support, as well as the nature of MoO_x species that are on it. Lou *et al.* [25] showed that the polymeric MoO_x species over SBA-15 possess higher rates of ethane consumption due to the higher reducibility of the polymeric MoO_x species. Chen *et al.* [27] studied propane ODH over MoO_x/ZrO₂ catalysts and showed that the decrease in the rate of propane consumption could be attributed to the increasing M=O bond strength. Further, for the oxidation of propane over MoO_x/Al₂O₃, by the same authors, it was suggested that the propane reaction rates decreased as the molybdenum surface density increased from the typical monolayer coverage to 3-dimensional structures such as crystalline MoO₃. This, they attributed to the poor accessibility of propane to the Mo centres at higher Mo loadings.

The ODH product yields for the support and catalysts are shown in Table 3.2. The product yields increased with an increase in molybdenum loading up to 10 wt%, whereas a further increase in molybdenum content to 18 wt% resulted in a decrease in the ODH product yield. With the decreasing content of monomeric MoO_x species, the yield towards octenes decreased, however, with an increase in polymeric MoO_x species, the yield towards aromatics increased. This indicates that over monomeric MoO_x species, the primary oxidation of *n*-octane to octenes was favoured, whereas, over the polymeric MoO_x species, octenes oxidised further to aromatics due to the increased lattice oxygen availability from the polymeric MoO_x species.

Table 3. 2 Yields of octenes and aromatic products (Temperature = 450 °C, GHSV = 4000 h⁻¹ and C:O = 8:3).

	SBA-15	4%	7%	10%	18%
Total ODH yield	3.99	4.40	4.28	5.03	3.14
Octenes	3.99	4.29	4.08	4.05	2.63
1-octene	0.94	0.66	0.69	0.55	0.44
<i>trans</i> 2-octene	1.01	1.12	1.05	1.05	0.68
<i>cis</i>-2-octene	0.71	0.73	0.63	0.69	0.47
<i>trans</i> 3-octene	0.51	0.86	0.85	0.90	0.54
<i>trans</i> 4-octene	0.82	0.91	0.86	0.87	0.49
Aromatics	0.00	0.12	0.20	0.98	0.52
Ethyl benzene	0.00	0.02	0.08	0.44	0.21
Styrene	0.00	0.05	0.09	0.29	0.19
xylene	0.00	0.04	0.03	0.26	0.11

Under the catalytic conditions studied, the highest yield was obtained for the *trans* 2-octene isomer, followed by *trans* 3-octene, *trans* 4-octene, *cis* 2-octene and then 1-octene. The *trans*-isomers are thermodynamically more stable than the *cis*-isomers, as the bulky groups are positioned in opposite directions. The *cis* 2-octene was the only *cis*-isomer observed to form in the reaction.

The octene breakdown gives a general idea about the activation position in the carbon chain of *n*-octane. The percentage activation at each carbon atom was calculated by normalising the number of moles of octenes formed during the reaction, shown in Appendix 1 (A1.3.5) A3.5, which showed that around 45% of activation was achieved alone at the C2 position, whereas the rest, 55% activation, occurred at C1, C3 and C4. The activation at C3 and C4 was found to be comparable. The activation at these positions are reported to be difficult, because of the thermodynamic and steric requirement of the octyl radical species, which play a vital role in deciding the activation of a carbon atom in the carbon chain, although the activation energies for activation at C2, C3 and C4 are not very different [29, 30]. The least activated position was at C1. The lower yield of 1-octene can be related to the observation made previously that 1-octene preferentially undergoes 1-6 cyclisation, followed by dehydrogenation to give ethyl benzene and styrene, whereas, *trans* 2-octene undergoes 2-7 cyclisation to give o-xylene [29].

The 1-octene isomer possesses six sequential saturated carbon atoms which can act as a backbone for the formation of aromatics, whereas, in case of other octene isomers, unsaturation at carbon number 2, 3 and 4 brings rigidity in the carbon chain [42].

Overall, the total ODH products yield was found highest with the 10 wt% Mo/SBA-15 catalyst under the conditions tested. This motivated a study to investigate the effect of temperature, carbon to oxygen ratio and GHSV toward improving the yield of the ODH products.

3.3.2.2 Effect of Temperature on 10 wt % molybdenum supported on SBA-15

The data given in Table 3.3 shows the effect of temperature on the *n*-octane conversion and product selectivity for the 10 wt% molybdenum loaded catalyst. The conversion increased with an increase in temperature and increased suddenly at 450 °C, possibly due to the activated oxygen species and to a lesser extent by the polymeric MoO_x species. With a further increase in temperature, a further gradual increase in conversion was recorded.

Table 3.3 *n*-Octane conversion and products selectivity of the 10 wt% molybdenum supported on SBA-15 (C:O = 8:3, GHSV = 4000 h⁻¹)

Temp. °C	Conv. %	C1-C6			C ₈		C6-C7		Oxygenated	
		Alkenes	Octenes	Aromatics	Dienes	Octanones	aromatics	CO	CO ₂	aromatics
350	0.7	0	53	0	0	0	0	0	47	0
400	3.3	22	37	8	4	4	2	0	19	4
450	15.2	19	27	6	1	0	2	26	21	1
500	19.6	26	24	9	1	0	2	20	19	0
550	20.9	27	21	12	1	0	3	19	17	0

At 350 °C, only octenes and CO₂ were detected; the formation of these products at this temperature is possibly due to the activated oxygen species (CO₂ formation) and exposed surface hydroxyl groups (octenes formation) of the catalyst [37]. When the temperature was increased to 400 °C, a significant decrease in the octenes selectivity was recorded and this was compensated by an increase in cracked products, aromatics, dienes and oxygenated aromatics selectivity. At 450 °C, the octenes selectivity decreased further with a subsequent increase in CO selectivity, which possibly indicates the consecutive oxidation of octenes by the lattice oxygen [43]. When the temperature was increased even further, the selectivity to aromatics increased, however, the octenes selectivity did not show a significant change. The selectivity to

cracked products was found to be similar over the increasing temperature range, suggesting that these products are probably forming directly from octane.

3.3.2.3 Effect of C:O ratio over 10 wt% molybdenum supported on SBA-15

To verify the conversion dependence on the oxygen content, the temperature was kept constant at 450 °C and the oxygen concentration in the feed was varied. The C:O ratios studied were 8:2, 8:3 and 8:4. The effect of the C:O ratio over the catalytic activity of the 10 wt% Mo/SBA-15 catalyst is shown in Figure 3.9.

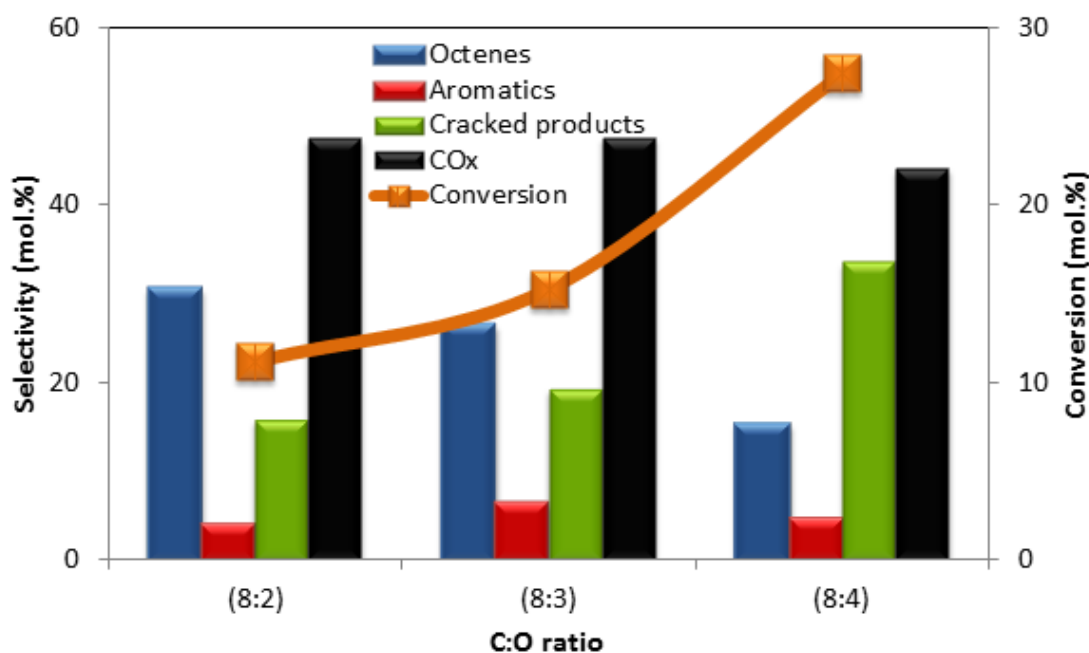


Figure 3.9 Effect of C:O ratio over the catalytic activity of 10 wt% molybdenum supported on SBA-15 (Temperature = 450 °C, GHSV = 4000 h⁻¹)

The conversion of *n*-octane was found to be dependent on the oxygen concentration in the feed. The lowest conversion was observed with the C:O ratio of 8:2, whereas the highest conversion was found with a ratio of 8:4. This can be explained by an increase in the strength of the oxidative environment which easily activates *n*-octane to thermodynamically stable products such as H₂O and CO₂ [28]. The oxygen content in the feed also influenced the product profile of the catalyst. The highest octenes selectivity was observed when the feed is enriched with the

hydrocarbon. At this ratio (8:2), the oxygen in the feed is utilized for the reoxidation of the reduced phase of the catalyst and further degradation of octenes is prevented. However, in the case of more oxygen in the feed, the increased oxygen content results in either consecutive or over oxidation of the products formed. This is evident from the CO and CO₂ selectivity data (Appendix 1, Table A1.3.1). With an increase in the oxygen content, the selectivity to CO increased, whilst the selectivity to CO₂ decreased. The increase in oxygen content also resulted in a decrease in the octene selectivity and contributed to the formation of cracked products. The aromatics selectivity increased initially with oxygen content in the feed and then decreased with the feed containing the highest oxygen concentration. The CO_x selectivity was similar over the 8:2 and 8:3 ratios and showed a decrease with a further increase in oxygen concentration, with a subsequent increase in cracked product selectivity.

3.3.2.4 Effect of GHSV

To investigate the effect of varying the GHSV, the catalytic testing was carried out at a temperature of 450 °C and at a C:O ratio of 8:3 (Figure 3.10 and Figure 3.11).

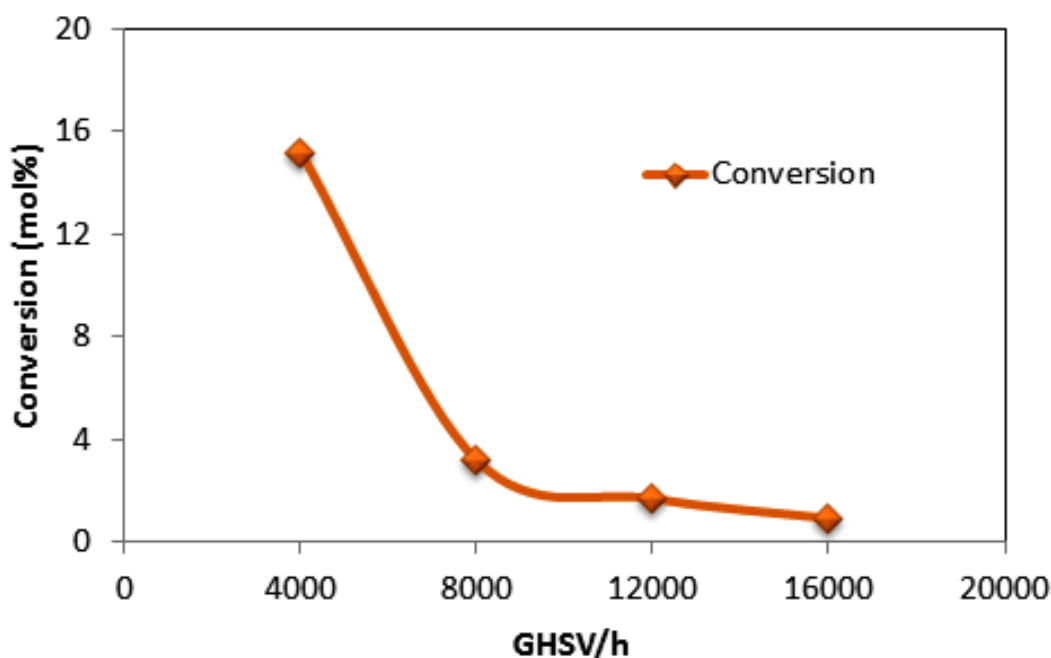


Figure 3.10 Effect of GHSV on *n*-octane conversion with 10 wt% molybdenum supported on SBA-15 (Temperature = 450 °C and C:O = 8:3)

The GHSV investigated were 4000, 8000, 12000, and 16000 h⁻¹. The conversion as expected decreased with an increase in the GHSV (Figure 3.10), due to the decreased residence time of the feed over the catalyst. The products observed at a GHSV of 4000 h⁻¹ were octenes, aromatics, cracked products, CO and CO₂, whereas octenes, cracked products and CO₂ were the only products observed at the highest GHSV tested.

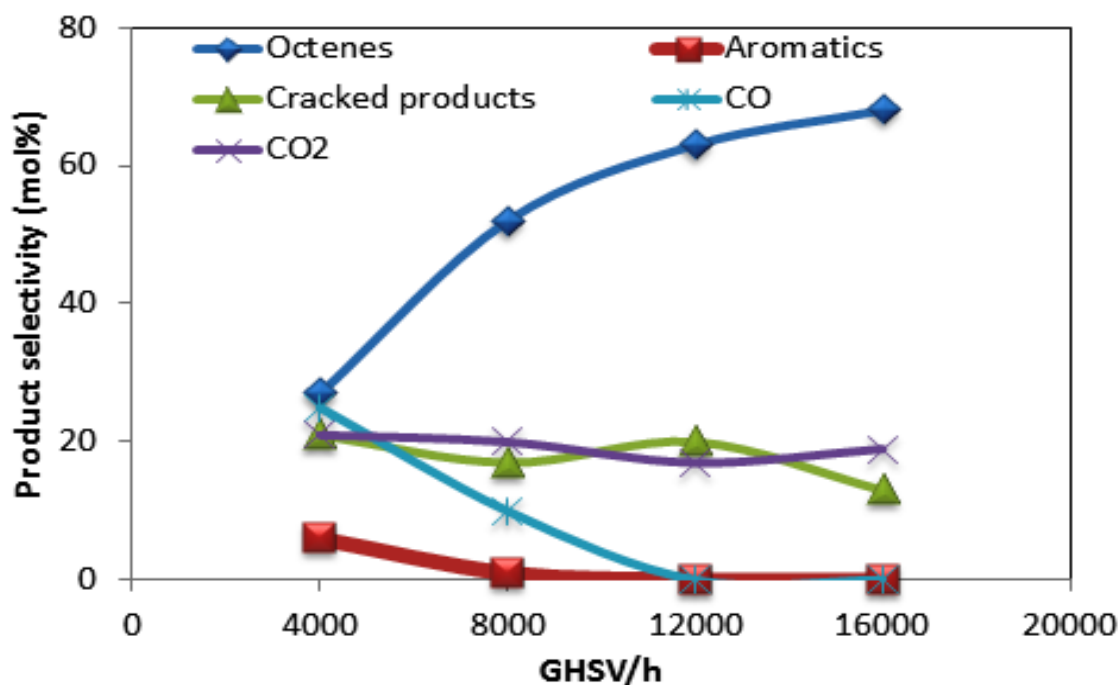


Figure 3.11 Effect of GHSV on selectivity to different products on 10 wt% molybdenum supported on SBA-15 (Temperature = 450 °C and C:O = 8:3)

The octenes selectivity increased from 24% at 4000 h⁻¹ to approximately 70% at 16000 h⁻¹. Concurrently, CO selectivity and to a lesser extent, aromatics selectivity decreased in this same range of space velocity. However, cracked products and CO₂ selectivity remained relatively stable. These observations indicate that octenes, CO₂ and cracked products are most likely the primary products of *n*-octane ODH, whereas CO and aromatics were formed from secondary oxidation of octenes.

3.4 Summary and conclusions

At lower loadings of molybdenum (4 and 7 wt%), MoO_x was shown to exist predominantly as monomeric and to a lesser extent, as polymeric MoO_x species, although the presence of crystalline MoO₃ species was observed at 7 wt% molybdenum loading. At a loading of 10 wt%, co-existence of polymeric MoO_x and crystalline MoO₃ was detected. A further increase in the molybdenum loading resulted in the formation of crystalline MoO₃ on the support.

Under the reaction conditions, the support was found to be active, but produced mainly cracked products and CO_x. The introduction of metal oxide, up to a loading of 7 wt% on SBA-15, caused a decrease in the *n*-octane conversion, probably due to the interaction of molecular oxygen with the support being minimized as less of the support surface is exposed. The conversion, however, increased with an increase in the metal loading above 7 wt% but remained lower than over the bare support. Over the 4 wt% molybdenum catalyst, the formation of octenes was observed as the dominant product, however, at molybdenum loadings of 10 and 18 wt%, the octenes selectivities decreased due to secondary oxidation to form aromatics as well as *n*-octane forming cracked products and CO_x. The highest yield to octenes was observed over the 4% molybdenum loaded catalyst, where the crystalline phase of molybdenum is absent and monomeric MoO_x species dominated. Overall, ODH products yields were higher over polymeric MoO_x species and were found to be at their highest concentration for the 10 wt% molybdenum loaded catalyst. When the reactions of the 10 wt% catalyst were studied as a function of temperature, the aromatic selectivity increased with temperature. When the same catalyst was tested by changing the oxygen content in the feed, the conversion increased with an increase in the oxygen content, however, the selectivity to ODH products decreased with increasing O₂ content. The GHSV studies revealed that aromatics and CO are secondary products, whereas octenes, CO₂ and cracked products are the primary products of *n*-octane oxidative dehydrogenation.

Acknowledgements

This work was financially supported by SASOL, THRIP and the NRF. We also thank the electron microscope unit, UKZN, for microscopic work.

References

- [1] F. Cavani, F. Trifirò, *Catal. Today* 36 (1997) 431-439.
- [2] G. Centi, J.T. Gleaves, G. Golinelli, F. Trifirò, in: P. Ruiz, B. Delmon (Eds.), *Stud. Surf. Sci. Catal., Els.*, 1992, pp. 231-246.
- [3] L.M. Madeira, M.F. Portela, *Catal. Rev.* 44 (2002) 247-286.
- [4] E.A. Mamedov, V. Cortés Corberán, *Appl. Catal. A: Gen.* 127 (1995) 1-40.
- [5] G. Karamullaoglu, S. Onen, T. Dogu, *Chem. Eng. Proces* 41 (2002) 337-347.
- [6] L.E. Cadus, M.F. Gomez, M.C. Abello, *Catal. Lett.* 43 (1997) 229-233.
- [7] O. Desponds, R.L. Keiski, G.A. Somorjai, *Catal. Lett.* 19 (1993) 17-32.
- [8] T. Mizushima, K. Fukushima, H. Ohkita, N. Kakuta, *Appl. Catal. A: Gen.* 326 (2007) 106-112.
- [9] T. Ressler, J. Wienold, R.E. Jentoft, T. Neisius, *J. Catal.* 210 (2002) 67-83.
- [10] M.A. Banares, H.C. Hu, I.E. Wachs, *J. Catal.* 150 (1994) 407-420.
- [11] K. Aoki, M. Ohmae, T. Nanba, K. Takeishi, N. Azuma, A. Ueno, H. Ohfuné, H. Hayashi, Y. Udagawa, *Catal. Today* 45 (1998) 29-33.
- [12] A. Christodoulakis, S. Boghosian, *J. Catal.* 260 (2008) 178-187.
- [13] M. Ruszel, B. Grzybowska, M. Gąsior, K. Samson, I. Gressel, J. Stoch, *Catal. Today* 99 (2005) 151-159.
- [14] H. Liu, E. Iglesia, *J. Catal.* 208 (2002) 1-5.
- [15] Y. Miao, G. Lu, X. Liu, Y. Guo, Y. Wang, Y. Guo, *J. Mol. Catal. A: Chem.* 306 (2009) 17-22.
- [16] G. Tsilomelekis, A. Christodoulakis, S. Boghosian, *Catal. Today* 127 (2007) 139-147.
- [17] A.N. Desikan, W.M. Zhang, S.T. Oyama, *J. Catal.* 157 (1995) 740-748.
- [18] F. Arena, A. Parmaliana, *J. Phys. Chem.* 100 (1996) 19994-20005.
- [19] M.R. Smith, L. Zhang, S.A. Driscoll, U.S. Ozkan, *Catal. Lett.* 19 (1993) 1-15.

- [20] J.P. Thielemann, T. Ressler, A. Walter, G. Tzolova-Müller, C. Hess, *Appl. Catal. A: Gen.* 399 (2011) 28-34.
- [21] M. Faraldos, M.A. Bañares, J.A. Anderson, H. Hu, I.E. Wachs, J.L.s.G. Fierro, *J. Catal.* 160 (1996) 214-221.
- [22] F. Cavani, F. Trifirò, *Catal. Today* 24 (1995) 307-313.
- [23] M.B. Ward, M.J. Lin, J.H. Lunsford, *J. Catal.* 50 (1977) 306-318.
- [24] R.B. Watson, U.S. Ozkan, *J. Catal.* 208 (2002) 124-138.
- [25] Y. Lou, H. Wang, Q. Zhang, Y. Wang, *J. Catal.* 247 (2007) 245-255.
- [26] K. Chen, S. Xie, A.T. Bell, E. Iglesia, *J. Catal.* 198 (2001) 232-242.
- [27] K. Chen, S. Xie, E. Iglesia, A.T. Bell, *J. Catal.* 189 (2000) 421-430.
- [28] E.A. Elkhalfa, H.B. Friedrich, *Catal. Lett.* 141 (2011) 554-564.
- [29] V.D.B.C. Dasireddy, S. Singh, H.B. Friedrich, *Appl. Catal. A: Gen.* 421-422 (2012) 58-69.
- [30] E.A. Elkhalfa, H.B. Friedrich, *Appl. Catal. A: Gen.* 373 (2010) 122-131.
- [31] V.D.B.C. Dasireddy, H.B. Friedrich, S. Singh, *Appl. Catal. A: Gen.* 467 (2013) 142-153.
- [32] D. Zhao, J. Feng, Q. Huo, N. Melosh, G.H. Fredrickson, B.F. Chmelka, G.D. Stucky, *Science* 279 (1998) 548-552.
- [33] L. Cao, T. Man, M. Kruk, *Chem. Mater.* 21 (2009) 1144-1153.
- [34] Z.D. Huang, W. Bensch, L. Kienle, S. Fuentes, G. Alonso, C. Ornelas, *Catal. Lett.* 122 (2008) 57-67.
- [35] J.A. Melero, J. Iglesias, J.M. Arsuaga, J. Sainz-Pardo, P. de Frutos, S. Blazquez, *Appl. Catal. A: Gen.* 331 (2007) 84-94.
- [36] T. Mizushima, Y. Moriya, N.H.H. Phuc, H. Ohkita, N. Kakuta, *Catal. Comm.* 13 (2011) 10-13.
- [37] S. Pradhan, J.K. Bartley, D. Bethell, A.F. Carley, M. Conte, S. Golunski, M.P. House, R.L. Jenkins, R. Lloyd, G.J. Hutchings, *Nat Chem* 4 (2012) 134-139.
- [38] T.Y. Stoylkova, C.D. Chaney, H.T. Lechert, C.P. Bezouhanova, *Appl. Catal. A: Gen.* 203 (2000) 121-126.
- [39] C. Boyadjian, B. van der Veer, I.V. Babich, L. Lefferts, K. Seshan, *Catal. Today* 157 (2010) 345-350.
- [40] K. Chen, E. Iglesia, A.T. Bell, *Stud. Surf. Sci. Catal.*, 136 (2001) 507-512.

- [41] J. Haber, E. Lalik, *Catal. Today* 33 (1997) 119-137.
- [42] H.B.Friedrich, E. A. Elkhalfa, *J. Mol. Catal. A: Chem.* 392 (2014) 22–30.
- [43] L.M. Madeira, M.F. Portela, *Appl. Catal. A: Gen.* 281 (2005) 179-189.

Chapter 4

Oxidation of *n*-octane over NiMoO₄ and NiMoO₄/SBA-15 as catalysts

Abstract

In this study, the oxidative dehydrogenation of *n*-octane was carried out using unsupported NiMoO₄ and SBA-15 supported NiMoO₄ catalysts. The catalysts were prepared by the co-precipitation method and characterised using XRD, ICP-OES, SEM, TEM, and TPR. With the supported catalyst, XRD showed the existence of both α - and β -phases of the NiMoO₄. A study of the effect of C:O ratio revealed that a carbon to oxygen ratio of 8:1 was best to achieve highest selectivity towards octenes. A decrease in C:O ratio to 8:2 and 8:3 gave increased CO_x selectivity. The catalytic testing results showed that the unsupported α -NiMoO₄ phase was more active than the unsupported β -phase, and supported α - and β -phases. Although the α -NiMoO₄ produced octenes as the dominant product, when it was supported on SBA-15, an increase in the selectivity to aromatics was observed. The unsupported β -phase also showed octenes as the dominant product, however, when it was supported on SBA-15, it resulted in decrease in the selectivity to octenes and CO_x, accompanied by a significant increase in cracked products selectivity. Based on the conversion and selectivity profile at lower temperatures, i.e. 350 and 400 °C, with the supported catalysts, the activation of *n*-octane is proposed to occur via surface oxygen, whereas, at higher temperatures (i.e. 450 and 500 °C) the reactions were driven by the lattice oxygen. Among the octene isomers, *trans* 2-octene was dominant, while, among the aromatics, styrene was preferred over ethyl benzene and xylene.

Keywords: NiMoO₄, SBA-15, NiMoO₄/SBA-15, *n*-octane and ODH.

4.1 Introduction

The oxidation of the linear paraffins has become an important topic of research over the past few decades. Paraffins are abundant and also can be easily sourced as by-products from

many Gas to Liquid (GTL) plants operating worldwide, are less expensive than olefins and can be catalytically transformed to the more desirable aromatics or olefins. Traditionally, olefins are obtained through dehydrogenation (DH) processes [1]. Despite having high olefin selectivity, DH is accompanied by some drawbacks, namely, high energy demands, coking, frequent regeneration of the catalyst is needed and a low equilibrium constant between the reaction and product. The drawbacks can be overcome by introducing oxygen in the system, which makes the process exothermic, thereby reducing the activation energy of the reaction. In addition to that, it also avoids coking, which is associated with the dehydrogenation processes and is not equilibrium limited.

Metal molybdates were found to be effective in the ODH of lower alkanes due to their interesting features, viz. structural defects, lattice oxygen mobility and thermal behaviour [2-4]. Several molybdenum catalysts have been tested for the activation of lower alkanes and some of them were found to be very effective in the oxidative dehydrogenation (ODH) of these alkanes [5-7]. Nickel molybdate, NiMoO_4 , was found to be effective in the oxidation of ethane [8], propane [9, 10], butane [11] and *n*-hexane [12, 13] to their corresponding alkenes. NiMoO_4 exists in two different polymorphs, viz. α - NiMoO_4 and β - NiMoO_4 , which exhibit different properties and selectivity patterns in alkane oxidation [8, 12, 14]. NiMoO_4 exists at room temperature as the α -phase, whereas, the β - NiMoO_4 is obtained by heating the α - NiMoO_4 phase to temperatures above 700 °C. α - NiMoO_4 has an octahedral geometry, whereas the β - NiMoO_4 exists in a tetrahedral geometry [12]. The change in the geometry affects the lattice oxygen reactivity, which has been observed in several studies [12, 13, 15]. In most cases, the α - NiMoO_4 phase was found to be more active than the β - NiMoO_4 phase, but the β - NiMoO_4 was more selective to ODH products. The room temperature α -phase was found to be more active and selective for ethane oxidation to ethene than its metastable β -phase [8], but in the case of propane, the metastable phase was found to be more selective to propene than the room temperature phase [16]. A similar observation was noted with *n*-hexane oxidation [12]. Cauzzi and co-workers [17] reported that the selective and high temperature metastable β -phase can be stabilized at room temperature by supporting it on SiO_2 . In addition, supporting the mixed metal oxides was found to be effective in terms of improving their surface area, allowing easier removal of heat and stabilization of the high temperature phase at lower temperatures, and coking, which is associated with unsupported NiMoO_4 is also avoided. Dias and co-workers [15] carried out isobutane oxidation using $\text{NiMoO}_4/\text{SiO}_2$ catalysts. Their results showed that at a 13 wt% loading of NiMoO_4 on SiO_2 , a

higher percent of the metastable β -phase was present, which gave a higher selectivity towards isobutene. When the wt% loading exceeded 26%, the α -phase of NiMoO_4 was dominant, resulting in a decrease in isobutene selectivity [15].

In this study, the high surface area mesoporous material, SBA-15, was used as a support for NiMoO_4 and its efficiency was investigated for the oxidation of *n*-octane. The effect of C:O ratio was investigated over the α -phase of unsupported NiMoO_4 for the oxidation of *n*-octane and the optimised C:O ratio was further employed for the catalytic testing of unsupported and supported NiMoO_4 oxides.

4.2 Experimental

4.2.1 Catalysts preparation

Ammonium heptamolybdate, tetrahydrate ($(\text{NH}_4)_6\text{Mo}_7\text{O}_{24}\cdot 4\text{H}_2\text{O}$, Merck) and nickel nitrate, hexahydrate ($\text{NiNO}_3\cdot 6\text{H}_2\text{O}$, Sigma Aldrich) were used as sources for molybdenum and nickel respectively. The synthesis of NiMoO_4 was carried out by the co-precipitation method [12]. In a typical synthesis, 14.5 g of $\text{NiNO}_3\cdot 6\text{H}_2\text{O}$ and 7.5 g of $(\text{NH}_4)_6\text{Mo}_7\text{O}_{24}\cdot 4\text{H}_2\text{O}$ was dissolved in 100 mL of deionised water to achieve a Ni to Mo molar ratio of 1:1. The prepared solutions were then added slowly to a round bottom flask. The pH of the solution was maintained at 5.7 using aqueous HNO_3 and aqueous NH_3 with the temperature fixed at 45 °C. The reaction mixture was then heated to 85 °C and filtered hot. The solid was dried in an oven and calcined in air at 550 °C for 2 h. The β - NiMoO_4 phase was obtained *in situ* in the reactor by heating it to 720 °C and during the catalytic testing the temperature was maintained above 300 °C. SBA-15 was synthesized using the method proposed by Cao *et al.* [18]. Tetra ethyl ortho silicate (TEOS, Aldrich) was used as a silica source and Pluronic P123 (PEP-PPO-PPE) ($\text{EO}_{20}\text{-PO}_{20}\text{-EO}_{20}$, M.W=5800, Aldrich), as a template. In the preparation, 14.6 g of Pluronic P123 and 0.161 g of the NH_4F were dissolved in 540 mL of 1.3 M HCl and stirred for 1 h. After complete dissolution of the polymer, 30 mL of TEOS was added drop wise to the solution. The resulting gel was stirred for 24 h at room temperature and then transferred to a closed vessel and treated hydrothermally at 100 °C for 24 h. The treated material was then filtered under vacuum and washed with deionised water and dried at room temperature. The material was then calcined at 550 °C for 5 h to remove the organic polymer template. Supported catalysts were also prepared by the co-precipitation method. For the 20% NiMoO_4 loaded catalyst, calculated amounts of the Ni and Mo precursors were added drop wise to the slurry of SBA-15, ensuring that the pH was maintained at 5.7.

4.2.2 Catalysts characterisation

The SBA-15 was characterised by using an Anton Parr Small Angle X-ray Scattering (SAXS) instrument with a line and point collimation 1X-ray tube. The X-ray source used was a sealed Cu tube and the X-ray generator used was PW3830 from PAN analytical operated at 40 kV and 50 mA. The diffraction patterns of the catalysts were obtained using Bruker D8 Advance instrument equipped with the Anton Parr XRK 900 reaction chamber and a TCU 750 temperature control unit. A Cu radiation source ($\lambda = 1.5406 \text{ \AA}$) was used for X-Ray generation. The amount of molybdenum and nickel in the catalysts were determined by inductively coupled plasma-optical emission spectroscopy (ICP-OES) using a Perkin Elmer Optima 5300 DV instrument. A Micrometrics Tristar II was used to determine the surface area, pore volume, and pore diameter of the sample. The samples were degassed by flowing nitrogen at 90 °C for 1 h and at 200 °C, overnight. TEM micrographs were obtained using a Jeol TEM 1010 electron microscope and the images were captured by iTEM software, while the SEM images were recorded using a Zeiss Ultra Plus instrument.

4.2.3 Catalytic Testing

Gas-phase catalytic oxidation of *n*-octane over supported and unsupported NiMoO₄ was carried out in a continuous flow fixed bed reactor (300 mm stainless steel tube, 10 mm I.D.) with temperatures ranging from 350 to 500 °C. The isothermal zone of the reactor tube was determined by conducting a temperature profile of the reactor tube and the catalyst 1 mL by volume of mesh size 600-1000 μm was placed at the centre of the isothermal zone region. The empty spaces below and above of the catalyst in the reactor tube was filled with 24-grit carborundum and the ends were plugged with glass wool. The temperature at the catalyst bed and the furnace were monitored using K-type thermocouples controlled by CB-100 RK temperature control units. A high precision isocratic pump (Lab Alliance Series II) was used to introduce the feed into the reactor with a flow rate of 0.05 mL/min. The reactor lines were maintained at a temperature of 200 °C using heating tape.

The concentration of *n*-octane in the gaseous mixture was maintained at 11.3 % (v/v) using air as an oxidant and nitrogen as a diluent to achieve a flow rate of 67 mL/min. The total volume of the gaseous products at the outlet was measured using a wet gas flow meter (Ritter Drum-Type Gas Meter). The products were analyzed using Perkin Elmer Clarus 400 FID and TCD gas chromatographs equipped with a SGE BP-PONA capillary column (0.25 mm I.D., 50 m length) and a SUPELCO Carboxen (0.53 mm I.D., 30 m length) column,

respectively. A Perkin Elmer Clarus 500 GC-MS was used to identify the unknown products. The calculated carbon balance was between 98-102%. All the data points were obtained in duplicate with an error of 2%.

4.3 Result and discussions

4.3.1 Characterisation of the catalyst

4.3.1.1 Powder X-ray diffraction

The X-ray diffractograms of unsupported α -NiMoO₄ and α -NiMoO₄ supported on SBA-15 are shown in Figure 4.1.

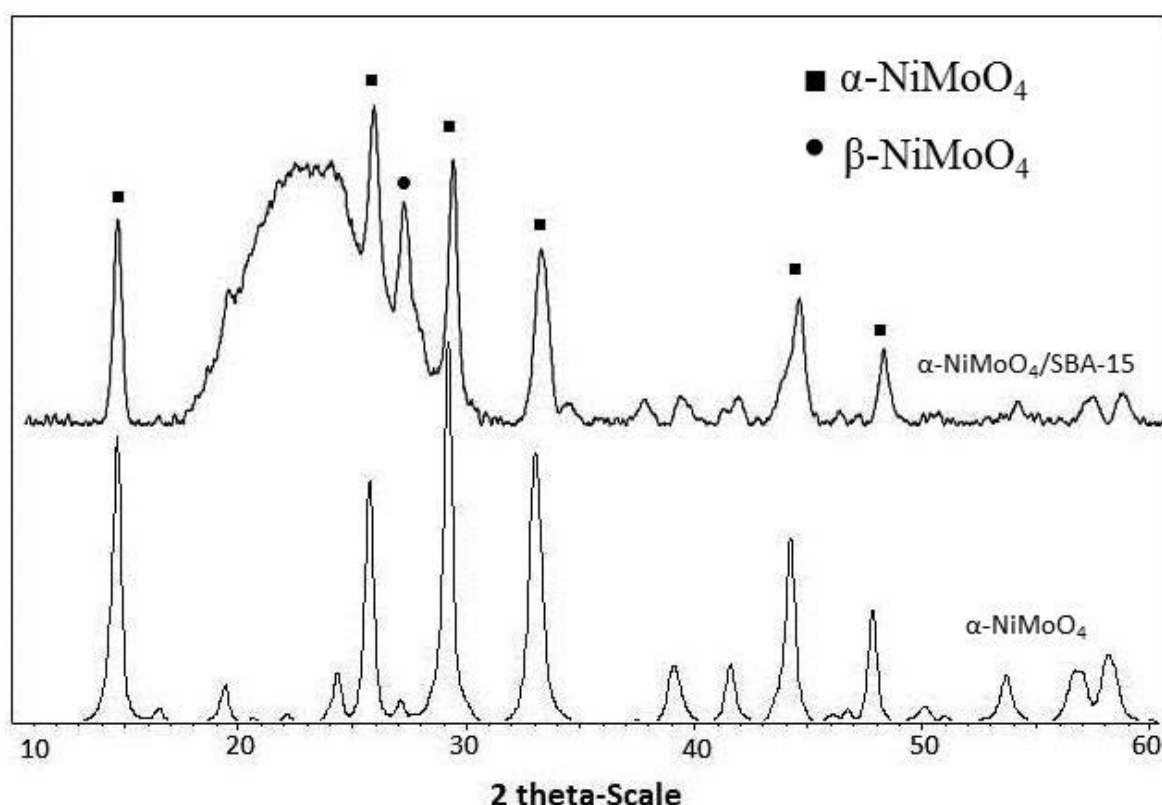


Figure 4.1 XRD of the unsupported α -NiMoO₄ and α -NiMoO₄ supported on SBA-15 catalysts.

In the case of unsupported NiMoO₄, only the thermodynamically stable α -phase was observed. The characteristic peaks for this phase were observed at 2θ values of 14.6°, 24.5°, 26.3°, 29.0°, 33.0°, 44.0°, and 48.0° [12]. The strongest peak observed was at a 2θ angle of 29.0° which is ascribed to the (100) plane. However, when NiMoO₄ was supported on SBA-15, a broad reflection was observed at 2θ values between 20° to 30° which is associated with silica [19] and the characteristic peaks for α -NiMoO₄ were found at $2\theta = 14.5^\circ, 25.6^\circ, 26.9^\circ, 27.5^\circ, 28.9^\circ, 32.9^\circ, 34.0^\circ, 44.0^\circ$ and 47.8° , with a strong peak at 26.9°. In addition to the peaks

for α -NiMoO₄, a peak for β -NiMoO₄ was also observed at a 2θ angle of 27.5° and is consistent with what is found in literature [17]. The existence of both α - and β -NiMoO₄ on SiO₂ has been reported before [15], and the formation of the β -phase on SiO₂ was explained by the interaction of NiMoO₄ with the surface of the support, which contributes to the stabilisation of the β -NiMoO₄ at room temperature [15, 17].

4.3.1.2 SEM and TEM analyses

The SEM images of unsupported NiMoO₄ and NiMoO₄ on SBA-15 are shown in Figure 4.2(A) and (B) respectively and the TEM images for the same catalysts can be seen in Figure 4.2(C) and (D) respectively.

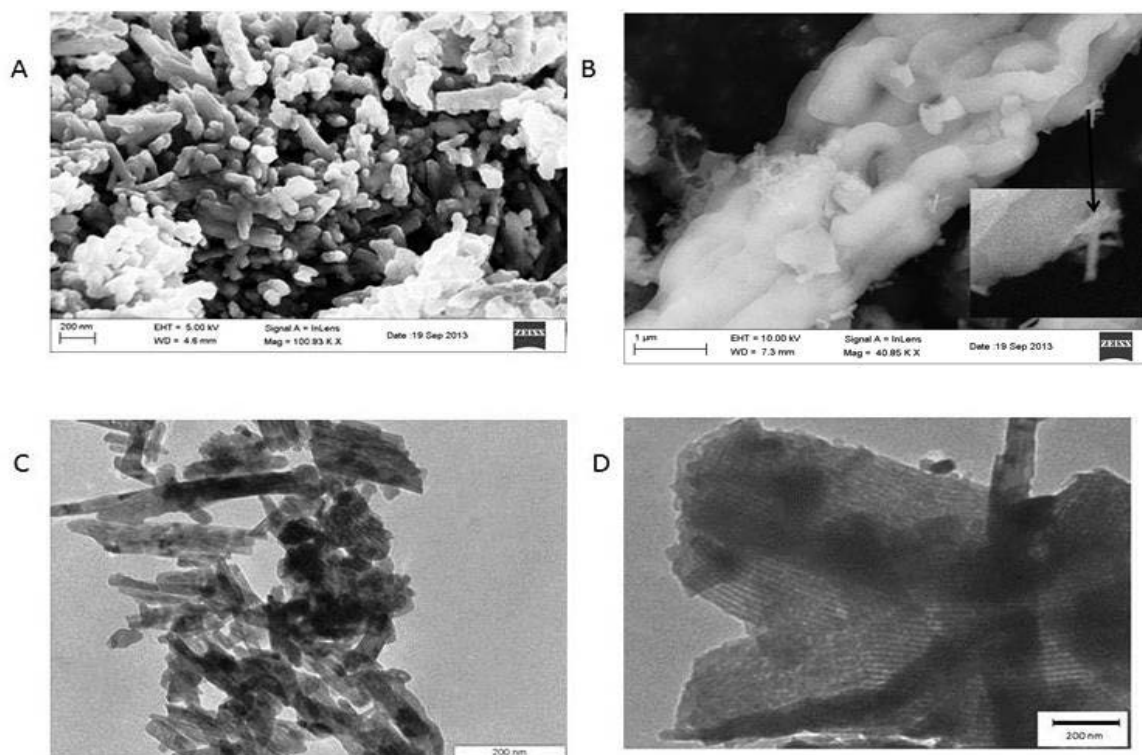


Figure 4.2 SEM images of unsupported NiMoO₄ (A) and supported NiMoO₄ (B); TEM images of unsupported (C) and supported NiMoO₄ (D).

The SEM images show that the unsupported NiMoO₄ possesses a rod-like morphology with varying lengths. These rods are composed of nanosheets of NiMoO₄, which can be seen in the TEM images (Figure 4.2C) [20]. In Figure 4.2(B), small needle shaped nanorods were observed on the characteristic wheat-like morphology of SBA-15. These NiMoO₄ nanorods aggregated to form a cluster as shown in Figure 4.2 (C) [20]. The sheet-like structure of

NiMoO₄ can be seen in Figure 4.2(D) over the 2-dimensional hexagonal ordering of the SBA-15. The NiMoO₄ displayed a thin plate-like morphology with varying shapes and sizes, when it was supported on SBA-15.

4.3.1.3 BET Studies

Surface area, pore volume and pore diameter analyses of the support and prepared catalysts are shown in Table 4.1.

Table 4.1 Effect of NiMoO₄ loadings over the surface area and pore volume on SBA-15

Catalysts	BET surface area/ m²g⁻¹	Pore volume/ cm³g⁻¹	Pore diameter/ nm
NiMoO ₄	52	0.12	10
SBA-15	771	1.30	7
20% NiMoO ₄ /SBA-15	332	0.86	10

When the NiMoO₄ was supported on SBA-15, a significant decrease in the surface area of SBA-15 was observed (771 to 332 m²g⁻¹). Similar observations were noted with the pore volume, which decreased from 1.30 cm³g⁻¹ to 0.86 cm³g⁻¹. The pore diameter showed an increase from 7 to 10 nm. The increase in the pore diameter is probably due to the filling of smaller pores of the support, which subsequently resulted in an increase in the average pore diameter of the catalyst.

4.3.1.4 Temperature programmed reduction study

The TPR of unsupported and supported NiMoO₄ is shown in Figure 4.3.

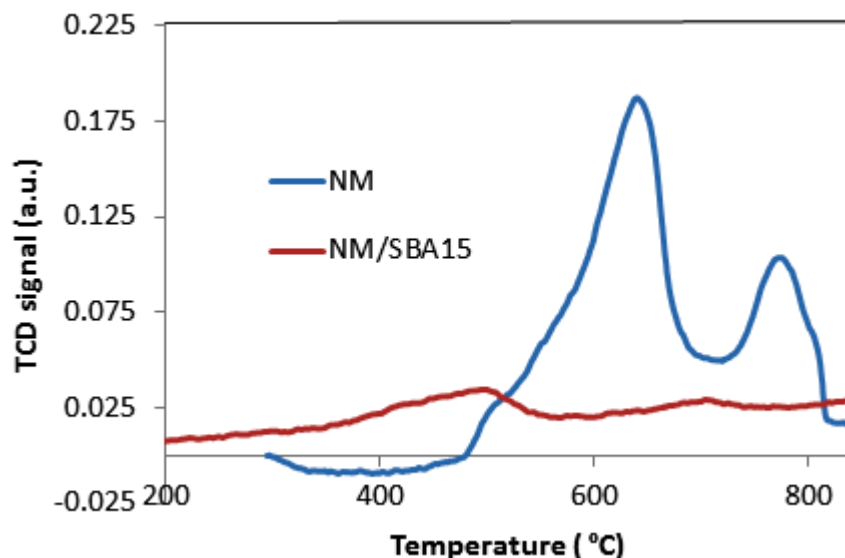


Figure 4.3 TPR of NiMoO₄ and NiMoO₄ supported on SBA-15 (NM = NiMoO₄).

The unsupported and supported catalysts showed two reduction events as observed in Figure 4.3. For unsupported NiMoO₄, the first reduction peak at 632 °C could be attributed to the reduction of NiMoO₄ to a number of possible species such as metallic nickel, MoO₂ and or Ni₄Mo [12]. The high temperature reduction peak accounts for the reduction of MoO₂ to metallic Mo or Ni-Mo alloys or may be intermetallic Ni₃Mo [12]. The reduction temperature of NiMoO₄ was shifted to a lower temperature, 489 °C when it was supported on SBA-15. A similar observation was also reported by Dias *et al.* [15]. The high temperature peak also showed a shift from 764 to 696 °C. The amount of H₂ consumed by the supported NiMoO₄ catalyst was lower than the H₂ consumed by unsupported NiMoO₄ due to the higher content of reducible species.

4.3.2 Catalytic results

4.3.2.1 Blank reaction details

All the reactions were performed in the temperature range of 350 to 500 °C at a GHSV of 4000 h⁻¹. Prior to the catalytic testing, the blank reaction was carried out with 24-grit carborundum, packed in a reactor tube at a C:O ratio of 8:3. The conversion and product selectivity of the blank reaction is shown in Figure 4.4.

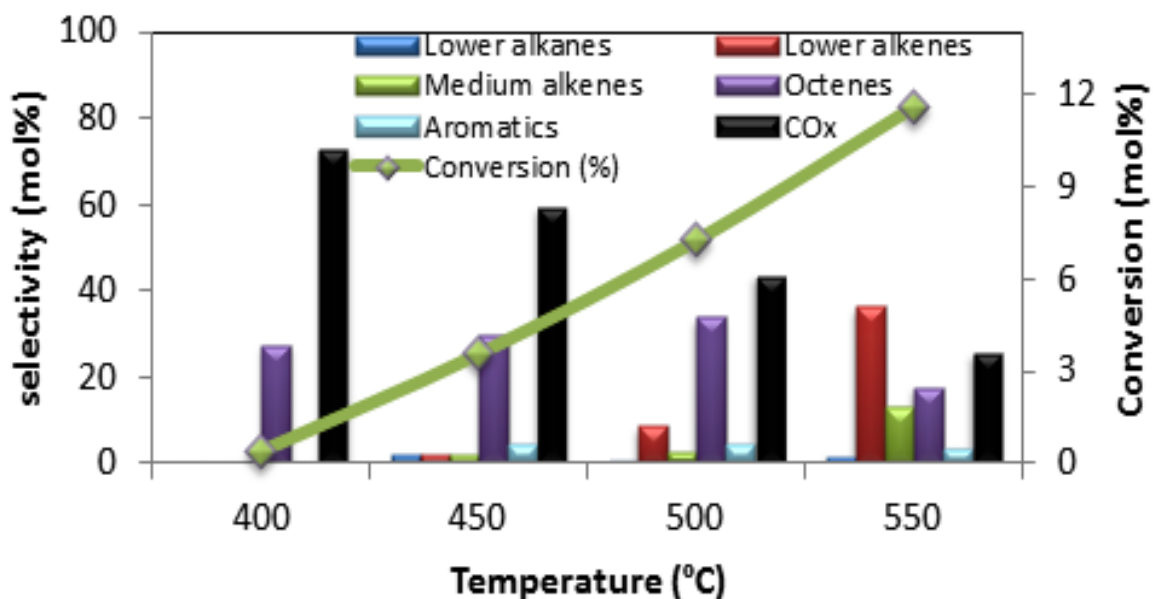


Figure 4.4 Blank reaction results with a carborundum packed reactor tube at a C:O ratio of 8:3 with a GHSV of 4000 h⁻¹.

The conversion increased with an increase in temperature. The lowest conversion was observed at 350 °C and the highest 7.7% was at 500 °C. The dominant product of the reaction at 350 °C was CO_x, however, its selectivity decreased with an increase in temperature with the subsequent appearance of octenes and cracked products. The cracked products included mainly C₂ - C₆ alkenes. Aromatic products were only observed at 450 and 500 °C and their selectivity remained constant. In the absence of a catalysts, it is concluded that the products that are formed are due to gas phase radical reactions [21].

4.3.2.2 Effect of C:O ratio for unsupported α -NiMoO₄

Figure 4.5 shows the effect of the C:O ratio at a GHSV of 4000 h⁻¹ on the conversion of *n*-octane over α -NiMoO₄.

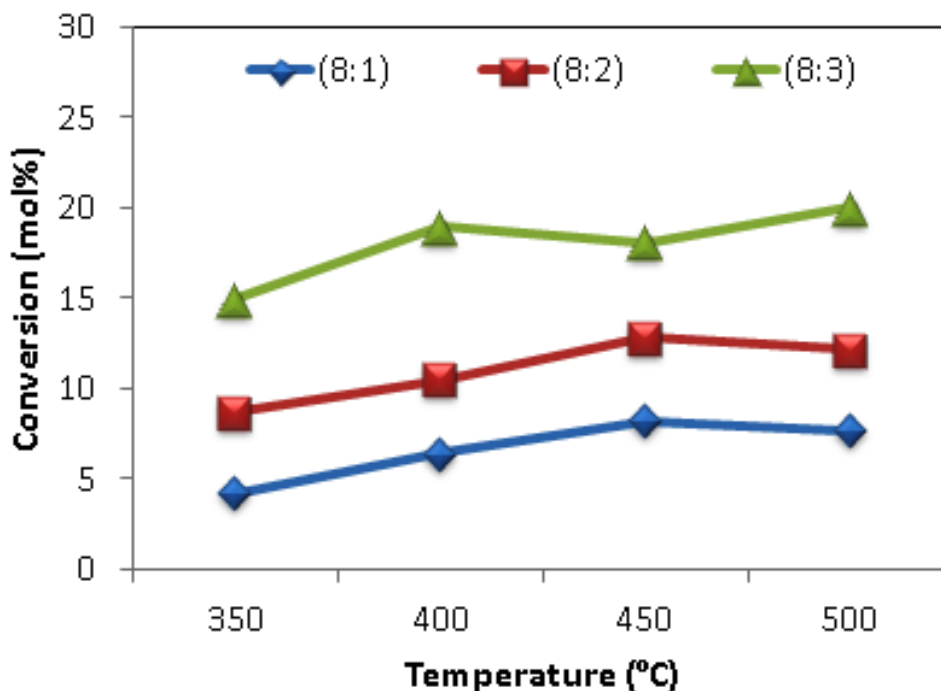


Figure 4.5 Effect of C:O ratio on conversion of *n*-octane over unsupported NiMoO₄ at a GHSV of 4000 h⁻¹.

As expected, the conversion of *n*-octane increased with an increase in temperature and oxygen concentration in the feed. The lowest conversion at all temperatures was observed with a C:O ratio of 8:1. However, at the C:O ratios of 8:1 and 8:2, a slight decrease in conversion was noted at 500 °C, probably due to the reduction of the active NiMoO₄ phase. This was not evident for the 8:3 ratio, since oxygen is likely present in a concentration which allows for the re-oxidation of the reduced NiMoO₄ phase. An increase in oxygen content also resulted in the generation of more physisorbed oxygen species on the surface of the catalyst. These species are claimed to be responsible for the increased conversion and formation of carbon oxides resulting in a decrease in the selectivity to ODH products [13].

The oxygen conversion for all C:O ratios is shown in Figure 4.6. Complete oxygen conversion occurred with the C:O ratio of 8:1 from 400 °C, whereas for the other two ratios, complete oxygen conversion was observed at 500 °C. The oxygen conversion for these two ratios was found to be greater than 80% at temperatures of 450 °C and higher, due to the operating redox cycle. The higher oxygen conversion at the C:O ratio of 8:3 compared to the other ratios at 350 °C is due to the excess oxygen in the feed being utilized for the production of CO₂.

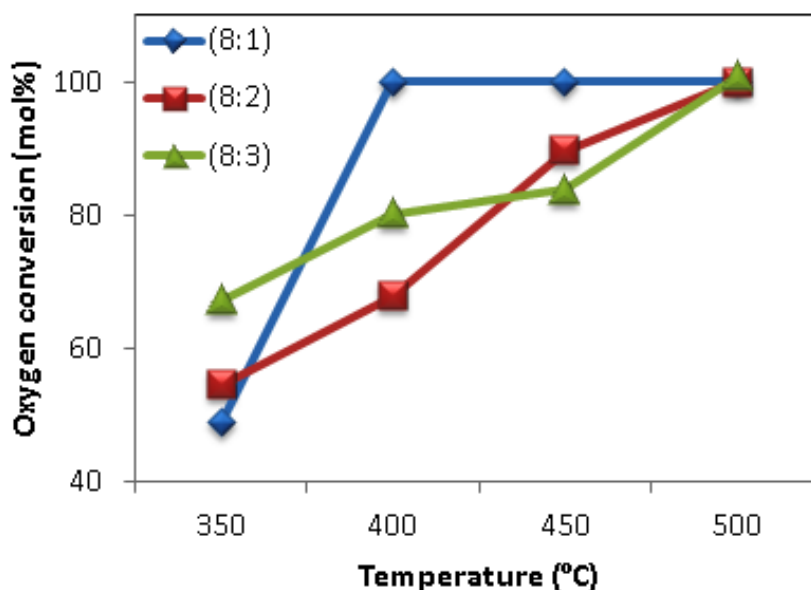


Figure 4.6 Oxygen conversion at varying C:O ratios over unsupported α -NiMoO₄ at a GHSV of 4000 h⁻¹.

The selectivity towards the products at different C:O ratios is shown in Figure 4.7. The oxygen concentration in the feed was shown to impact the products selectivity significantly. As the concentration of oxygen in the feed increased, the octenes selectivity decreased and the selectivity to aromatics and, mainly, CO_x increased. At a C:O ratio of 8:1, octenes were the major products observed at all temperatures, however, selectivity decreased with an increase in temperature, which is possibly due to their secondary oxidation to aromatics and CO_x. At 500 °C, aromatics recorded a slight drop in selectivity, which could be due to the loss in availability of lattice oxygen, since not enough oxygen is available for reoxidation of the reduced phase. The complete consumption of the oxygen at this C:O ratio of 8:1 was also evidenced in Figure 4.5 at 500 °C, which shows that the oxygen is the limiting factor for the conversion, as well as the formation of octenes and to some extent, aromatics. In this hydrocarbon rich feed, the gaseous oxygen is mostly utilised for the reoxidation of the reduced phase which prevents further degradation of the octenes. When the carbon to oxygen ratio was reduced to 8:2, a drop in the octene selectivity was observed, due to the direct oxidation (combustion) of the hydrocarbon feed to CO₂ and the consecutive oxidation of the formed alkenes to CO [9]. At the highest oxygen concentration (8:3), the lowest octenes and highest CO_x selectivity was noted. The increased oxygen content in the feed drives the process to produce thermodynamically stable products such as CO_x and H₂O [23].

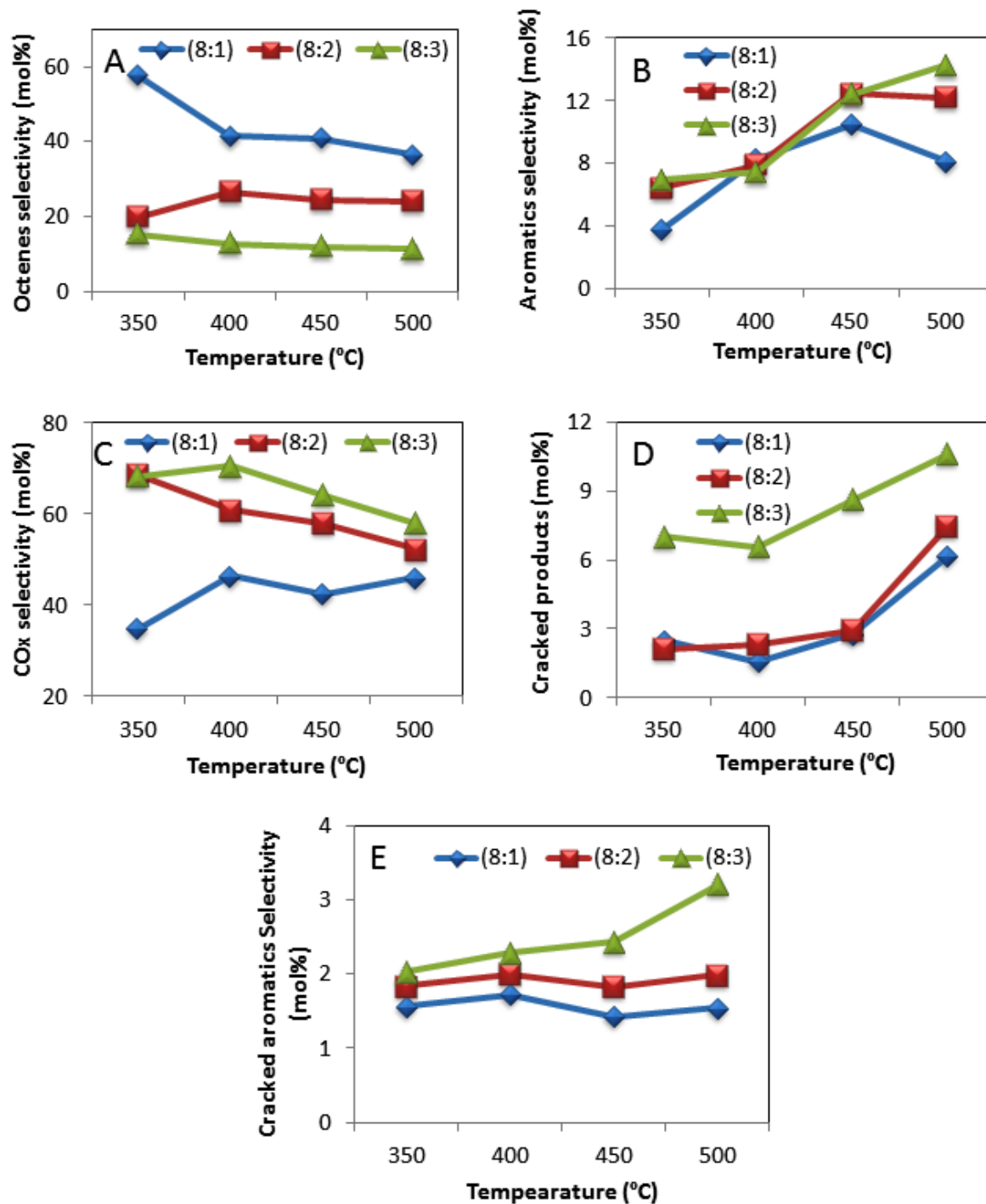


Figure 4.7 Octene (A), aromatics (B), CO_x (C), cracked (D) and cracked aromatics (E) products at different C:O ratios as a function of temperature over unsupported α -NiMoO₄.

The variation in the temperatures was shown to affect the product profile as well. Throughout, an increase in temperature resulted in a decrease in the octene selectivity with a subsequent rise in selectivity towards aromatics [23-25]. In addition, the aromatics selectivity increased with increasing oxygen content. A slight decrease in the aromatics

selectivity was observed at 500 °C for the C:O ratio of 8:1, as the supply of lattice oxygen was depleted. The carbon oxides selectivity is shown in Figure 4.8. With the oxygen lean feed, the CO_x selectivity was found to be lowest, whereas with an oxygen rich environment, a pronounced formation of CO_x was observed. The CO production was found to increase with an increase in oxygen concentration in the feed. This indicates that an increase in oxygen content provides an increasing lattice oxygen supply, which favours the consecutive oxidation of octenes, whereas CO₂ formation proceeds through the parallel reaction with weakly adsorbed oxygen species on the surface of catalyst [22].

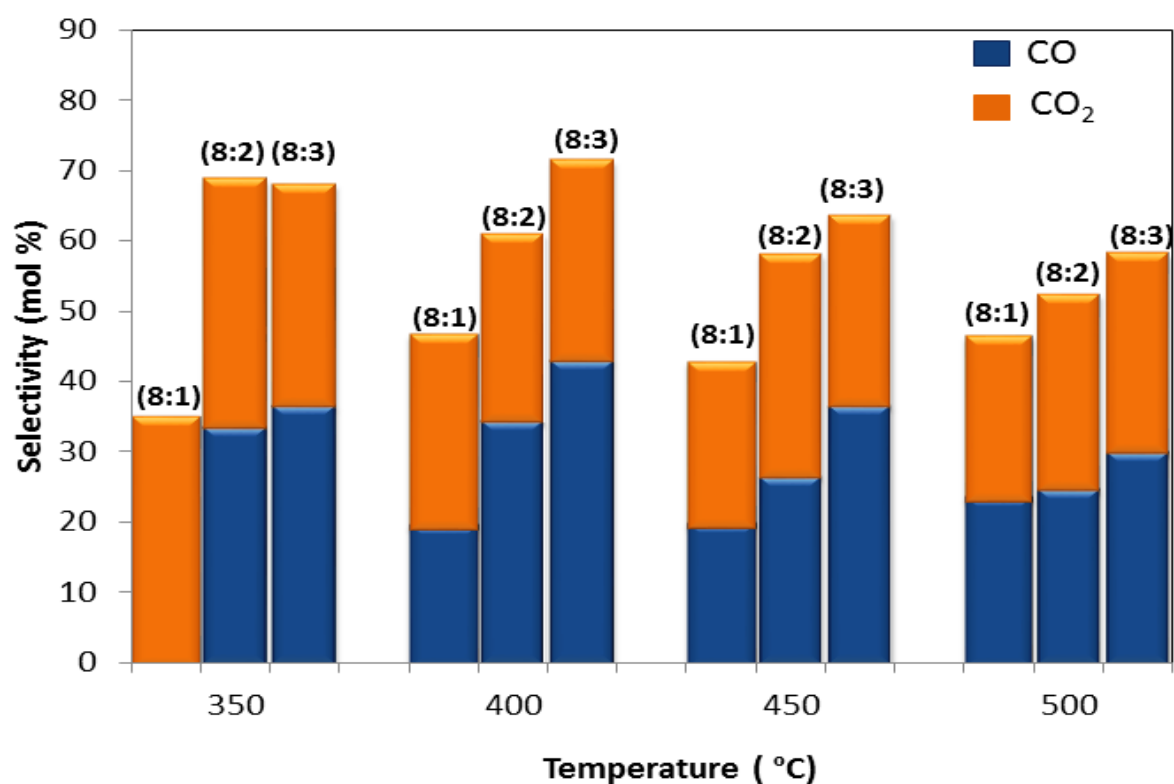


Figure 4.8 CO and CO₂ selectivity at different C:O ratios at a GHSV of 4000 h⁻¹ over α -NiMoO₄ catalyst as a function of temperature.

4.3.2.3 Comparison of *n*-octane conversion for supported and unsupported NiMoO₄

The catalytic testing of the unsupported and supported phases of NiMoO₄ was carried out at an optimum C:O ratio of 8:1 at a GHSV of 4000 h⁻¹. The results obtained for the catalytic testing is shown in Figure 4.9.

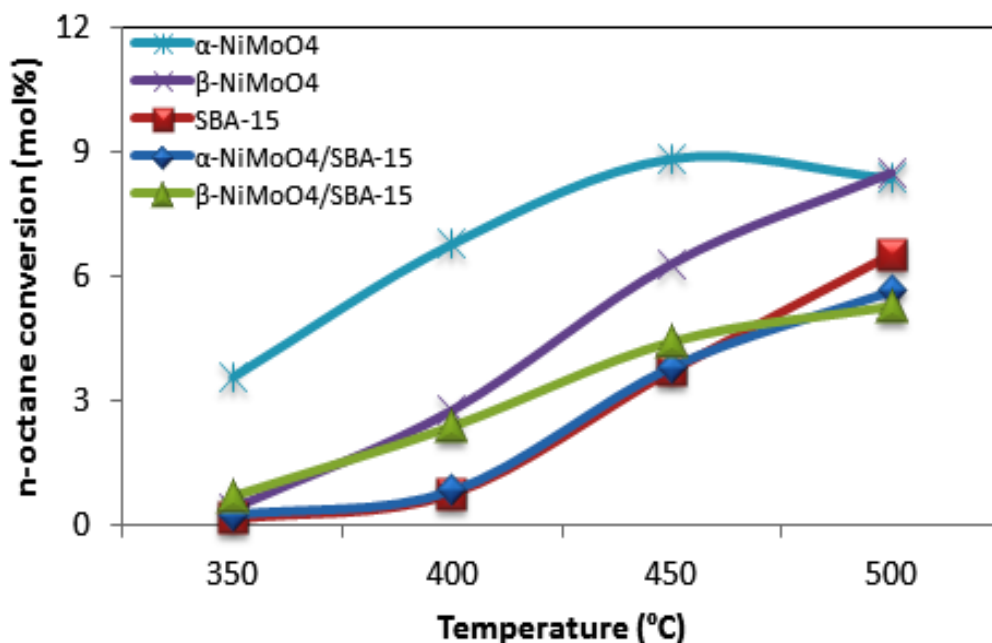


Figure 4.9 Conversion of *n*-octane over different catalysts at a C:O ratio of 8:1 at a GHSV of 4000 h⁻¹.

The β -phase was generated *in situ* by heating the α -NiMoO₄ to 720 °C and then cooling it down to 350 °C before testing. In comparison to other catalysts, unsupported α -NiMoO₄ exhibited higher conversion at all temperatures. The high activity of the α -phase is related to its structural features, such as high surface area and lattice oxygen reactivity [12]. In addition, it was shown that, the α -phase loses lattice oxygen faster than the β -phase, which contributes to its higher reactivity compared to its polymorph [4]. In comparison, the unsupported β -phase showed a lower feed conversion at all temperatures, except at 500 °C.

When comparing the supported catalysts, the β -NiMoO₄ on SBA-15 exhibited a slightly higher conversion than α -NiMoO₄ supported on SBA-15 in the temperature range studied. The reason for the differences in the activity could be the lower surface area of the β -phase compared to the octahedrally co-ordinated α -phase, thereby increasing the exposed surface area of the support for the gaseous oxygen when compared to the α -phase [8]. This may explain the formation of activated gaseous oxygen to form activated oxygen species to produce oxygenates rather than ODH products [26]. This was not observed with the α -phase, since the octahedral geometry, which has a high surface area, hinders the gaseous oxygen from interacting with the surface of the support to generate O₂²⁻.

With the bare SBA-15, the conversion increased with a rise in temperature. No conversion was noted at 350 °C, whereas, the highest conversion (7%) was observed at 500 °C which

was ascribed to the homogeneous gas phase radical reactions. Activation of *n*-octane over SBA-15 takes place by surface reaction with the aid of O₂ to produce these free radicals [26]. The unsupported NiMoO₄ produced octenes, CO_x, C₈ aromatics and cracked aromatics (C₆ and C₇), with minor amounts of C₁ to C₆ cracked products. However, with the supported catalysts, along with octenes and CO_x, a significant amount of cracked products (C₁-C₆) and oxygenates were observed. All the catalysts, except SBA-15 and β-NiMoO₄ supported on SBA-15, showed octenes as their dominant products at all temperatures.

4.3.2.4 Comparison of product selectivity for all catalysts as a function of temperature

The selectivity to the different products as a function of temperature obtained during catalytic testing of the different catalysts is shown in Table 4.2.

In general, at lower temperatures (350 and 400 °C), octenes were produced as primary products, but as the temperature increased to 450 °C and higher, secondary oxidation of octenes became favourable to produce aromatics, cracked products and CO_x. With the β-NiMoO₄/SBA-15 catalyst, support surface reactions were found to dominate causing a decrease in the selectivity to octenes which were compensated by the formation of oxygenates and cracked products.

With α-NiMoO₄, at 400 °C, octene selectivity decreased and then remained constant over the increasing temperature range. This decrease was accompanied by an increase in the selectivity to aromatics, since the octenes are acting as precursors for their formation [27]. The increase in temperature also resulted in increased CO_x selectivity. A similar drop in octenes selectivity was also noted over the β-NiMoO₄, but the extent of non-selective secondary oxidation of the octenes was found to be lower than over the α-NiMoO₄ and thus, decreased selectivity to CO_x was noted. The difference in the reactivity of both the phases are credited to their different structural properties [4]. The β-phase was found to be more selective towards ODH products than its other polymorph for the oxidation of propane, butane and *n*-hexane [12, 16, 28]. Madeira *et al.* [22] suggested that the α-NiMoO₄ has a higher number of weakly adsorbed oxygen species on its surface, which are associated with total oxidation and this accounted for the lower selectivity to ODH products. In contrast, the lower exposed surface area of the tetrahedral β-phase is able to lower the amount of adsorbed oxygen species on its surface, which results in higher octene selectivity.

Table 4.2 Catalytic testing of the catalysts at a C:O ratio of 8:1 and at a GHSV of 4000 h⁻¹.

Catalysts	Conv. %	Temp. %	Octenes %	Aroma-tics C8	Aromatics (<C8) %	COx %	Oxygena tes %	C1-C6 %	Dienes %
α-NM	3.5	350	58	4	2	35	0	2	0
	6.7	400	42	8	2	46	0	2	0
	8.8	450	41	11	1	42	0	3	2
	8.5	500	37	8	2	46	0	7	1
β-NM	0.4	350	97	0	0	0	0	3	0
	2.8	400	67	0	0	27	0	3	3
	6.2	450	53	11	3	26	0	4	3
	8.5	500	55	15	2	18	0	7	3
SBA-15	0.1	350	100	0	0	0	0	0	0
	0.8	400	78	0	0	16	3	3	0
	3.7	450	40	0	0	23	4	33	0
	6.5	500	31	5	0	17	0	46	1
α-NM/SBA15	0.2	350	100	0	0	0	0	0	0
	0.8	400	67	0	0	29	0	4	0
	3.8	450	53	0	1	36	3	7	0
	5.6	500	20	23	1	43	2	11	0
β-NM/SBA15	0.7	350	32	0	0	0	43	25	0
	2.7	400	40	0	0	6	12	42	0
	4.4	450	36	2	0	7	17	38	0
	5.3	500	40	4	0	12	2	42	0

(NM= NiMoO₄)

When SBA-15 was tested alone under similar conditions, it showed a decreasing trend to octenes selectivity with an increase in temperature. At 400 °C, along with octenes, formation of cracked products was also observed. The activation of *n*-octane over SBA-15 takes place due to the activated oxygen species, whereas, the formation of cracked products occurs due to the electrophilic O⁻ species, which are formed by the dissociation of the O₂²⁻ species [26, 29]. Stoylkova *et al.* [26] suggested that an insertion of these activated oxygen species into the hydrocarbon takes place on the surface of the mesoporous silica to produce oxygenated hydrocarbons, such as substituted furans and pyrans, however, cleavage of these activated precursors (hydrocarbon peroxide) results in the formation of ketones. The aromatics were formed only at higher temperatures, with substantial selectivity to CO_x and cracked products,

which suggests that the appearance of the aromatics could likely be favoured by two routes, namely, by the thermal activation of octenes as well as to some extent by the SBA-15 support itself. The thermal route toward formation of these aromatic products is supported by the analyses of the data obtained for the blank reactions (Appendix 1, A1.4.1), which show the appearance of aromatics and C8 olefins.

When the SBA-15 supported catalysts were tested at temperatures of 350 and 400 °C, the α -NiMoO₄/SBA-15 exhibited a similar conversion to the support, but with a totally different product profile. This implies that the surface structure of the SBA-15 underwent modification in the presence of the active phases, which results in the formation of these products. Above 450 °C, the bare SBA-15 gave a selectivity lower than 40% to octenes but in the presence of the α -phase, the selectivity of ODH products increased due to the reactions being driven by lattice oxygen.

The α -phase of the supported catalyst also showed a similar behaviour to the unsupported α -phase in terms of CO_x production, which suggests that the surfaces of these systems are very similar in defining the CO_x selectivity. However, the aromatization of octenes was generally favoured over the unsupported catalyst, except at 500 °C, where the supported α -NiMoO₄ gave a comparatively higher selectivity. The interface between the silica surface and octahedral co-ordinated α -phase with a minor amount of the β -phase is likely to be the active site for the cyclisation and dehydrogenation of the octenes. The basic character introduced by the small amount of the β -NiMoO₄ at the active site and the higher mobility of the lattice oxygen improves the catalyst's ability to participate in the redox reaction and thus allows favourable conditions for the formation of aromatics [30].

Although the supported β -phase has basic character, the support surface reactions were found to dominate over ODH and produced oxygenates, thus lowering the selectivity to ODH products. Molybdates have an ability to activate oxygen as demonstrated by Pradhan *et al.* [31] when using iron molybdate catalysts to activate *n*-decane in the temperature range of 350 °C to 450 °C. In addition, Stoylkova *et al.* [26] showed that mesoporous silica also has an ability to activate gaseous oxygen to form activated oxygen species. It is thus suspected that the higher selectivity to oxygenates for the supported β -NiMoO₄ catalyst is due to the higher surface area of the support rather than the phase itself. Subsequently, the β -NiMoO₄ supported on SBA-15 shows a higher tendency to form oxygenated products when compared to the supported α -phase. The oxygenated products showed a decrease in selectivity at

500°C, since the decomposition of the hydroperoxides species, O_2^{2-} , is favoured to produce O^- species, generating alkyl radicals to produce mainly cracked products.

4.3.2.5 Product selectivity at isoconversion

The selectivities to the various products were examined at an isoconversion of approximately 5% for the various catalysts. The results are shown in Figure 4.10.

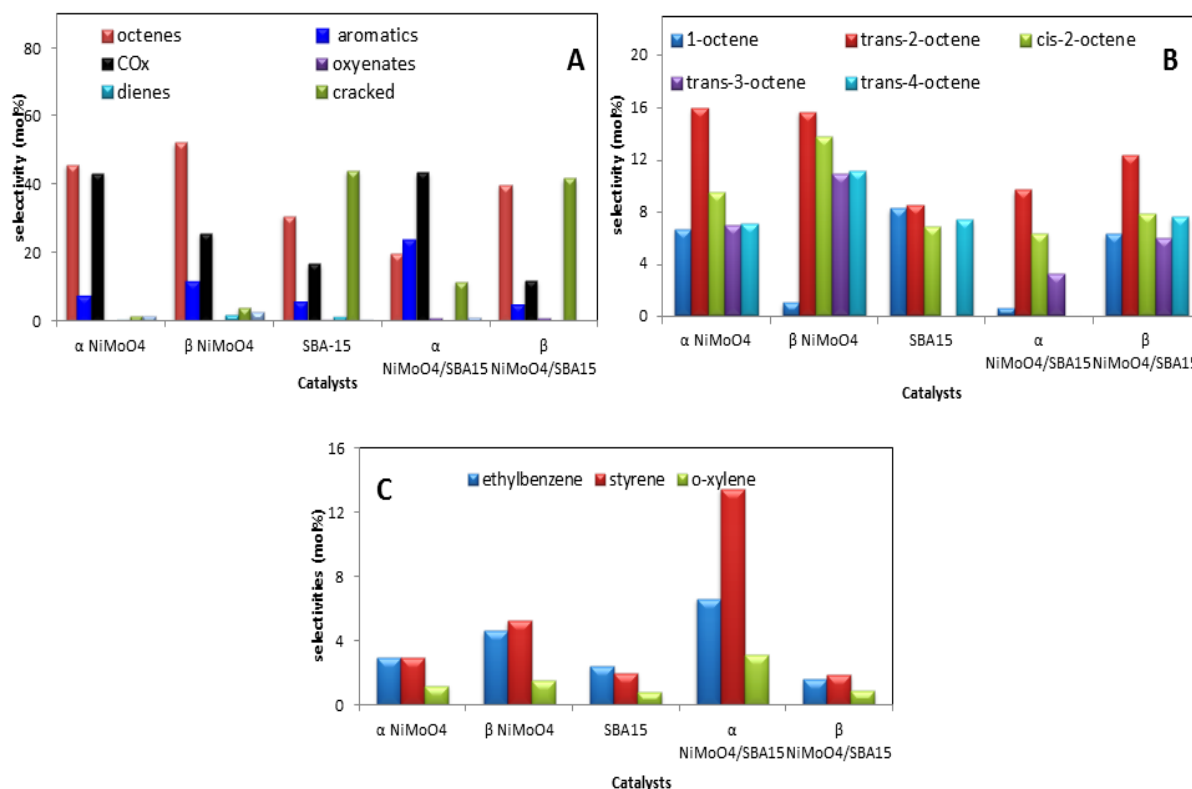


Figure 4.10 Product distribution at isoconversion (A) different products selectivity (B) octenes breakdown (C) Aromatics breakdown.

Both the unsupported phases of NiMoO₄ showed a high ODH product selectivity, however, the β -phase showed a higher selectivity compared to the α -phase. Comparatively, the CO_x selectivity was higher over the α -phase than the β -phase. The variation in the reactivity of both the unsupported phases was assigned to the differences in the lattice oxygen reactivity, as well as geometry of the phases, which affects the Mo-O bond strength [16]. Kaddouri *et al.* [4] reported, when looking at the ODH of propane, that the lattice oxygen consumption rate for the β -phase was shown to be higher than the α -phase, which results in a higher olefin selectivity.

Under similar reaction conditions, the bare SBA-15 support showed a significant selectivity to cracked products. On the SBA-15 support, the activation of *n*-octane takes place via the adsorbed oxygen which forms O_2^{2-} species. The dissociation of these peroxy species causes the formation of O^- species, which promotes the formation of cracked products [32].

With the α -phase supported on SBA-15, the cyclisation of octenes to aromatics was found to increase at the expense of octenes. However, it is noteworthy that the improved performance of the catalyst cannot be related to one phase, but possibly it is a combined effect of the α - and β -phase of $NiMoO_4$ and SBA-15 support. Zăvoianu *et al.* [30] concluded that in the presence of the β -phase, the α -phase exhibits an improved selectivity towards the formation of ODH products. The higher mobility of the lattice oxygen of the β -phase was said to be responsible for its increased ability to participate in redox processes [4, 33]. The higher CO_x selectivity for the supported α -phase is similar to the unsupported phase indicating its tendency to combust the hydrocarbons.

The octenes and aromatics breakdown for all the catalysts is shown in Fig. 4.10 B and C respectively. The octenes observed were 1-octene, *trans* 2-octene, *cis* 2-octene, *trans* 3-octene, and *trans* 4-octenes. The octene isomeric selectivity decreased in the order, *trans* 2-octene > *trans* 3-octene > *cis* 2-octene > 1-octene > *trans* 4-octenes. The least favoured octene is thus *trans*-4-octene, since the hydrogen radical abstraction becomes difficult due to the steric requirements at position 4. Increased selectivity to *cis* 2-octenes, *trans* 3-octenes, and *trans* 4-octenes were found with the unsupported β -phase, however, both the unsupported α - and β -phases exhibited similar selectivity to *trans* 2-octenes. The unsupported α -phase showed higher selectivity to 1-octene compared to the unsupported β -phase.

When α - $NiMoO_4$ was supported on SBA-15, no 1-octene was observed, while β - $NiMoO_4$ on SBA-15 showed the presence of 1-octene. Previous work stated that 1-octene is highly reactive and is consumed to produce ethyl benzene and further dehydrogenates (oxidatively) to give styrene [23]. The aromatic selectivity over unsupported α - $NiMoO_4$ was low due to over-oxidation of the octenes, while with unsupported β - $NiMoO_4$, aromatics selectivity increased since this phase is known to promote ODH reactions [4].

It was observed that when α - $NiMoO_4$ was supported on SBA-15, an increase in the selectivity to aromatics occurred, while no 1-octene was seen. This was found to be in agreement with the report that 1-octene undergoes rapid cyclisation to give ethyl benzene as this is the only isomer has six sequential sp^3 hybridised carbon atoms, as in the other octene isomers, the

double bond present at the carbon position of 2, 3 and 4 brings rigidity in the carbon chain and thus lowers their ability to undergo cyclisation to form ethyl benzene [23]. In addition, the α -NiMoO₄/SBA-15 also facilitates the formation of styrene by oxidative dehydrogenation of the formed ethyl benzene. The β -NiMoO₄/SBA-15 catalyst showed lower selectivity towards aromatics due to two parallel mechanisms operating at the same time; that is, lattice oxygen activation of *n*-octane to produce octenes and the surface activated oxygen resulting in the formation of cracked products, oxygenates, and CO_x. Xylene formation was least favoured over these catalytic systems, which suggests that the catalytic systems do not favour C₂-C₇ cyclisation, but rather favour C₁-C₆ cyclisation to produce ethyl benzene and styrene. The styrene was the dominant aromatic product, followed by ethyl benzene and xylene. The unsupported α -phase showed a comparable selectivity to ethyl benzene and styrene, while, the unsupported β -phase showed an increase in styrene selectivity. The formation of benzene and toluene was also observed, probably resulting from the oxidative cracking of styrene.

4.4 Conclusion

In the absence of support, the pure α -NiMoO₄ phase is obtained, whereas in the presence of the support, together with the α -NiMoO₄, a minor amount of the β -NiMoO₄ was also observed. This was confirmed with XRD. Higher conversion was achieved with the higher C:O ratio of 8:3, while at a lower ratio of 8:1, lower conversion was observed. At the lower ratio, good selectivities towards octenes were found, while with an increase in oxygen content in the feed, increased selectivity to CO_x resulted. At a C:O ratio of 8:1, the limited supply of oxygen was utilised for the reoxidation of the reduced phase, thus preventing further oxidation to more stable CO_x. Testing at the same conversion revealed that unsupported α -NiMoO₄ showed a lower selectivity to octenes than the unsupported β -NiMoO₄. However, when the α -NiMoO₄ was supported on SBA-15 a higher selectivity to aromatics was found than over the β -phase, probably due to the presence of minor amount of β -phase along with the dominant α -phase causing a synergistic effect. In the case of β -NiMoO₄ supported on SBA-15, the formation of oxygenates was favoured.

Acknowledgements

This work was financially supported by SASOL, THRIP, and the NRF. We also thank the electron microscope unit, UKZN, for microscopic work.

References

- [1] J.H.McCain, M.M Bhasin, B.V Vora, T Imai, P.R Pujadó, *Appl. Catal. A: Gen.* 221 (2001) 397-419.
- [2] P.L. Gai-Boyes, *Catal. Rev.* 34 (1992) 1-54.
- [3] Y.S. Yoon, N. Fujikawa, W. Ueda, Y. Moro-oka, K.W. Lee, *Catal. Today* 24 (1995) 327-333.
- [4] A. Kaddouri, R. Del Rosso, C. Mazzocchia, P. Gronchi, D. Fumagalli, J. *Therm. Anal. Calor.* 66 (2001) 63-78.
- [5] A. Christodoulakis, S. Boghosian, *J. Catal.* 260 (2008) 178-187.
- [6] M.A. Bañares, S.J. Khatib, *Catal. Today* 96 (2004) 251-257.
- [7] S. Kotanjac, M. van Sint Annaland, J.A.M. Kuipers, *Chem. Eng. Sci.* 65 (2010) 441-445
- [8] A. Kaddouri, R. Anouchinsky, C. Mazzocchia, L.M. Madeira, M.F. Portela, *Catal. Today.* 40 (1998) 201-206.
- [9] R. Del Rosso, A. Kaddouri, R. Anouchinsky, C. Mazzocchia, P. Gronchi, P. Centola, *J. Mol. Catal. A: Chem.* 135 (1998) 181-186.
- [10] F. Dury, E.M. Gaigneaux, P. Ruiz, *Appl. Catal. A: Gen.* 242 (2003) 187-203.
- [11] L.M. Madeira, M.F. Portela, *Catal. Rev.* 44 (2002) 247-286.
- [12] B. Pillay, M.R. Mathebula, H.B. Friedrich, *Appl. Catal. A: Gen.* 361 (2009) 57-64.
- [13] B. Pillay, M. Mathebula, H. Friedrich, *Catal. Lett.* 141 (2011) 1297-1304.
- [14] M. Sautel, G. Thomas, A. Kaddouri, C. Mazzocchia, R. Anouchinsky, *Appl. Catal. A: Gen.* 155 (1997) 217-228.
- [15] C.R. Dias, R. Zavoianu, M.F. Portela, *Catal. Comm.* 3 (2002) 85-90.
- [16] C. Mazzocchia, C. Aboumrad, C. Diagne, E. Tempesti, J.M. Herrmann, G. Thomas, *Catal. Lett.* 10 (1991) 181-191.
- [17] D. Cauzzi, M. Deltratti, G. Predieri, A. Tiripicchio, A. Kaddouri, C. Mazzocchia, E. Tempesti, A. Armigliato, C. Vignali, *Appl. Catal. A: Gen.* 182 (1999) 125-135.
- [18] L. Cao, T. Man, M. Kruk, *Chem. Mater.* 21 (2009) 1144-1153.
- [19] T.W. Atsushi Ishihara, Hiroyuki Nasu, Tadanori Hashimoto, *Appl. Catal. A: Gen.* 478 (2014) 58–65.

- [20] M.-C. Liu, L. Kang, L.-B. Kong, C. Lu, X.-J. Ma, X.-M. Li, Y.-C. Luo, *RSC Adv.* 3 (2013) 6472-6478.
- [21] A.A. Lemonidou, A.E. Stambouli, *Appl. Catal. A: Gen.* 171 (1998) 325-332.
- [22] L.M. Madeira, M.F. Portela, *Appl. Catal. A: Gen.* 281 (2005) 179-189.
- [23] E.A. Elkhalfa, H.B. Friedrich, *Catal. Lett.* 141 (2011) 554-564.
- [24] M. Narayanappa, V.D.B.C. Dasireddy, H.B. Friedrich, *Appl. Catal. A: Gen.* 447-448 (2012) 135-143.
- [25] E.A. Elkhalfa, H.B. Friedrich, *Appl. Catal. A: Gen.* 373 (2010) 122-131.
- [26] T.Y. Stoylkova, C.D. Chanev, H.T. Lechert, C.P. Bezouhanova, *Appl. Catal. A: Gen.* 203 (2000) 121-126.
- [27] V.D.B.C. Dasireddy, S. Singh, H.B. Friedrich, *Appl. Catal. A: Gen.* 421-422 (2012) 58-69.
- [28] R.M. Martin-Aranda, M.F. Portela, L.M. Madeira, F. Freire, M. Oliveira, *Appl. Catal. A: Gen.* 127 (1995) 201-217.
- [29] A. Bendandi, G. Fornasari, M. Guidoreni, L. Kubelkova, M. Lucarini, F. Trifirò, *Top. Catal.* 3 (1996) 337-354.
- [30] R. Zăvoianu, C.R. Dias, A.P.V. Soares, M.F. Portela, *Appl. Catal. A: Gen.* 298 (2006) 40-49.
- [31] S. Pradhan, J.K. Bartley, D. Bethell, A.F. Carley, M. Conte, S. Golunski, M.P. House, R.L. Jenkins, R. Lloyd, G.J. Hutchings, *Nat. Chem.* 4 (2012) 134-139.
- [32] B.v.d.V. Cassia Boyadjian, Igor V. Babich, Leon Lefferts, K. Seshan, *Catal. Today.* 157 (2010) 345-350.
- [33] J.L. Brito, J. Laine, *Appl. Catal.* 72 (1991) L13-L15.

Chapter 5

Summary and Conclusion

The oxidative dehydrogenation (ODH) of *n*-octane was carried out using molybdenum based catalytic systems. The study included testing of unsupported MoO₃, MoO₃ supported on SBA-15 and unsupported NiMoO₄, and NiMoO₄ supported on SBA-15.

The results, when testing the unsupported MoO₃ catalyst, showed a change in the selectivity profile as the C:O ratio and temperature were varied. Under catalytic conditions, when no oxygen were present in the feed, octenes were found to dominate over the reduced phase of MoO₃, that is, over MoO₂, but at considerably low conversions of *n*-octane. This was observed up to 500 °C. At the highest temperature studied (550 °C), only cracked products were observed. The introduction of oxygen in the feed to give a C:O ratio of 8:2 caused an increase in conversion of *n*-octane, with a decrease in octenes selectivity and at the same time an increase in CO_x selectivity. At a C:O ratio of 8:1, the fuel rich conditions favoured formation of octenes, which were observed to be the most selective products formed.

The used catalysts studied at a C:O ratio of 8:1 displayed peaks for MoO₂, Mo₄O₁₁ and less intense peaks for MoO₃, whilst the catalyst studied at a C:O ratio of 8:0 showed peaks only for MoO₂. At the highest concentration of oxygen in the feed, no peaks for MoO₂ were detected using XRD. The feed with a C:O ratio of 8:1 at 550 °C was found to be optimum to give the highest selectivity to octenes (54%) and aromatics (10%). Among the octenes and aromatics, 1-octene (16% selectivity) and styrene (4% selectivity) were the dominant products observed respectively.

When molybdenum oxide was supported on SBA-15 with weight loadings of 4, 7, 10 and 18 wt%, several phases were found depending on the loading which impacted the conversion of *n*-octane and the selectivities of the product that formed. The catalysts were characterised with XRD, Raman, SEM, TEM and surface area analyses. The formation of predominantly monomeric, with minor amounts of polymeric, MoO_x species was detected at 4 wt% molybdenum loading. When the molybdenum loading was increased to 7%, crystalline MoO₃ was observed, as confirmed with Raman and XRD, in addition to the species observed at 4 wt% loading. With 10% molybdenum supported on SBA-15, the peaks for crystalline

MoO₃ and polymeric MoO_x species were more pronounced with the absence of monomeric MoO_x species, however at 18 wt% molybdenum loading, the presence of crystalline MoO₃ on the surface of SBA-15 was noted. For the catalytic testing, the bare SBA-15 was found active, but non-selective towards ODH products with a selectivity of more than 60% to cracked products and CO_x at the 450 °C. At the same temperature, with the introduction of metal oxide on the support at 4 and 7 wt% loadings, the cracked products and CO_x selectivity decreased with a corresponding increase in ODH products selectivity. However, further increase in molybdenum loading brought about an increase in selectivity towards non-selective oxidation products due to the aggregation of the molybdenum oxides species on the surface of the support, providing a catalyst that behaves more like the bare support. The octenes yield (4%) was highest over the 4 wt% loaded catalyst, whereas the 10 wt% molybdenum loaded catalyst gave the highest yield (1%) to aromatics. Overall, the ODH yield was higher over the 10% molybdenum supported on SBA-15 catalyst. When the catalytic testing of the 10 wt% molybdenum loaded catalyst was carried out as a function of temperature, aromatics selectivity increased to a maximum of 12% at 550 °C. The GHSV studies for the same catalytic system revealed that octenes, cracked products, and CO_x are the primary products of the ODH of *n*-octane, whereas CO and aromatics are formed due to secondary oxidation. The conversion of *n*-octane and the extent of non-selective oxidation increased with increase in the oxygen content in the feed.

Unsupported NiMoO₄ and NiMoO₄ supported on SBA-15 were also tested as catalysts for the oxidative dehydrogenation of *n*-octane. The characterisation results of the unsupported NiMoO₄ showed the presence of only α -phase, however, when the NiMoO₄ was supported on SBA-15, it showed the appearance of the minor β -phase, in addition to the dominant α -phase even prior to the heat treatment of the catalysts. The β -phase was generated *in situ* by heating the α -phase to 720 °C.

The catalytic testing of the unsupported α -phase was carried out while varying the oxidative environment i.e. with changing C:O ratios of 8:1, 8:2 and 8:3. The *n*-octane conversion predictably increased with an increase in oxygen concentration. At lower concentration of oxygen, the octenes selectivity was observed to be highest and thereafter decreased with an increase in oxygen concentration. When the unsupported β -phase was generated *in situ* and tested at the optimum C:O ratio of 8:1 as a function of temperature (350 to 500 °C), it displayed lower conversions than the unsupported α -phase, but showed improved selectivity towards octenes.

The SBA-15 supported α -NiMoO₄ with a slight amount of β -NiMoO₄, displayed the highest aromatics selectivity (23%) at the same ratio (8:1). With β -NiMoO₄ supported on SBA-15, a lower selectivity to aromatics was observed and a higher selectivity to oxygen and oxygenates and cracked products. The highest octenes selectivity was observed over both the unsupported phases (α - and β -) with trans 2-octenes being the most dominant isomer formed, whereas α -NiMoO₄ supported on SBA-15 gave the highest selectivity to aromatics with styrene being the most selective. The CO_x selectivity was highest for both the unsupported and supported α -NiMoO₄ compared to β -phase. The catalytic testing of the bare SBA-15 under the same conditions of testing as the catalysts, that is at a C:O ratio of 8:1, gave the highest selectivity to octenes up to 450 °C, after which cracking became the dominant process of converting the *n*-octane.

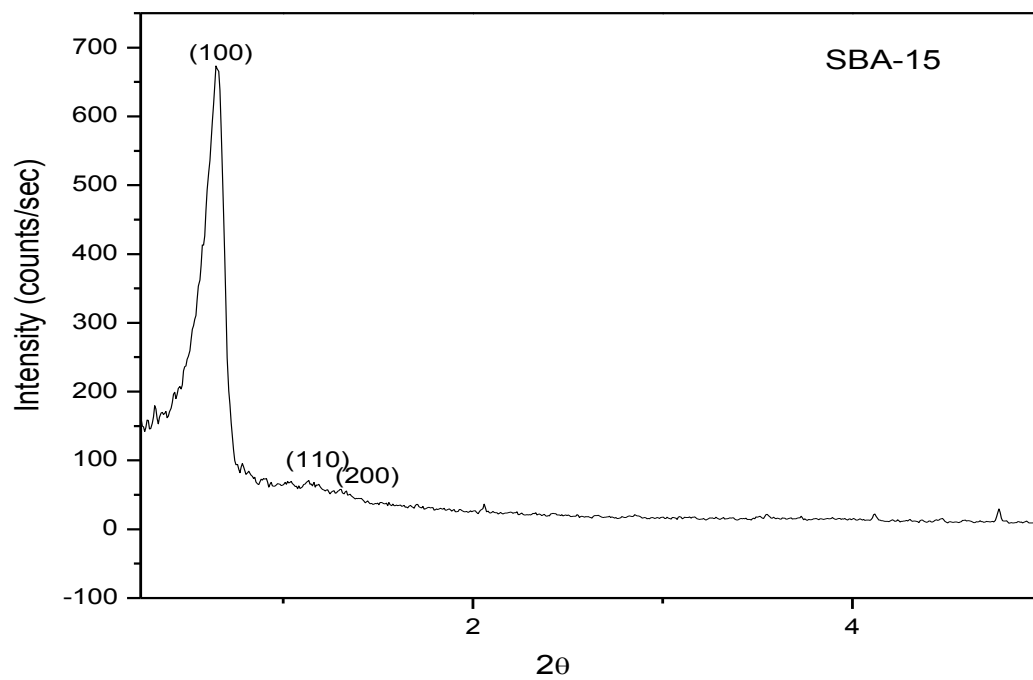
Appendix-1(Figures and Tables)

A1.2.1

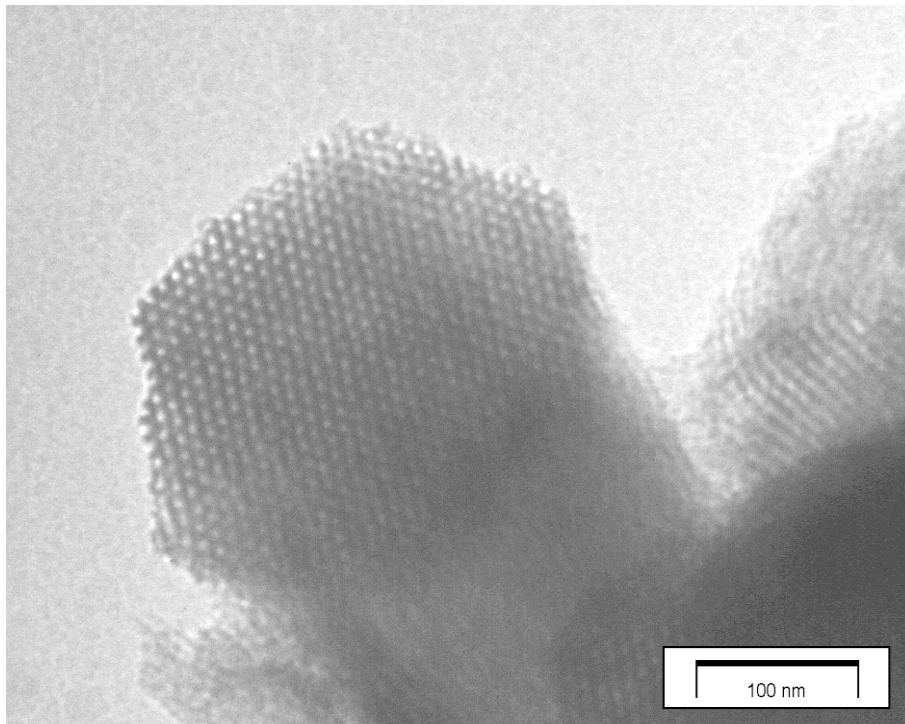
Table A1.2.1 Conversion and product selectivities of n-octane oxidation in a 24 grit carborundum packed reactor tube at C: O ratio of 8:0 at a GHSV of 4000 h⁻¹.

Temperature/ °C	500 °C	550 °C
<i>n</i> -octane conversion (%)	0.4	0.7
Selectivity		
C ₁ -C ₃ alkane	42	5
C ₂ -C ₄ alkenes	44	73
C ₅ -C ₆ alkenes	14	21

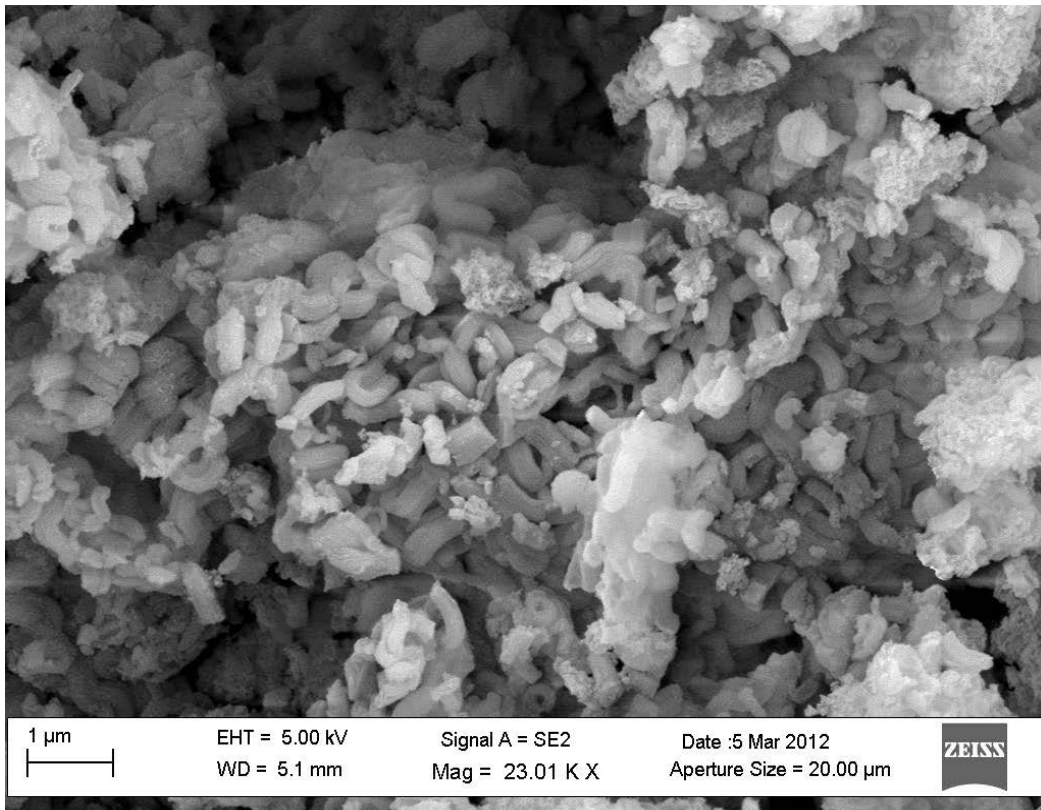
A1.3.1 SAXS for SBA-15



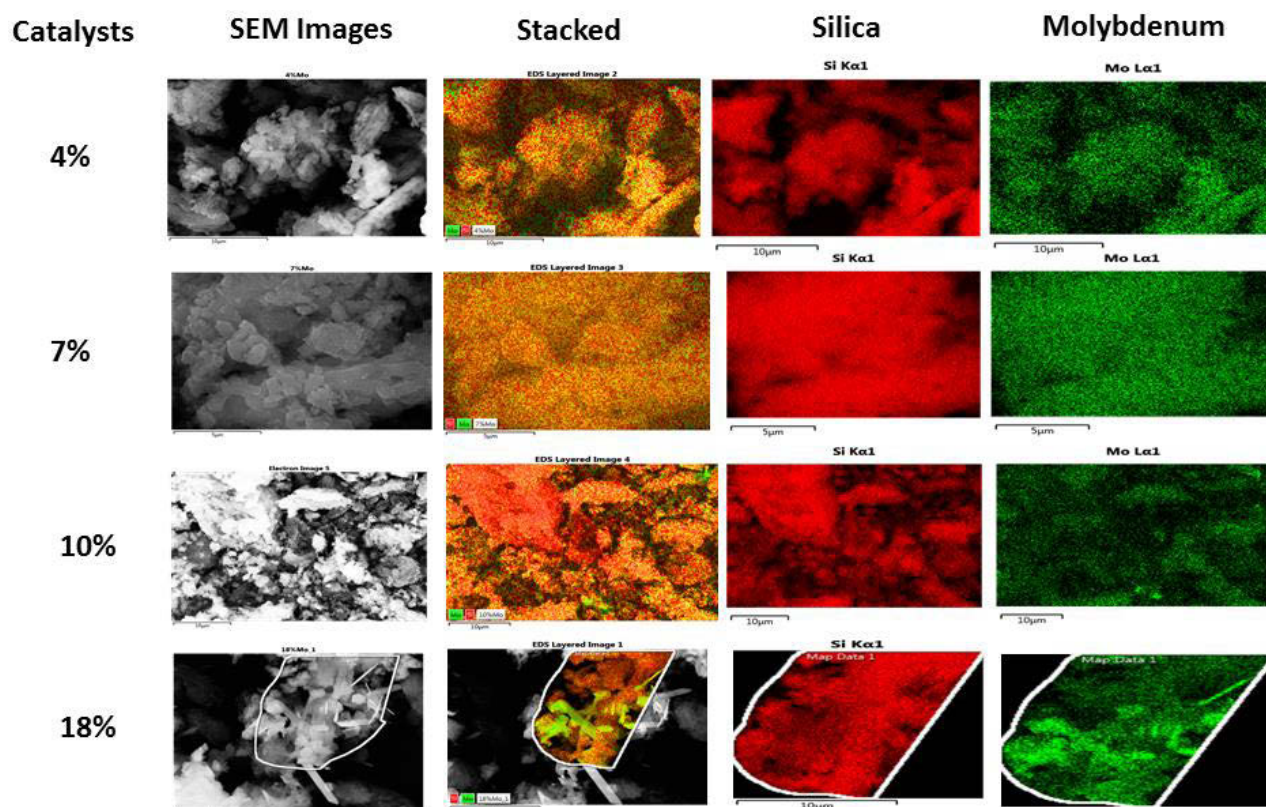
A1.3.2 TEM image of SBA-15



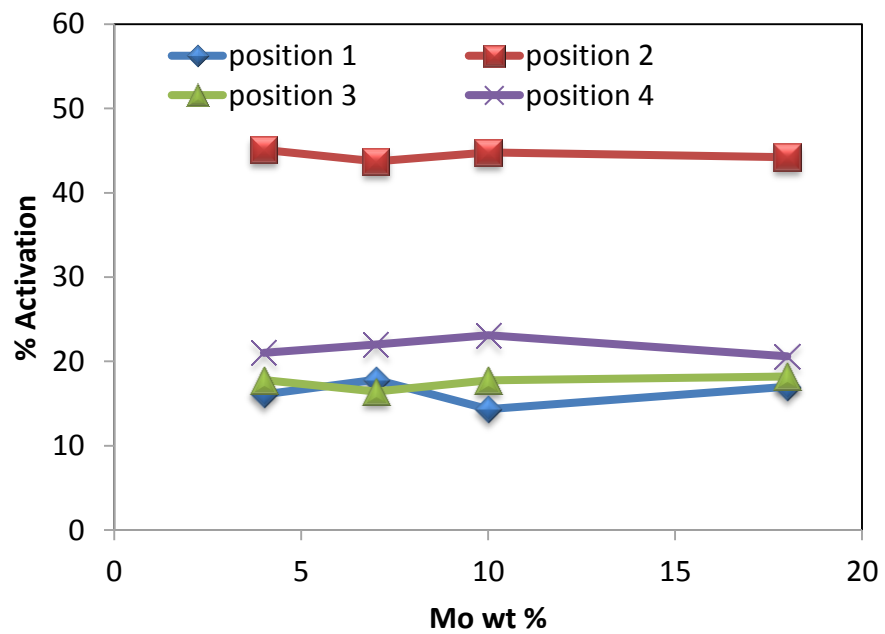
A1.3.3 SEM image of SBA-15



A1.3.4 EDS mapping of catalysts



A1.3.5 % Activation of *n*-octane

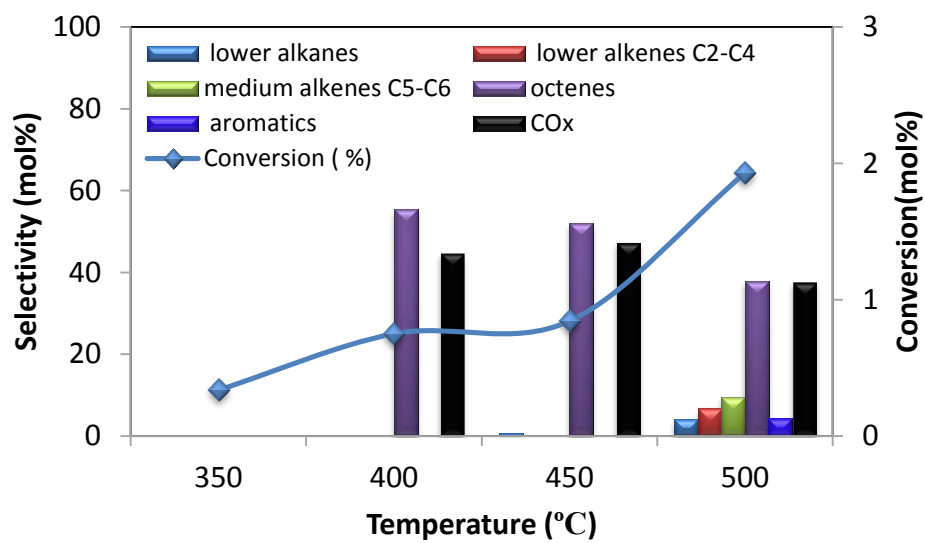


A1.3.6

Table CO and CO₂ breakdown with varying oxygen ratio at 450 °C at a GHSV of 4000 h⁻¹.

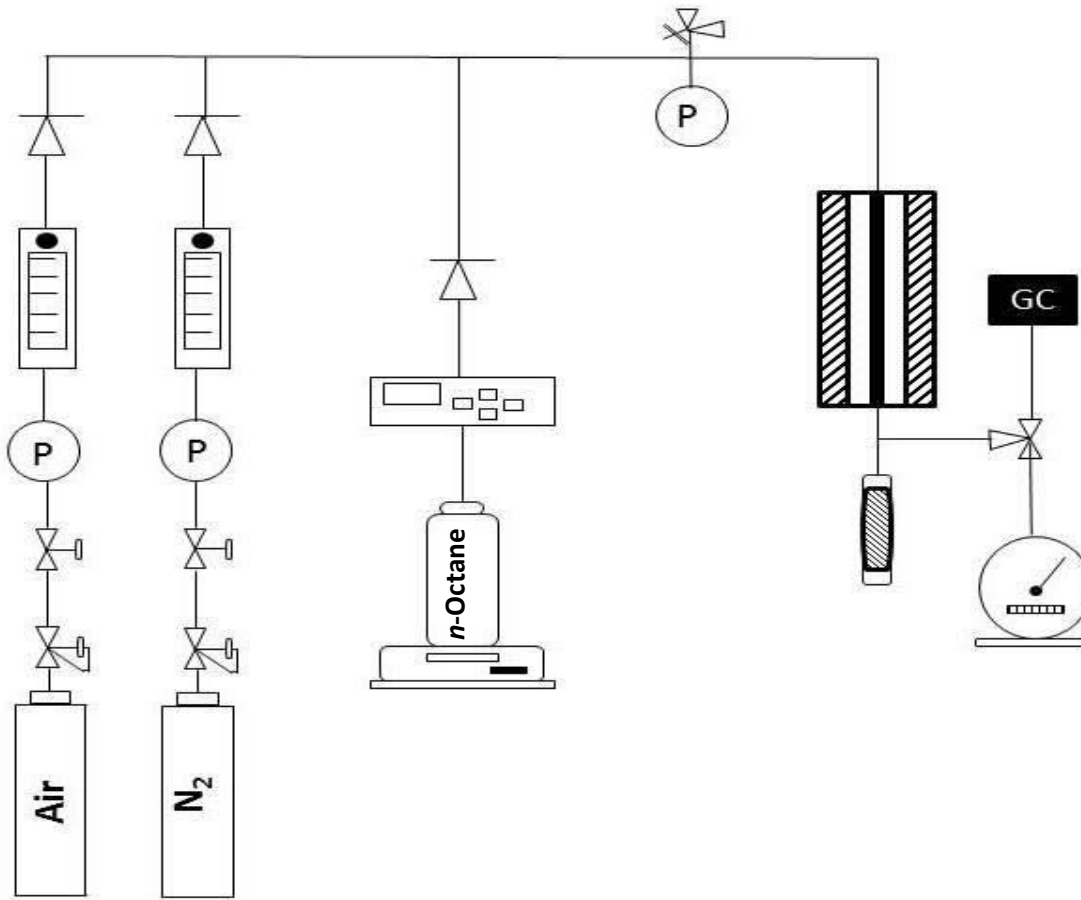
	C:O ratio		
	(8:2)	(8:3)	(8:4)
CO	21.48	24.50	25.93
CO₂	26.04	21.16	18.21


A1.4.1 Blank reaction results with C:O = 8:1 at a GHSV of 4000 h⁻¹.

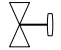



Appendix-2(Product quantification)

A2: Reactor set up:




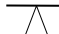
 Pressure regulator


 ball valve


 Pressure relieve valve

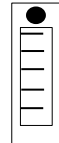
 Pressure gauge

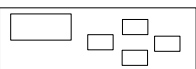
 Reactor tube

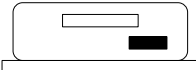
 one way valve


 Wet gas flow meter

 Catch pot coated with chilled lines

 Rotameters

 HPLC pump

 Balance

 Heating block

A3. Gas chromatographic method for analysing gaseous, organic and liquid samples

Channel Parameters:

Run Time: 30.00 min

Sampling Rate: 3.1250 pts/s

Carrier Parameters:

Carrier A Control: He (300 Kpa)

Column A length: 50.00 m

Vacuum Compensation: Off

Diameter: 530 μ m

Split Ratio: 150:1

Initial Set point: 2.0 ml/min

Valve Configuration and Setting:

Valve 1: SPLIT On

Valve 2: NONE

Valve 3: NONE

Detector Parameters:

	Detector A
Detector	FID
Range	1
Time Constant	200
Auto zero	ON
Polarity –	
Detector A Gas Flows	
Air: 450.0 ml/min	
Hydrogen: 45.0 ml/min	

Heated Zones:

Injector A: CAP

Setpoint: 220 °C

Detector A: 250 °C

Oven Program:

Cryogenics: Off

Total Run Time: 30.0 min

Initial Temp: 40°C

Max. Temp: 300 °C

Initial Hold: 15.0 min

Equilibration Time: 0.2 min

Ramp 1: 20.0 °C/min to 100 °C, hold for 5.0 min

Ramp 2: 20.0 °C/min to 200 °C, hold for 2.0 min

Processing Parameters:

Bunch Factor: 2 points

Noise threshold: 50 µV

Area Threshold: 100.0 µV

Peak Separation Criteria:

Width Ratio: 0.2

A4. GC-Method used for analyzing carbon oxides (TCD)

Channel Parameters:

Run Time: 7.0 min

Sampling Rate: 6.25 pts/s

Carrier Parameters:

Carrier B Control: He (300 KPa)

Column B length: 30.00 m

Vacuum Compensation: Off

Diameter: 530 μ m

Split Flow: 500.0 ml/min

Initial Set point: 6.0 ml/min

Valve Configuration and Setting:

Valve 1: SPLIT On

Valve 2: NONE

Valve 3: NONE

Detector Parameters:

	Detector B
Detector	TCD
Range	3
Time Constant	200
Autozero	ON
Polarity	-
Detector B Gas Flows	Helium: 30.0 ml/min

Heated Zones:

Injector B: CAP

180

Set point: 220 °C

Detector B: 250 °C

Oven Program:

Cryogenics: Off

Total Run Time: 7.0 min

Initial temp: 40 °C

Max. Temp: 250 °C

Initial Hold: 2.50 min

Equilibration Temp: 0.5 min

Ramp 1: 20.0 °C/min to 80 °C, hold for 2.5 min

Processing Parameters:

Bunch Factor: 2 points

Noise threshold: 1 μ V

Area Threshold: 100.0 μ V

Peak Separation Criteria:

Width Ratio: 0.2

Valley-to-peak Ratio: 0.01

Table A2.1 Standards used for calibration

Chemical	Supplier Purity	(%)
<i>n</i> -Octane	Merck	99
1-Octene	Aldrich	98
<i>trans</i> 2-Octene	Fluka	98
<i>cis</i> 2-Octene	Alfa Aesar	98
<i>trans</i> 3-Octene	Aldrich	98
<i>trans</i> 4-Octene	Fluka	98
<i>cis</i> 4-Octene	Alfa Aesar	97
1, 7-Octadiene	Fluka	97
Ethyl benzene	Alfa Aesar	99
<i>o</i> -Xylene	Alfa Aesar	99
Styrene	Aldrich	99
Ethylcyclohexane	Fluka	99
<i>n</i> -heptane	Fluka	99.8
1-heptene	Aldrich	97
<i>n</i> -hexane	ACROS	99.5
1-hexene	ACROS	97
<i>n</i> -Nonane	Fluka	99
Cyclooctane	Fluka	99
<i>cis</i> -Cyclooctene	Aldrich	95
<i>cis,cis</i> -1,5-Cyclooctadiene	Fluka	98
Propyl cyclopentane	Fluka	98
2,4-Dimethylhexane	Fluka	99
2-ethyl-1-hexanol	Fluka	98

1-Octanol	Alfa Aesar	99
Octanal	Aldrich	99
2-Octanone	Fluka	97
3-Octanone	Fluka	97

Table A2.2 Gaseous standards used for calibration.

Component	Percentage (%)
Methane	2.0

A5. GC analysis

The reaction products obtained from reactor were quantified using Gas Chromatography (GC). To this end, a Perkin Elmer Clarus 400 instrument was used which was equipped with a Thermal Conductivity Detector (TCD) for the sequential analysis of carbon oxides using a Carboxen 106 PLOT column and a Flame Ionization Detector (FID) for all other organic products using a 50m PONA column, respectively.

A6. FID Sampling

Gaseous organic products were analysed on the FID by injecting a 0.2 ml gas sample withdrawn at the specific analysis time. The GC chromatogram for a gaseous sample is shown in Figure A1.

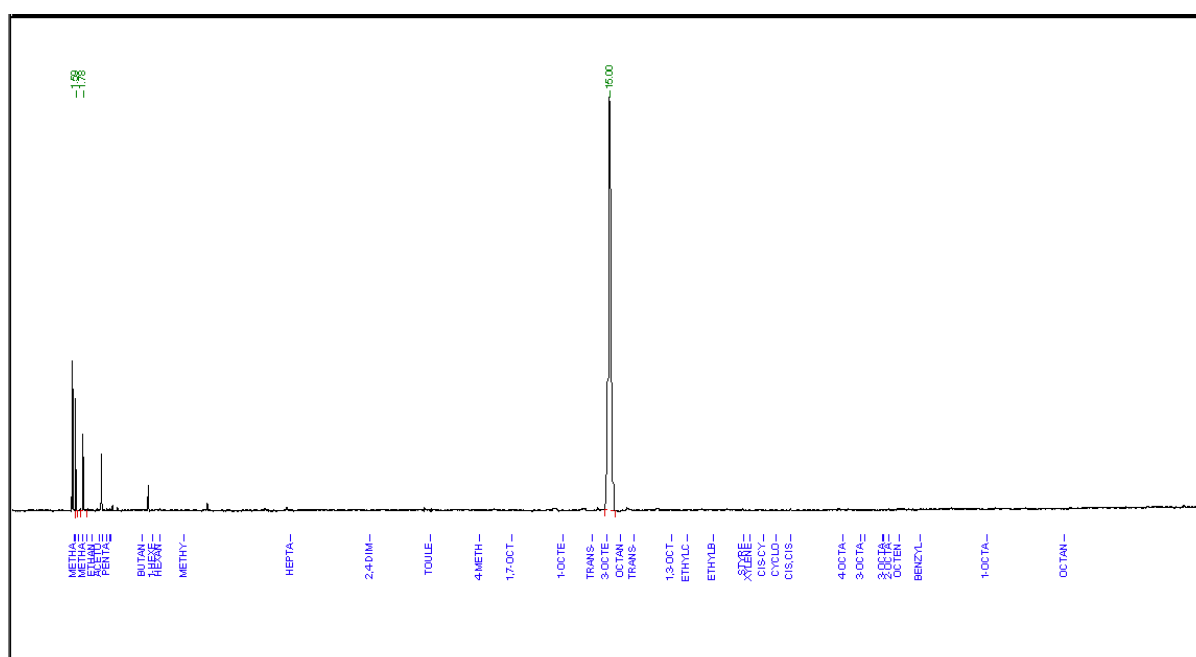


Figure A2.1 GC-FID chromatogram for a gaseous sample

Liquid organic products that condensed in the catch-pot (sample cylinder) were drained *via* the needle valve and accurately weighed. In some cases, two distinct layers were observed i.e. an organic layer and an aqueous layer. These were then carefully separated and re-weighed to obtain their individual contributions to the total mass of liquid products. The GC

method to analyse these layers is explained below. Chromatograms were then obtained for each of the layers separated. GC- chromatograms for an organic layer and an aqueous layer was shown in Figure A2 and Figure A3.

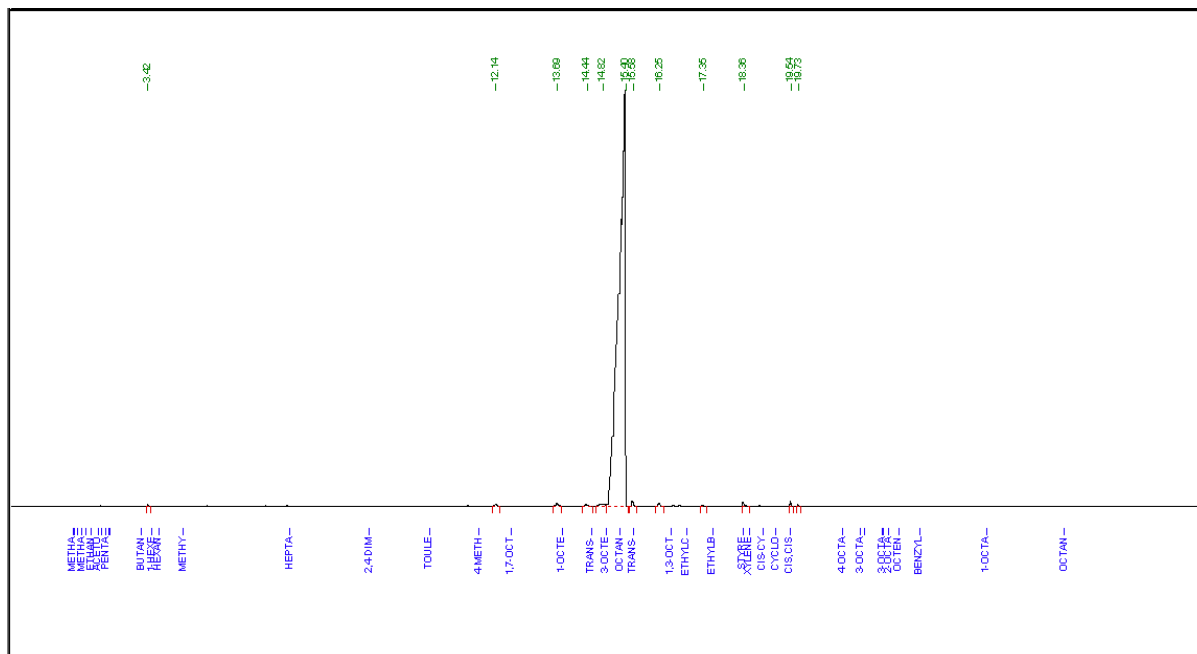


Figure A2.2 GC-FID chromatogram for a organic layer

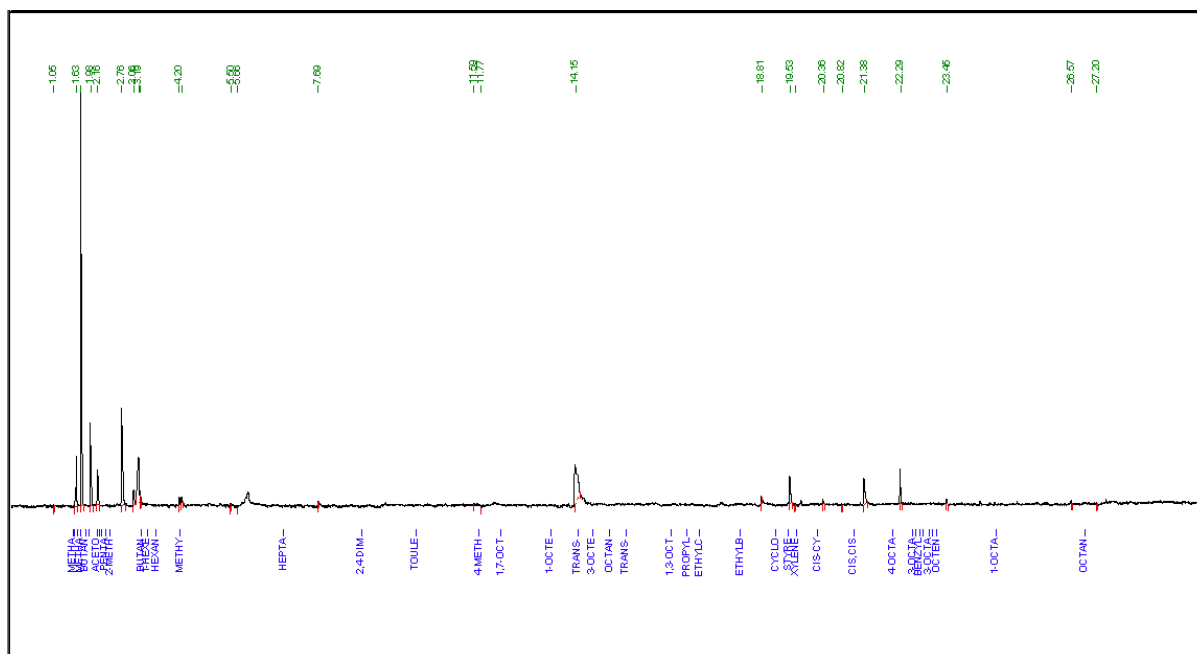


Figure A2.3 GC-FID chromatogram for a aqueous layer

A7. TCD sampling

Both carbon monoxide and carbon dioxide were produced during the various reactions. These were analysed by withdrawing a 100 μl gas sample using a 500 μl gas tight syringe Supplied by Scientific Glass Engineering Pty. Ltd. (SGE). GC chromatograph of carbon monoxide and carbon dioxide (CO_x) is showed in Figure 4. The carbon monoxide has a retention time of 0.65 min while the CO_2 appears at 2.25 min. as showed in Figure below.

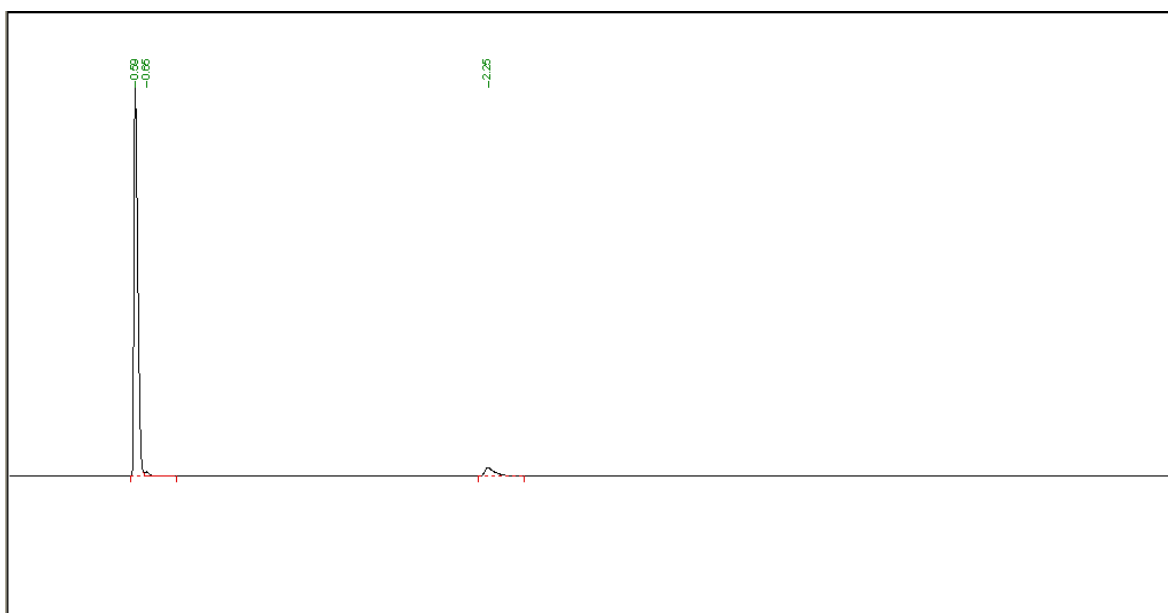


Figure A2.4 GC-TCD chromatogram of gaseous CO_x .

A8. KF calculation

In order to quantify the data obtained from the chromatograms during one analysis to usable data, such as yield and conversion, parameters including run time, mass of feed used, mass of Products collected and gas flow rates were recorded in the data sheet showed in Figure A5. The water content of the individual layers in the liquid products was determined by Karl Fischer Analysis using a Metrohm 870 KF Titrino Plus instrument. The values obtained were used to correct the mass of the organic and aqueous layers as shown in the example below.

Table A2.3 Data sheet for react

GHSV	4000	4000	4000	4000	4000
Time(hour)	1.5	1.5	1.5	1.5	1.5
Temperature(°C)	350	400	450	500	550
Mass of octane(initial)	2	2	2.02	2.04	2.04
Mass of octane (final)	0	0	0	0	0
Mass of Octane in	2	2	2.02	2.04	2.04
Moles of Octane in	0.01750854	0.01750854	0.01768362	0.0178587	0.0178587
Moles of carbon in	0.14006828	0.14006828	0.14146897	0.1428696	0.1428696
Out gas (initial)	28182.68	28188.15	28192.55	28196.86	28200.4
Out gas (final)	28186.4	28191.85	28196.05	28200.34	28203.82
Out gas flow(L)	3.72	3.7	3.5	3.48	3.42
out gas flow(ml)	3720	3700	3500	3480	3420
Total mass of liquid	1.966	1.9123	2.005	2.1079	1.9877
Mass of Organic layer	1.966	1.9123	1.786	1.7099	1.5775
Mass of Aqueous layer	0	0	0.219	0.398	0.4102
% of water in Organic	0	0	1.16	1.36	1.12
% of water in Aqueous	0	0	60	75	69
Actual mass of organic	1.966	1.9123	1.786	1.7099	1.5775
Actual mass of aqueous	0	0	0.219	0.398	0.4102
moles of water	0	0	0.01216667	0.0221111	0.0227889
Conversion :					
Moles of Octane in	0.01750854	0.01750854	0.01768362	0.0178587	0.0178587
Moles of Octane out	1.72E-02	1.67E-02	1.50E-02	1.42E-02	1.31E-02
Conversion (%)	1.76	4.75	15.2	20.2	26.86
Carbon balance:					
Moles of Carbon in	0.14006828	0.14006828	0.14146897	0.1428696	0.1428696
Moles of Carbon out	0.13786874	0.13428157	0.14598496	0.1562182	0.14768
Carbon balance	98.4	96	103	101	101

Mass of organic phase layer = 1.786 gm

% of water in organic layer = 1.16

Actual mass of organic layer = 1.789 gm

A8. Calculation of response factors (RF):

Assign *n*-octane a RF of 1 and calculate all other Response Factors relative to this:

Mass of *n*-octane in standard solution = 0.0073 g

Mass of *trans*-2-octene in standard solution = 0.00715g

Injection volume = 0.1 μ l

Peak area of *n*-octane = 46684.56

Peak area of *trans*-2-octene = 51712.54

The RF of *n*-octane was considered as 1 and Response Factor calculations was carried out relative to *n*-octane

Mass of *n*-octane in standard solution = 0.0075

Mass of *trans* 2-octene in standard solution= 0.00715

Injection volume= 0.1 μ L

Peak area of *n*-octane= 46684.56

Peak area of *trans*-2-octene= 50712.21

Response factor of *trans*-2-octene= $\frac{\text{peak area of trans-2-octene} \times \text{mass of n-octane}}{\text{mass of trans-2-octene} \times \text{peak area of n-octane}}$

Table A2.4 Relative response factor of *trans* 2-octene

Injection volume (μ l)	Amount of <i>trans</i> 2-octene	Peak area of <i>trans</i> 2-octene	Amount of <i>n</i> -octane injected	Peak area of <i>n</i> -octane	Relative response factor (RF)
0.1	0.00071	51714,89	0.000703	46684.56	0.91
0.2	0.00153	113606.4	0.001416	94552.7	0.9
0.3	0.00225	158300.4	0.002109	136843.9	0.91
0.4	0.00285	229129.7	0.002813	205058.5	0.91

Average response factor of *trans* 2-octene= 0.91

Table A2.5 Retention times, Response factors and gradient of the calibration graph of compounds

Component	R. T. (min)	R.F	Equation (y=..)
1-pentene	2.432	0.93	1.01E+14
2-methyl-2-propanol	2.477	0.72	8.13E+14
<i>n</i> -Pentane	2.37	0.76	8.81E+14
1-hexene	3.52	0.95	1.36E+14
<i>n</i> -Hexane	3.692	0.93	1.32E+14
Methylcyclopentane	4.311	0.92	1.24E+14
<i>n</i> -Heptane	6.98	0.91	1.63E+14
2, 4-dimethylhexane	8.97	0.94	1.79E+14
Toluene	10.47	1.12	1.57E+14
4-methylheptane	11.72	1.14	1.83E+14
1, 7-octadiene	12.52	0.90	1.85E+14
1-octene	13.8	0.98	1.90E+14
3-octene	14.9	0.98	1.75E+14
Trans-4-octene	14.53	0.97	1.83E+14
<i>n</i> -Octane	15.26	1	1.82E+14
Trans-2-octene	15.59	0.94	1.79E+14
1,3-octadiene	16.523	0.92	1.54E+14
Ethyl cyclohexane	16.92	0.90	1.87E+14
Propyl cyclopentane	16.93	1 0.95	1.75E+14
Ethyl benzene	17.58	1.13	1.93E+14
Styrene	18.34	1.17	1.75E+14
xylene	18.49	1.15	1.92E+14

cis-cyclooctene	18.829	1.20	1.78E+14
cyclooctane	19.16	1.16	1.90E+14
cis.cis-1,5-cyclooctadiene	19.52	1.12	1.84E+14
4-octanone	20.839	0.73	1.32E+14
3-octanone	21.28	0.91	1.87E+14
2-octanone	21.394	0.84	1.80E+14
3-octanol	21.83	0.76	1.51E+14
octanal	21.84	0.71	1.40E+14
2-octanol	21.992	0.78	1.46E+14
octene oxide	22.244	0.85	1.61E+14
benzyl alcohol	22.765	0.89	1.28E+14
1-octanol	24.446	0.85	1.86E+14
octanoic acid	26.396	0.61	1.23E+14

A9. Determination of moles of *trans* 2-octene from a liquid organic sample

Mass of the organic layer = 1.786 g

Percentage peak area of *trans* 2-octene = 0.91

Calculated Response Factor = 1.0519

Corrected area = Percentage peak area ÷ Response factor = 0.91 ÷ 1.0519 = 0.9677

$$\text{Normalised area (\%)} = \frac{\text{corrected area}}{\text{Sum of corrected areas of all the products in sample}} \times 100$$

$$= 0.866$$

$$\text{Mass Component (g)} = \frac{\text{normalised area}}{100} \times \text{mass of organic layer}$$

$$= \frac{(0.8601 \times 1.786)}{100} = 0.01525 \text{ gm}$$

$$\begin{aligned} \text{Moles component out (moles)} &= \frac{\text{mass of component}}{\text{molar mass of component}} \\ &= \frac{0.01525}{112.21} = 0.000135 \end{aligned}$$

$$\begin{aligned} \text{Moles of carbon out} &= \text{moles component out} \times \text{carbon number} \\ &= 0.001087 \text{ moles of carbon} \end{aligned}$$

A10. Determination of moles of butane from a gaseous organic sample

The gaseous samples were identified with the help of GCMS and their quantification was carried out by using methane as a standard gas by using the equation below

Initially, the constant was derived by using equation

$$\text{Constant} = (\text{Rf of methane} / \text{Area of methane}) \times \text{Vol. \% of methane}$$

The values obtained by injecting 0.2 μL in the GC-FID are

$$\text{Injection volume} = 0.2 \mu\text{L}$$

$$\text{Methane area} = 90000$$

$$\text{Methane Rf} = 1$$

$$\text{Constant} = (1/90000) \times 0.02$$

$$= 2.22 \times 10^{-7}$$

$$\text{Ethylene area from gaseous sample from reaction} = 17629.91$$

$$\text{Corrected area} = \text{Area} / \text{Rf}$$

$$= 17629.91/1$$

$$= 17629.91$$

Further, the corrected area was entered in the following formula to get the Mol. %,

Mol. %= Corrected area \times constant \times (molecular weight of methane/ molecular weight of unknown)

$$\text{Mol. \%} = 17629.91 \times 2.22 \times 10^{-7} \times (16/28)$$

$$\text{Mol \%} = 0.223871\%$$

Then, the volume of gas out was calculated from Mol. %

$$\text{Volume of gas out} = \text{Mol. \%} \times \text{gas out/min}$$

$$= 0.223 \% \times 67 \text{ mL/min}$$

$$= 0.0538 \text{ mL/min}$$

Moles out were calculated by using ideal gas equation

$$PV = nRT$$

Where,

$$P = 10000 \text{ Pa}$$

$$V = 0.0538 \text{ ml/min}$$

$$R = 8.314 \text{ L kPa K}^{-1} \text{ mol}^{-1}$$

$$T = 298 \text{ K}$$

$$\begin{aligned} \text{Number of moles of ethylene} &= 100000 \text{ Pa} \times 0.0538 \text{ ml/min} \times 0.000001 / (8.314 \text{ kPa K}^{-1} \\ &\quad \text{mol}^{-1} \times 298 \text{ K}) \end{aligned}$$

$$= 0.00000217$$

$$\text{Moles of Carbon} = 0.00000217 \times 2$$

$$= 0.00000434$$

$$\text{Total moles of Carbon} = 0.00000434 \times \text{Reaction time (min.)}$$

$$= 0.00000434 \times 120 \text{ min.}$$

$$= 0.00052$$

A11. Determination of moles of CO from gaseous sample

The number of moles of CO and CO₂ were obtained by plotting the graph of vol. % of CO and CO₂ by using two different concentration of gases of CO and CO₂. The gases used were

- 1% of CO and CO₂ with nitrogen as a make-up gas
- 5% of CO with nitrogen as a make-up gas
- 10% of CO₂ with nitrogen as a make-up gas

The standard were injected in TCD and areas were obtained for 0.2 μL injection are

CO vol. %	Area	CO ₂ vol. %	Area
0.01	2500.00	0.01	5000.00
0.05	12400.00	0.10	50700.00

The slopes were obtained by plotting the area as a function of Vol. %.

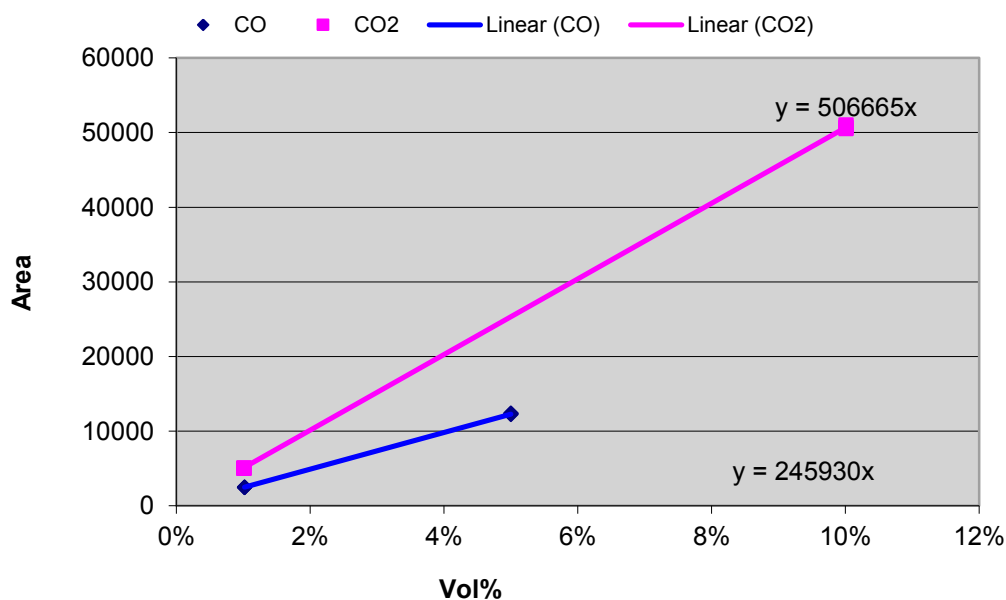


Figure A5 Graph represents the area as a function of Vol. % for CO and CO₂ standard.

The obtained slopes were used to calculate Vol. %,

$$\text{Vol. \%} = \text{Area of CO}_2/\text{Slope}$$

$$= 14195.62/506665$$

$$= 2.80 \%$$

$$\text{Vol. ml/min} = 2.80 \times 68 \text{ (mL/min)}$$

$$= 1.90 \text{ mL/min}$$

Further, the number of moles of CO₂ was calculated by using ideal gas equation, as showed in above,

$$\mathbf{PV=nRT}$$

Where,

$$P= 10000 \text{ Pa}$$

$$V= 1.90 \text{ ml/min}$$

$$R= 8.314$$

$$T= 298\text{K}$$

$$\text{Number of moles of ethylene} = 100000 \times 1.90 \times 0.000001 / (8.314 \times 298)$$

$$= 0.0000768$$

$$\text{moles of Carbon oxide/ hour} = 0.0000768 \times 60$$

$$= 0.000461 \text{ moles/hour}$$

